Technical Report Documentation Page

1. Report No. FHWA/TX-14/0-6635-1	2. Government Accession No.	3. Recipient's Catalog No.
4. Title and Subtitle Water Quality and Hydraulic Performance of Permeable Friction Course on Curbed Sections of Highways		5. Report Date August 2013; Published November 2014 6. Performing Organization Code
7. Author(s) Laura C. Sampson, Alexandra V. Houston, Randall J. Charbeneau, and Michael E. Barrett		8. Performing Organization Report No. 0-6635-1
9. Performing Organization Name and Address Center for Transportation Research The University of Texas at Austin 1616 Guadalupe Street, Suite 4.202 Austin, TX 78701		10. Work Unit No. (TRAIS) 11. Contract or Grant No. 0-6635
12. Sponsoring Agency Name and Address Texas Department of Transportation Research and Technology Implementation Office P.O. Box 5080 Austin, TX 78763-5080		13. Type of Report and Period Covered Technical Report (November 2010–March 2013) 14. Sponsoring Agency Code
15. Supplementary Notes Project performed in cooperation with the Texas Department of Transportation and the Federal Highway Administration.		

16. Abstract

This paper presents the results of a study on the use of porous overlays on urban highways. Permeable friction course (PFC) is a layer of porous asphalt applied to the top of conventional asphalt highways at a thickness of around 50 mm. The first objective of the study was to determine the impact of porous asphalt on the quality of stormwater runoff on highways with a curb and gutter drainage system. The quality of highway stormwater runoff was monitored before and after the installation of PFC on an eight-lane divided highway in the Austin, Texas, area. Observed concentrations of total suspended solids from PFC were 92% lower than those in runoff from the conventional pavement. Concentration reductions were also observed for nitrate/nitrite and total amounts of phosphorus, copper, lead, and zinc. The data shows that the pollutant reductions on highway sections with curb and gutter are similar to those with a rural cross section. The effect of two different binder compositions was also compared, showing an increase in zinc when recycled rubber is used. The second objective focuses on the drainage capabilities of PFC. While porous overlays can reduce stormwater accumulation on roadways, conveyance capacity at high rainfall intensities is limited. Installing subgrade underdrains within PFC could further improve stormwater conveyance. This research determined the hydraulic profile of runoff as it approached an underdrain with varying flow rates and grades. The results could assist TxDOT in the sizing and configuration of drains based on rainfall intensity and roadway geometry.

17. Key Words Highway Runoff; Permeable Friction Course; Stormwater Management; Water Quality; Drainage Conveyance	18. Distribution Statement No restrictions. This document is available to the public through the National Technical Information Service, Springfield, Virginia 22161; www.ntis.gov.

19. Security Classif. (of report) Unclassified	20. Security Classif. (of this page) Unclassified	21. No. of pages 104	22. Price

Form DOT F 1700.7 (8-72) Reproduction of completed page authorized

THE UNIVERSITY OF TEXAS AT AUSTIN
CENTER FOR TRANSPORTATION RESEARCH

Water Quality and Hydraulic Performance of Permeable Friction Course on Curbed Sections of Highways

Laura C. Sampson
Alexandra V. Houston
Randall J. Charbeneau
Michael E. Barrett

CTR Technical Report:	0-6635-1
Report Date:	August 2013
Project:	0-6635
Project Title:	Water Quality Performance of Permeable Friction Course on Curbed Sections
Sponsoring Agency:	Texas Department of Transportation
Performing Agency:	Center for Transportation Research at The University of Texas at Austin

Project performed in cooperation with the Texas Department of Transportation and the Federal Highway Administration.

Center for Transportation Research
The University of Texas at Austin
1616 Guadalupe, Suite 4.202
Austin, TX 78701

http://ctr.utexas.edu/

Disclaimers

Author's Disclaimer: The contents of this report reflect the views of the authors, who are responsible for the facts and the accuracy of the data presented herein. The contents do not necessarily reflect the official view or policies of the Federal Highway Administration or the Texas Department of Transportation (TxDOT). This report does not constitute a standard, specification, or regulation.

Patent Disclaimer: There was no invention or discovery conceived or first actually reduced to practice in the course of or under this contract, including any art, method, process, machine manufacture, design or composition of matter, or any new useful improvement thereof, or any variety of plant, which is or may be patentable under the patent laws of the United States of America or any foreign country.

Notice: The United States Government and the State of Texas do not endorse products or manufacturers. If trade or manufacturers' names appear herein, it is solely because they are considered essential to the object of this report.

Engineering Disclaimer

NOT INTENDED FOR CONSTRUCTION, BIDDING, OR PERMIT PURPOSES.

Project Engineer: Michael E. Barrett
Professional Engineer License State and Number: Texas No. 82582
P. E. Designation: Research Supervisor

Acknowledgments

This research was funded by the Texas Department of Transportation under project 0-6635. Special thanks to Gary Lantrip of TxDOT. The help of Gary Franklin and the staff at Lower Colorado River Authority in sample processing is greatly appreciated. The project's efforts have been guided by previous work completed by Tina Standard and Brad Eck.

Table of Contents

List of Figures

List of Tables

Chapter 1. Introduction

1.1 Overview

As the populations of cities such as Austin continue to increase, land development is increasing across the United States and throughout the world. This growing trend in urbanization leads to natural land cover being replaced by roadways, sidewalks, parking lots, and other impervious surfaces. These development activities have a large impact on the surrounding watershed. When rainfall is kept from infiltrating into the ground, a greater quantity of runoff with an increased peak flow is produced. The concentration and makeup of pollutants in the runoff are also largely affected by the use of impervious surfaces. Increased flow rates can lead to dangerous driving conditions while pollution entering water bodies can destroy habitats and require expensive restoration. A space and cost-efficient stormwater management system that both provides safer driving conditions and prevents ecological degradation is needed.

As regulations for environmental protection become more stringent, best management practices (BMPs) are being used to reduce the negative impacts of impervious services. The Texas Commission on Environmental Quality (TCEQ) requires that a BMP be implemented to remove 80% of the increases in the total suspended solids (TSS) load created by land development over the Edwards Aquifer Recharge and Contributing Zones (Texas Administrative Code, 2005). The standard practices used to meet requirements in the Austin area include a slow sand filters and vegetated filter strips. These solutions address the need for pollutant management and reduce the peak flow into receiving bodies but do nothing to improve the safety of highways during storms. In addition they require additional right-of-way and can be expensive to construct and maintain.

Permeable friction course (PFC) is being used by the Texas Department of Transportation (TxDOT) to reduce ponding on roadways during storm events. PFC is a bituminous mixture produced with course aggregate that is usually placed at a thickness of 50 mm and has a porosity of about 20% (TxDOT, 2004). The porous PFC overlay is placed on top of an existing impervious concrete or asphalt highway. This design differs from fully porous pavements, which have much thicker pervious layers and are used on parking lots, driveways, and sidewalks rather than highways due to durability concerns.

After installation of PFC, rain that falls on the highway drains into the PFC layer and flows within the pavement, instead of on top of it, toward the edge of the road. By reducing the amount of water on the surface of the roadway, hydroplaning, skidding, splash and spray are all reduced, and visibility is improved (Van der Zwan et al., 1990). These benefits are expected to decrease the number of accidents during rainfall events. In addition to the safety benefits, the porous surface has been shown to absorb and reduce noise pollution, creating quieter neighborhoods (Bendtsen and Andersen, 2005).

In recent years, studies have also shown that PFC can improve the water quality of stormwater runoff. The concentration of pollutants such as TSS, Total Kjeldahl Nitrogen (TKN), nitrate and nitrite, and total and dissolved heavy metals have shown to be reduced in runoff after PFC installation (Ranchet, 1995; Berbee et al., 1999; Pagotta et al., 2000; Barrett et al., 2006; Eck et al., 2012b). Due to this previous research, TCEQ recently approved the use of PFC as a stormwater BMP in Texas on uncurbed roadways. The research in this report monitors the

stormwater quality of runoff from PFC on a highway with curbs and gutters. The results could be used to extend the use of PFC as a BMP for highways located in more urban areas.

While the use of PFC presents many advantages, there are also some concerns. When compared with conventional pavements, PFC has a greater initial cost due to the required high quality course aggregate. The initial cost can be offset if other structural BMPs such as those discussed previously are no longer required, making the safety and noise reduction benefits essentially free. Another concern is that over time the void space can become clogged due to the retention of suspended solids and other pollutants (Fwa et al., 1999). However, some research also suggests that the pore space is effective throughout the design life of the pavement (Eck et al., 2012b). In addition, while PFC improves the safety of driving conditions for many storms, sheet flow can still occur under high rainfall intensities. Along with the water quality monitoring, this research explores the combination of PFC with underdrains to further improve stormwater conveyance.

1.2 Objectives

This research study focused on two main areas of concern for porous overlays. The first objective was to determine whether the stormwater quality benefits associated with use of PFC on rural highways would also be observed on highway sections that include curb and gutter. The second objective was to conduct preliminary tests that could facilitate TxDOT guidance on the spacing and configuration of underdrains, improving stormwater conveyance and reducing standing water on roadways with PFC. The following tasks were required to meet these objectives:

- Survey of other DOTs
- Selection of two sampling sites in the Austin area that met certain of criteria
- Installation of an automatic sampler and flow meter at each sampling site, along with a rain gauge at each unless the selected sites were close in proximity
- Monitoring of sites and collection of runoff samples from storm events over a 2-year period
- Laboratory analysis for each of the collected runoff samples
- Compilation of runoff sample results from laboratory analysis into a database
- Statistical and graphical analysis of results to identify any trends or differences in data
- Identification of a laboratory appropriate material for PFC testing
- Selection of representative underdrain for use with PFC
- Design of small scale testing apparatus with underdrain
- Refurbishing of manometer system for water height measurements
- Method development for accurately measuring water levels within the pavement at various slopes and flow rates
- Identification of trends in hydraulic behavior that will assist future large-scale modeling endeavors

Chapter 2. Literature Review

2.1 Introduction

This chapter summarizes a review of previous literature applicable to the presented research. The first section will provide a background of hydraulic properties of porous media such as PFC. This review will cover research related to flow depth and hydraulic conductivity. The second section includes information on the water quality associated with conventional pavements as well as the limited available published data on water quality benefits of PFC. While data is published regarding the benefits of PFC on rural highways with vegetated strips, no literature was found on the benefits of PFC on curb and gutter sections of highways. The literature presented comes from online journals and articles from around the world, in combination with reports from previous studies conducted by researchers at the Center for Research in Water Resources (CRWR) at The University of Texas at Austin.

2.2 Hydraulic Properties Review

Porous Media Flow

Flow through porous media can be seen as taking one of two forms: linear or nonlinear. Most of the time, flow is modeled linearly using Darcy's Law, which defines a relationship between flow rate and hydraulic gradient (Darcy, 1856). Darcy's Law is the most basic equation used by scientists and engineers to describe flow of fluid through a porous medium. The equation has been transferred into many forms to meet the needs of various applications, but is often written as shown in Equation 1.

$$Q = KIA \qquad \text{(Eq. 1)}$$

where Q is the volumetric flow rate, I is the hydraulic gradient, and A is the cross-sectional area of flow. The variable K represents the hydraulic conductivity, which quantifies how easily fluid flows through the porous medium. Often a negative sign is placed on the right side of the equation to account for the direction of the hydraulic gradient, which is opposite to the natural flow from high to low hydraulic head.

Past studies have modeled flow though PFC as flow through unconfined aquifers (Jackson and Ragan, 1974). In an unconfined aquifer, the lower boundary of the flow region is an impermeable layer and the upper boundary is the water table. Assuming the impermeable base is approximately horizontal, the saturated thickness becomes smaller along the direction of flow and the hydraulic gradient becomes bigger. This allows for the Dupuit-Forchheimer assumptions to be applied to Darcy's Law. The first assumption is that the hydraulic gradient equals the slope of the water table and is proportional to the discharge. Lastly, head is assumed to be independent of depth, meaning the flow lines are only horizontal (Charbeneau, 2000). Evoking these assumptions and integrating Darcy's Law with respect to appropriate boundary conditions leads to a useful form of the Dupuit equation for steady, unconfined flow (Equation 2). (Note that Equation 2 is addressed in more detail in Section 3.7.)

$$Q = \frac{K}{2} * \frac{h_1^2 - h_2^2}{L} * w \qquad \text{(Eq. 2)}$$

The Dupuit equation is only appropriate for linear flows because it is derived from Darcy's Law. While Darcy's Law is applicable for most flow through porous media, nonlinear flow has been observed in past experiments. Nonlinear flow occurs most often at high velocities, but the transition point between linear and nonlinear flow is not well understood. Darcy's Law is valid when the inertial forces within the porous media are negligible compared to the viscous forces. A ratio of the relative importance of inertial effects compared to viscous effects is quantified by the Reynolds number (*Re*) (White, 1999). Equation 3 shows the definition of the non-dimensional Reynolds number as a function of specific discharge (q), fluid viscosity (μ), fluid density (ρ), and a characteristic length dimension (d).

$$R_e = \frac{\rho q d}{\mu} \qquad \text{(Eq. 3)}$$

Depending on the application within fluid mechanics, the length dimension (d) in Equation 3 varies. Pipe diameter is used for pipe flow and the hydraulic radius is used for open channels (White, 1999). However, modeling porous media flow is a bit more complicated due to particle size distribution and non-uniform flow paths. The variety of porous media characteristics has led to a variety of length dimensions throughout the literature. Some researchers use a value proportional to the intrinsic permeability of the medium. Collins (1961) suggests the use of $d = (k/n_e)^{1/2}$, where k is the intrinsic permeability and n_e is the effective porosity. Ward (1964) simplified the equation down to $d = k^{1/2}$. Others believe the length dimension should be based on a representative grain diameter size since the diameter of flow channels between the grains is related to the size of the flow channels. The mean diameter size, d_{50}, is often selected to represent the average flow channel (Bear, 1972). Because of its common use and the ease with which it is determined, d_{50} was selected for this report.

As R_e increases, inertial effects become more important and the flow begins to deviate from Darcy's Law. The exact point at which it begins to deviate is not very clear. Laminar flow is thought to exist until the Reynolds number reaches a value greater than 100. However, even without the presence of turbulence, a nonlinear flow relationship can be established from large microscopic inertial forces or microscopic interfacial drag within the media (Hassanizadeh and Gray, 1987). For coarse-grained media, Bear (1972) suggests that linear flow conditions will exist for a Reynolds number less than some value between 1 and 10 when calculated using the mean grain diameter, d_{50}.

This transitional range was studied and plotted by several researchers (Ergun, 1952; Ward, 1964; Venkataraman and Rama Mohan Rao, 1998). A graph of friction factor versus Reynolds number for porous media was developed by Ward (1964), using experimental data from various mediums such as ion exchange resin and gravel. The results were graphed along with fully laminar and fully turbulent relationships, as seen in Figure 2.1 This graph shows that even flows through porous media that are not turbulent can deviate from Darcy's Law. Despite relatively low specific discharges, non-linear forces will be considered in this research study to account for the inertial interactions observed at low Reynolds numbers by Ward (1964).

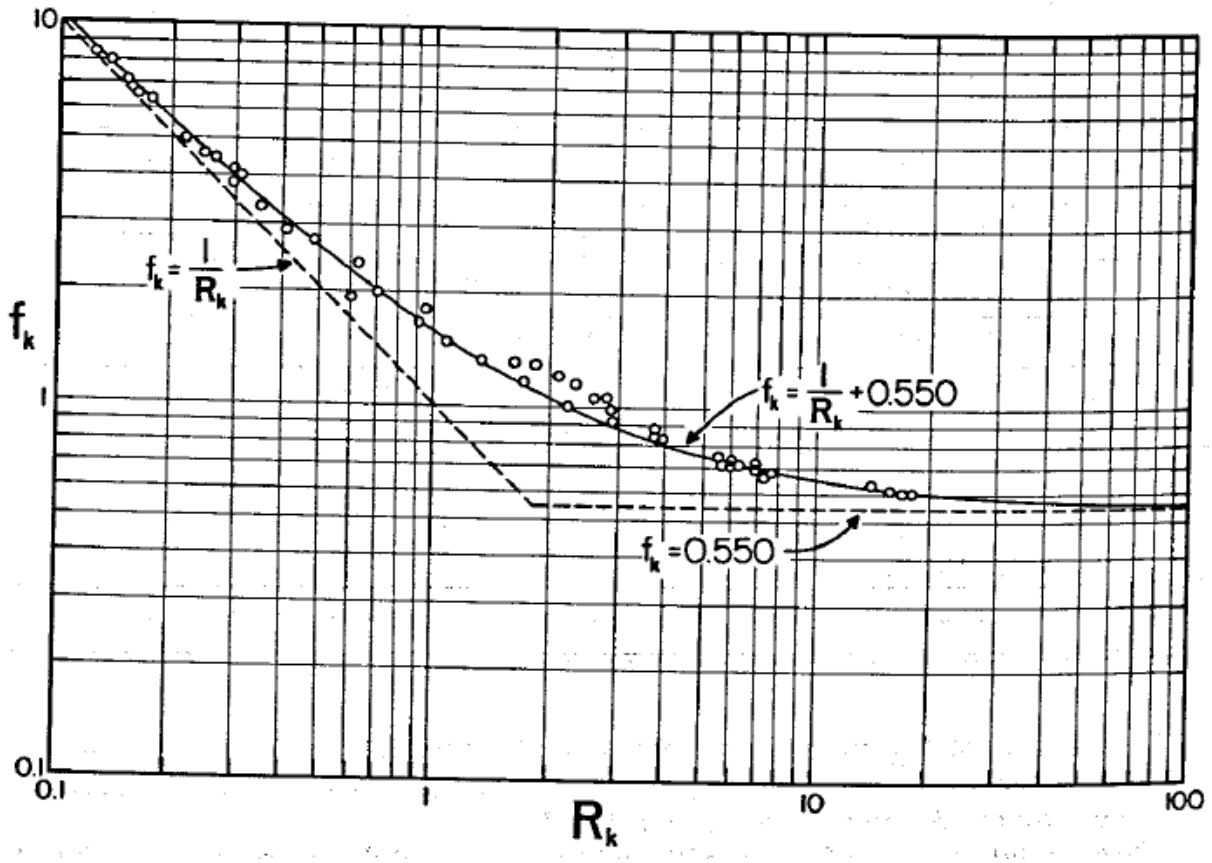

Figure 2.1: Relationship between Fanning friction factor and Reynolds number for single porous media (Source: Ward, 1964)

Eck et al. (2012a) suggested a different system for estimating the validity of Darcy's Law. The proposed method does not compute a porous media Reynolds number; instead the specific discharges obtained through Darcy's Law and a non-linear equation are compared directly. A ratio close to one corresponds to perfect agreement to Darcy's Law. Values lower than one show increasing importance on turbulent effects. This avoids the problem of selecting a length scale, D_p, for which there is no standard. Reynolds number is still widely used throughout the literature and will therefore be utilized in this research.

While Darcy's Law is almost universally accepted for linear flow through porous media, several formulas are used throughout the literature to model non-linear flow. A few authors have written empirical power laws to describe the flow behavior at large velocities (Isbach, 1931; Scheidegger, 1963; Wilkins, 1955). However, these equations assume nonlinear flow for all values of specific discharge and are only valid at large velocities. Another formula suggested by Forcheimer (1901) models the hydraulic gradient as a quadratic equation dependent on specific discharge. The form seen in Equation 4 includes empirical coefficients (α and β) that weigh the importance of inertial and viscous forces (Charbeneau, 2000).

$$I = \alpha q + \beta q^2 \qquad \text{(Eq. 4)}$$

In Equation 4, I is the hydraulic gradient and q is the specific discharge, as in previous equations. The value of α is the linear Forchheimer coefficient and β is the nonlinear Forchheimer coefficient. When linear flow is valid the coefficients will approach values of $\alpha = 1/K$ and $\beta = 0$, making the q^2 term negligible and reducing the Forcheimer equation to Darcy's Law. Since the specific discharges in this study are not high enough to assume non-linear flow, the Forchheimer equation will be used instead of the previously mentioned empirical power laws.

The Forcheimer coefficients (α and β) have been approximated by many researchers in terms of fluid and porous media properties (Ergan, 1952; Ward, 1964; Kovacs, 1981; Kadlec and Knight, 1996). In each approximation, the linear Forchheimer coefficient, α, depends on both the properties of the porous media as well as the properties of the fluid, while the nonlinear Forchheimer coefficient, β, depends only on the properties of the porous medium. Selected approximations were plotted along with experimental PFC data in a study conducted by Klenzendorf (2010). The results show that for a layer of PFC, the Kadlec and Knight approximations are most accurate (Figure 2.2).

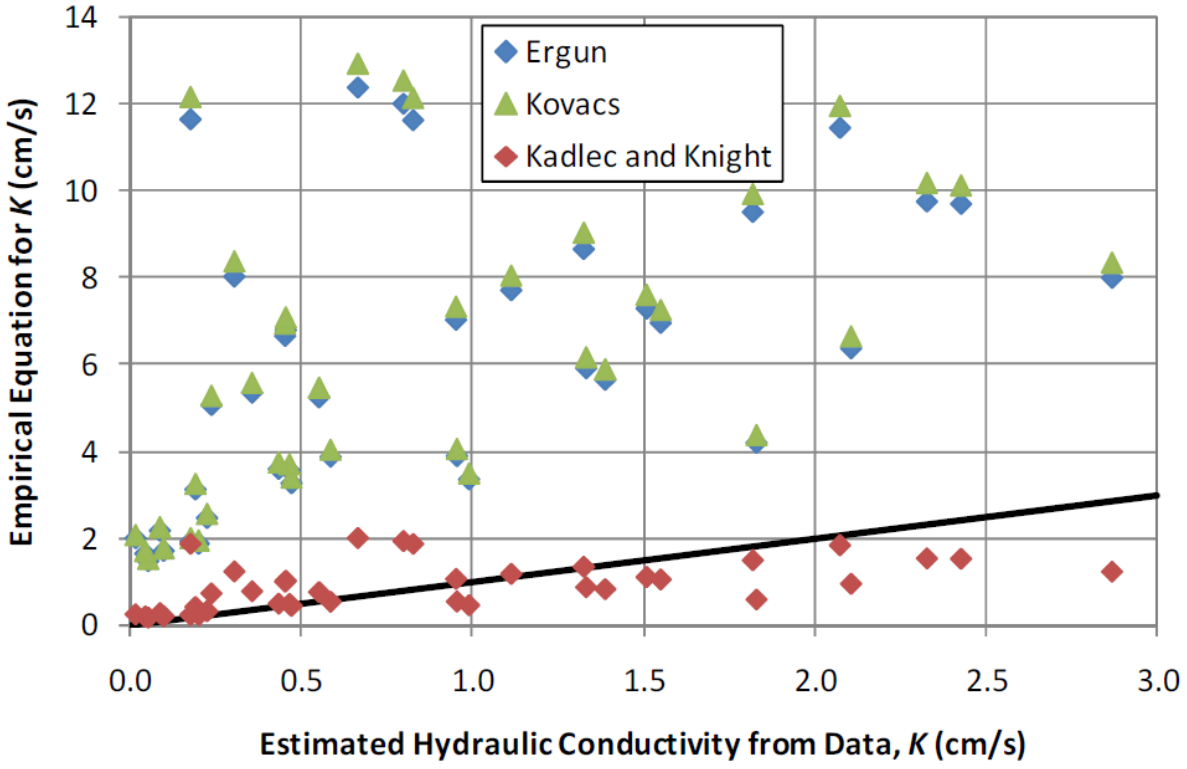

Figure 2.2: Forcheimer coefficient approximations compared with PFC data (Source: Klenzendorf, 2010)

Equations 5 and 6 show the linear and non-linear Forcheimer coefficients (α and β) approximated by Kadlec and Knight (1996) and tested for use with PFC by Klezendorf (2010). This study involves a PFC overlay and will further test the Kadlec and Knight Forcheimer coefficients with Ergun's and Ward's when modeling non-linear flow.

$$\propto = \frac{255\mu(1-n_e)}{\rho g n_e^{3.7} D_p^2} \quad \text{(Eq. 5)}$$

$$\beta = \frac{2(1-n_e)}{g n_e^3 D_p} \quad \text{(Eq. 6)}$$

Water Depth Modeling in PFC

One can model flow within PFC by assuming that it behaves as an unconfined aquifer. Several papers have been published regarding analytical models for water depth profiles within unconfined aquifers on sloping impervious surfaces. These studies address one-dimensional flow conditions under steady state flow with constant rainfall intensity. Darcy's Law and the Dupuit-Forcheimer assumptions have been applied since small hydraulic gradients are expected within the media.

Shallow soil overlying slopping bedrock with uniform accretion and flow is examined by Yates et al. (1985). Water table profiles for several aquifer configurations were found with two different boundary conditions. Heads numerically within 1% were found at various positions when comparing results between the exact solution and the non-linear finite difference and non-linear horizontal solutions. Loaiciga (2005) also derived steady state-water, Dupuit-based water surface equations for unconfined, slopping aquifers. A different method was used in his analysis by taking the hydraulic head approximated by the Dupuit assumptions and linearizing them with a transformed variable to find the equation of the phreatic profile. These studies showed that governing partial differential flow equations could be converted to first-order nonlinear ordinary differential equations in order to mathematically model steady state conditions in an unconfined aquifer.

Some researchers have applied this same analytical process specifically to porous pavement. Ranieri (2002) modeled water depths within a PFC layer to determine the thickness necessary to contain the entire runoff within the pore space. The model was dependent on roadway slope, hydraulic conductivity of the PFC layer, and rainfall intensity. The theoretical derivation utilizes the Boussinesq equation, which is based on Darcy conditions, to model the flow. A laboratory experiment was used to validate the equations. The experimental setup included a uniform rainfall simulator, a basin containing PFC, and piezometers to measure the water depth along the length of the slab. Ranieri noticed non-linear flow within the PFC layer and multiplied the hydraulic conductivity by a new correction factor, defined b^*, to account for deviation from a linear flow regime. The introduced factor was tested for three aggregates at different slopes and rainfall intensities.

Charbeneau and Barrett (2008) expand on the work by Yates et al. (1985) and Loaiciga (2005) by deriving analytic solutions to the governing equations of flow that are specific to PFC. Three ranges of rainfall intensity and a variety of boundary conditions are investigated, leading to the suggested analytic solutions. This work varies from that of Ranieri (2002), in that the issue of saturated PFC flow with the addition of overland sheet flow is addressed. Eck et al. (2012c) continued this work by creating a computer model based on these equations for both saturated and sheet flow within PFC.

Hydraulic Conductivity Measurements

Hydraulic conductivity is an important parameter used throughout all the flow and depth modeling efforts mentioned above. Many studies have been conducted on methods to measure the hydraulic conductivity of porous asphalt mixes due to its importance. Tests have been developed for both field and laboratory applications. Tan et al. (1997) uses a pressure transducer to measure the water depth as it falls through a porous asphalt sample inside a testing apparatus. A one-dimensional hydraulic conductivity is measured based on the non-linear Isbash equation mentioned above. Fwa et al. (1998) applied a similar method to additional materials and tested for both horizontal and vertical hydraulic conductivity. Hydraulic conductivity was tested in all three dimensions by an automatic field permeameter developed by Tan et al. (1999). A correction factor was also developed from a finite element model to calculate an effective isotropic hydraulic conductivity from the three-dimensional data.

Other devices have also been developed for use in the field calculation of drainage capacity. Many of these methods utilize a falling head test. Isenring et al. (1990) describe a field test developed by the Switzerland Institute of Technology called the IVT permeameter. The IVT permeameter is composed of a vertical pipe that is placed on the porous asphalt surface and sealed with putty at the base. A falling head test is conducted with 2.27 liters of water and the time elapsed is used to express drainage capacity. Texas uses a procedure detailed by TxDOT (2004). The field parameter is similar to the IVT permeameter. Rubber clamps are used to keep water from flowing around the pavement and a pipette is introduced as a timing device. The drainage capacity is reported as the time to drain 5.1 L of water.

Another falling head test device was designed at CRWR and described in Klenzendorf (2010). The apparatus consists of a 22.9 cm solid metal base plate with a 5.1 cm centered standpipe. A layer of vacuum grease is placed on the bottom side of the base plate to create a no flow boundary along the surface of the plate instead of using putty on the standpipe.

Porous Pavement with Underdrains

Jackson and Ragan (1974) were among the first to model flow through an entirely porous pavement. They concentrated on flow through the base course some distance below the impermeable pavement, rather than on water depth within the pavement. Darcy flow conditions were assumed and numerical solutions to the Dupuit-Forchheimer assumptions were developed. Jackson and Ragan used an explicit central difference scheme (CDS) finite difference model to solve the Boussinesq equation for a pavement with zero slope. It was found that peak discharge entering the drain could be related to hydraulic conductivity, effective porosity, rainfall intensity, and total storm volume. They determined that the relationships developed between flow and drain efficiency could be used for the design of spacing. The underdrains studied in this research differ from the ones of concern to Jackson and Ragan because they are installed in channels directly below the permeable pavement rather than in the configuration seen in Figure 2.3.

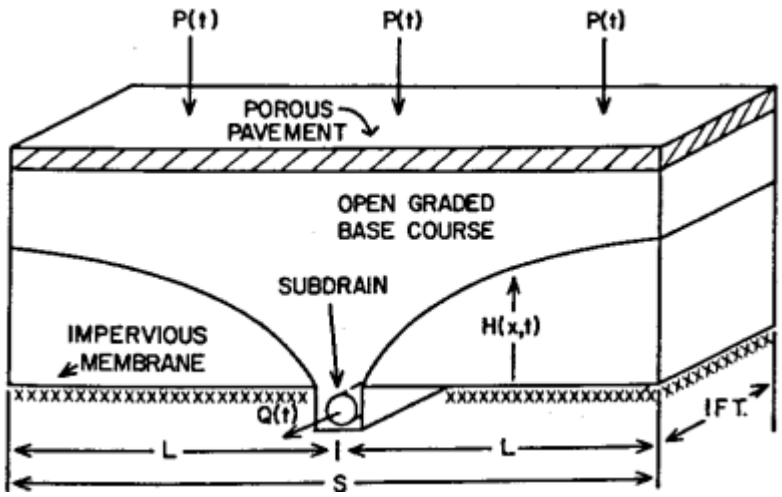

Figure 2.3: Subdrain within base course

Charbeneau and Barrett (2008) developed mathematical solutions based on rainfall intensity, PFC hydraulic conductivity, roadway slope, and maximum drainage path length for cases when the PFC drainage capacity is exceeded. The results provide both the estimates of the maximum drainage depth within the PFC and the maximum depth of sheet flow on the surface. The model equations presented can be used to calculate the necessary spacing between underdrains for controlling ponding runoff.

2.3 Water Quality Review

Permeable Friction Courses

The original purpose of porous pavement was enhanced highway safety and noise reduction. The water quality benefits are more recently becoming understood and appreciated. Therefore, less literature concerning the water quality impacts of porous pavements is available compared to what is written on drainage capacity and hydraulic conductivity. Even less is available regarding the water quality impacts along highways, since porous pavements were used more frequently on parking lots and rural roadways in the past.

Many of the initial investigations on the water quality of runoff from porous pavements were conducted in Western Europe. Stotz and Krauth (1994) analyzed runoff from a 40 mm thick porous asphalt section in Germany over the course of a year. Yearly pollutant loadings from impervious highway runoff in a previous study were used for constituent comparison. A reduction in the filterable solid loads of 50% was found. The authors also found a seasonal difference in the pollutant concentration, which could be attributed to winter maintenance.

In France, Ranchet (1995) investigated the impact of a porous overlay on runoff quality over a period of 2 years. The research was conducted at both an urban site and a divided freeway. At the urban site, runoff from both a PFC section and an impervious stone-matrix section were sampled and tested for contaminants. An 87% reduction in lead was seen at the urban site. At the freeway site, samples were taken and compared from both a conventional pavement section and a PFC overlay. A 62 and 67% reduction in total copper and total zinc respectively was found. TSS was less affected, with a reduction of only 7%. The reduction values in this study are lower than many later studies; this may be due to the orientation of the freeway, as the wind is likely to

transfer pollutants from the impervious lanes onto the pervious asphalt pavement at the test location.

Berbee et al. (1999) also compared runoff water quality from a 50 mm thick overlay and a conventional pavement surfaces in the Netherlands. The highways were similar, although more traffic was present on the porous overlay section. Runoff was collected in a gutter over 1-week periods and then analyzed for pollutant concentrations. The results showed significantly higher reductions in pollutant concentrations than the study conducted by Ranchett (1995). TSS concentrations were 91% lower, TKN 84% lower, and heavy metals ranged from 67 to 92% lower than in runoff from the conventional asphalt pavement.

The ability of porous asphalt overlays to retain heavy metals from runoff was investigated by Legret et al. (1999). Highway runoff containing heavy metals was sprayed over asphalt cores that had been clogged in the laboratory. The heavy metals were assumed to have been retained by the clogging material particles after rainfall simulations. Another French highway was studied by Pagotto et al. (2000). Runoff was collected and tested for contaminants before and after the placement of a 30 millimeter thick porous overlay. This study examined both total and dissolved metals. TSS was reduced by 81%, total metals were reduced between 33 and 78% and dissolved metals were reduced between 16 to 61%. Pagotta et al. (2000) assumed that the removed solids were physically filtered out and contained in the pore space of the pavements. The dissolved metal species were assumed to have adsorbed onto the pavement.

In recent years, US agencies have started to appreciate the potential that porous overlays offer as a water quality BMP. Research has started to be conducted in the United States to evaluate the effectiveness of PFC in this role. Eck et al. (2012b) collected water quality measurements for PFC and conventional pavement over 6 years near Austin, Texas, and 2 years in eastern North Carolina. The results in Texas are consistent with those from North Carolina, and both are consistent with the earlier studies from France, the Netherlands, and Germany. Concentrations of TSS were reduced by more than 90% and the heavy metals were also reduced significantly. Because the pavement in Austin was tested recently after installation and the North Carolina data was for a pavement up to 10 years old, the research shows that the water quality benefits of PFC can last through the typical design life of asphalt pavement. The expectation of stormwater quality benefits from PFC is somewhere between 8 and 10 years (NCHRP, 2009).

PFC overlays have been used throughout the world for a variety of uses, and the popularity is growing. The studies mentioned above were conducted in different countries, with various pavement mixes and under different highway design conditions. However, they all concluded that PFC provides a reduction in TSS and total metals compared to conventional asphalt pavement. A summary of pollutant concentrations from the literature noted is shown in Table 2.1.

Table 2.1: Summary of Pollutant Reduction in Literature

Constituent	Conventional Asphalt	PFC	Reduction Percent
TSS (mg/L)	46.0–222.0	6–18	81–94
TKN (mg/L)	1.10–2.11	0.64–1.2	10–67
Total Copper (µg/L)	24–30	6.8–20	33–75
Dissolved Copper (µg/L)	5.94–16	5.0–16	-77–24
Total Lead (µg/L)	11–40	0.9–8.7	78–93
Dissolved Lead (µg/L)	< 1.0	< 1.0	NA
Total Zinc (µg/L)	130–228	21–77	66–86
Dissolved Zinc (µg/L)	18–140	11–54	34–61

Curb and Gutter Sections

Most studies conducted on urban PFC occurred on highways with vegetated shoulders. While no research was found concerning PFC on curbed section, past studies suggest that pollutants can build up on the roadside and affect water quality in the presence of curbed sections. Stotz (1987) conducted research on three German highways, two with an impermeable system of curbs and sewers and one that included a catchment area drained through grass-covered ditches. Stotz concluded that drainage methods were more important than pavement type in determining the quality and quantity of highway runoff.

Other researchers came to similar conclusions when investigating stormwater runoff from traditional pavements. Sartor and Boyd (1972) found that the highest concentration of solids is in the gutter since the curb forms a barrier to any particles moving transversely. Likewise, Burch et al. (1985) suggested that without curbs, wind and turbulence was likely to remove much of the fine materials from the road. One goal of this research is to determine if curbs and gutters negatively affect pollutant removal by PFC.

Chapter 3. Materials and Methods

This chapter starts by addressing the setup, procedures, and analysis for the stormwater quality monitoring study. The second section focuses on the design and operation of the hydraulic modeling apparatus and underdrain testing for PFC.

3.1 Survey

A survey was conducted to determine how states are currently using PFC. The Department of Transportation (DOT) for each state was contacted either through email or by phone and asked if they used PFC on curbed surfaces and if so to what extent. A follow-up question was asked to determine whether the placement goes all the way to the curb, just to the edge of the gutter, or terminates near the edge of the traveled lane. The contacts for each DOT are shown in Appendix A.

3.2 Stormwater Sampling Locations

An analysis of stormwater runoff from conventional asphalt at the 35th Street overpass along the Mopac freeway was reported by Barrett et al. (1998). The two PFC sites selected for this study are located a few blocks north of the previous conventional asphalt study: between 35th and 45th Streets in Austin, Texas. Mopac is a highway with a curb and gutter section that was paved with a 1.5 in. thick PFC overlay in 2010. Different asphalt binder mixtures were used on the north and southbound lanes. This gives us the option to compare the water quality results from mixtures with different compositions and hydraulic conductivities. A satellite image of the sites is presented in Figure 3.1.

The sites were located off of exit lanes and the equipment was kept inside the fence lines of government facilities providing safe storage and accessibility. Monitoring equipment was installed and sampling began in November 2010 for both PFC sites. Runoff rates were recorded within the gutters and flow-weighted water quality samples were collected using an automated sampler. An ISCO 4230 Bubbler Flow Meter monitors the depth of water runoff in the gutter and calculates the corresponding flow rate every minute. The data is stored within the flow meter and is downloaded to a computer using ICSO Flowlink software.

Runoff samples are collected just upstream of the flow meter using an ISCO 3700 Portable Sampler. A peristaltic pump draws samples through a Teflon suction line and into a 10L Nalgene bottle. The gutter setup at Camp Mabry is shown in Figure 3.2. A stainless steel strainer is attached to the end of the suction line to keep debris from clogging the system. The bubbler flow meter and automatic sampler are within a locked storage box onsite. A solar panel on top of the box and a 12-volt marine battery within the box power the equipment. All tubing and wires from the equipment to the storage box are covered with conduit for protection. Camp Hubbard's equipment is shown in Figure 3.3. Rainfall data is sent to the flow meter from an ISCO 674 tipping bucket rain gauge located only at the Camp Hubbard site.

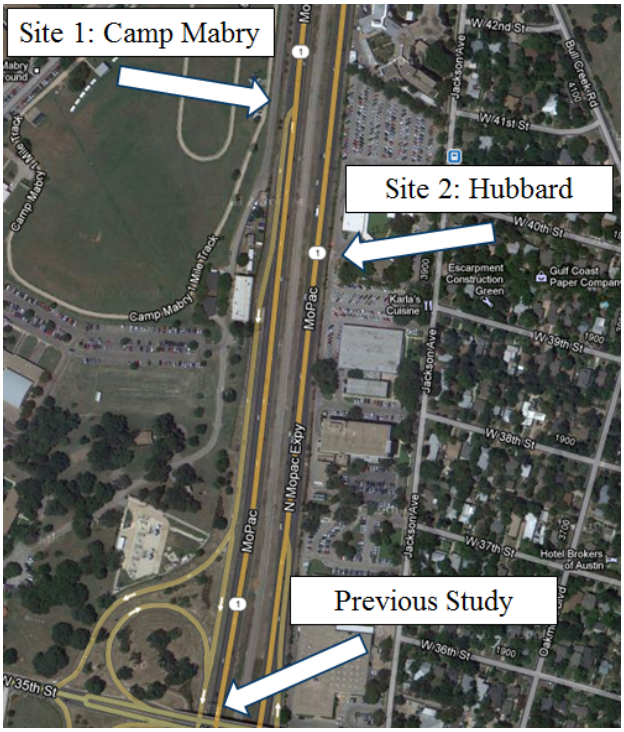

Figure 3.1: Satellite image of sites on Mopac (Google Maps, 2013)

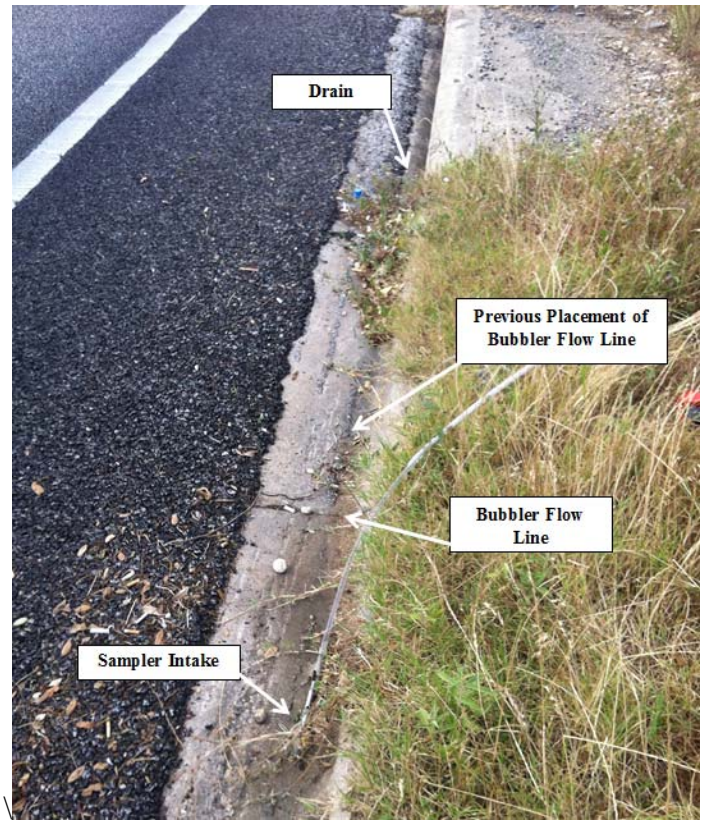

Figure 3.2: Gutter collection system

Figure 3.3: Storage box containing flow meter and sampler

3.3 Mixture Comparison and Permeability

The northbound lanes of Mopac are paved with an asphalt-rubber binder (A-R Binder), and the southbound lanes use a performance graded binder (PG 76). A-R mixtures use smaller aggregate sizes than do PG 76 mixtures as Table 3.1 indicates. A-R binders also require a minimum of 15% crumb rubber modified and in general costs more than the PG 76 binders (TxDOT, 2006).

Table 3.1: Percent Passing by Weight or Volume and Binder Content (Rand, 2006)

Sieve Size	PG 76 Mixtures	A-R Mixtures
¾”	100.0	100.0
½”	80.0–100.0	95.0–100.0
3/8”	35.0–60.0	50.0–80.0
#4	1.0–20.0	0.0–8.0
#8	1.0–10.0	0.0–8.0
#200	1.0–4.0	0.0–4.0
Binder Content, %		
	5.5–7.0	8.0–10.0

Some of the aggregate used on the northbound lanes was of poor quality. Figure 3.4 shows the coring sample taken from the exit lane of the northbound lanes of Mopac. The sample shows compaction and fracturing of the "B" aggregate, which results in rutting of the roadway surface.

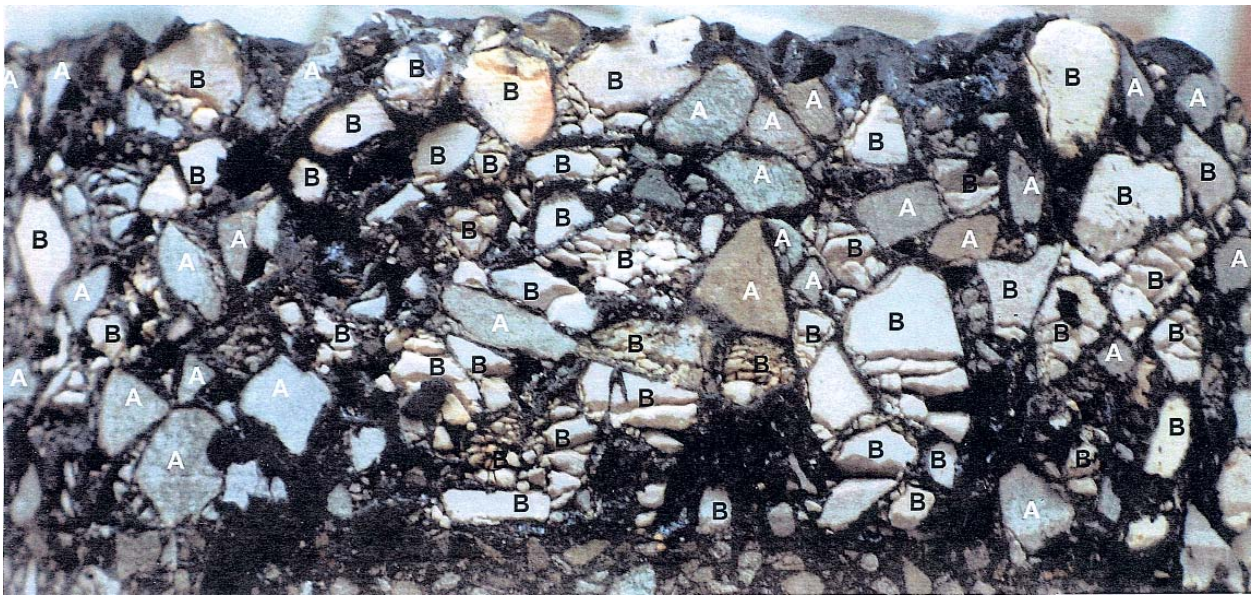

Figure 3.4: Coring sample from the northbound lanes of Mopac

On November 5, 2010, permeability tests were conducted at Camp Mabry and Camp Hubbard. A falling head test was performed in situ, and the procedure that was followed is provided in Klenzendorf et al. (2012). Both test locations were in the right hand traffic lane. TxDOT provided traffic control. Three tests were conducted at each location with the average of the time measurements used to compute the hydraulic conductivity.

3.4 Rating Curves

The flow rate was programmed according to the depth of the water measured in the gutter. The rating curve took some time to develop and is shown in Figure 3.5 for Camp Mabry. Manning's equation was initially used to predict flow rate as a function of water depth in the gutter; however, the resulting runoff volumes differed substantially from the rainfall volume. Generally Manning's equation works well, but the exact slope of the road was unknown and the runover of PFC into the gutter caused problems predicting the Manning's roughness coefficient. PERFCODE (Eck et al., 2012c) was then used to develop a rating curve by plotting the modeled flow against the measured level. This method proved to work and produced runoff coefficients that were acceptable.

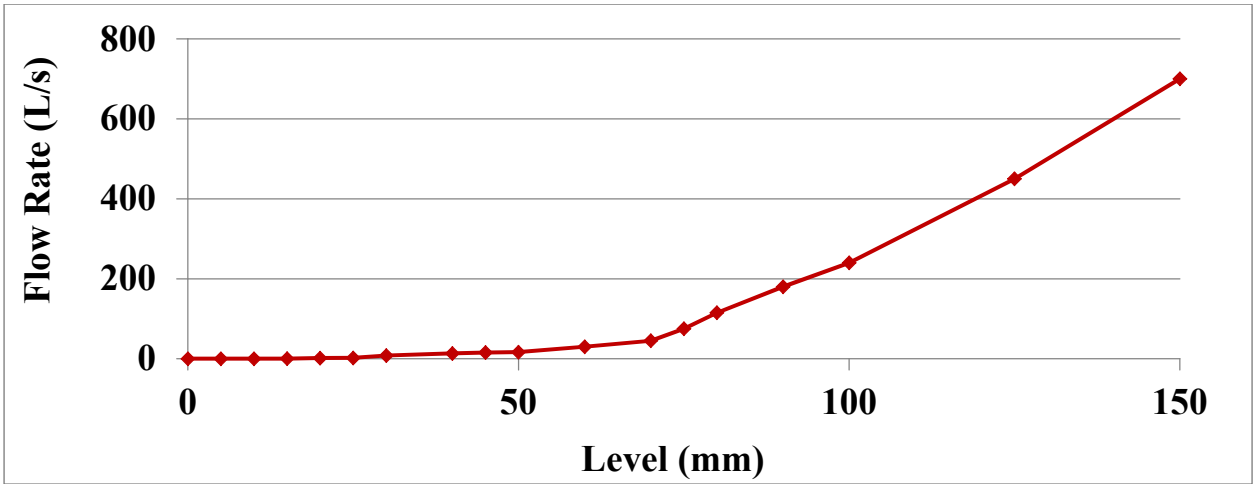

Figure 3.5: Rating curve for Camp Mabry site

The volume pacing for sample collection at Camp Mabry was programmed according to the estimated catchment area and the minimum design storm. Ten aliquots of 320 mL were chosen for the minimum design storm.

$$\text{Road width} = 18.28 \text{ m}$$

$$\text{Estimated catchment area} = 18.28 \text{ m} \times 150 \text{ m} = 2742 \text{ m}^2$$

$$\text{Minimum storm size} = 0.25 \text{ in}$$

$$\text{Minimum runoff volume} = 0.25 \text{ in} \times \frac{1 \text{ m}}{39.4 \text{ in}} \times 2742 \text{ m}^2 = 17.4 \text{ m}^3 = 17412 \text{ L}$$

$$\text{Volume of runoff per aliquot} = \frac{17412 \text{ L}}{10 \text{ aliquots}} = 1741 \frac{\text{L}}{\text{aliquot}}$$

The largest storm that could be sampled would be 53,976 liters—0.78 inch storm.

As with the Camp Mabry site, Manning's Equation was originally used to relate the depth and flow rate at Camp Hubbard, but once again this proved to not describe the relationship well. PERFCODE was once again used to develop the rating curve for the site. Figure 3.6 provides the rating curve for Camp Hubbard.

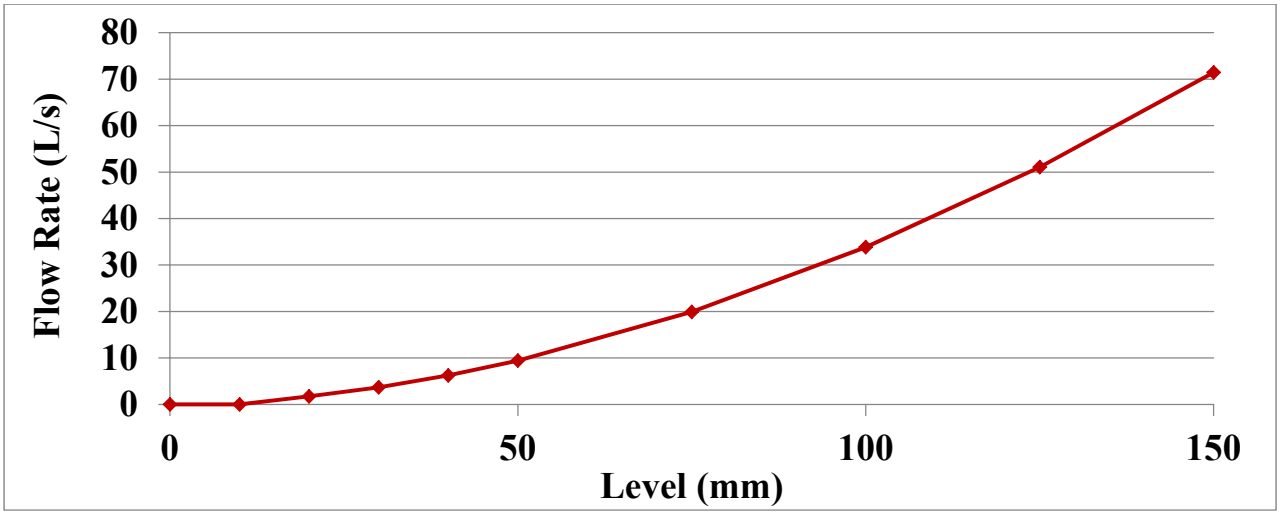

Figure 3.6: Rating curve for Camp Hubbard site

The volume of runoff that passes through the gutter at Camp Hubbard was used to pace the sampler. The volume pacing was programmed according to the estimated catchment area and the minimum design storm. Ten aliquots of 320 mL were chosen for the minimum design storm.

$$\text{Road width} = 16\ \text{m}$$
$$\text{Estimated catchment area} = 16\ \text{m} \times 105\ \text{m} = 1680\ \text{m}^2$$
$$\text{Minimum storm size} = 0.25\ \text{in}$$
$$\text{Minimum runoff volume} = 0.25\ \text{in} \times \frac{1\ \text{m}}{39.37\ \text{in}} \times 1680\ \text{m}^2 = 10.67\ \text{m}^3 = 10668\ \text{L}$$
$$\text{Volume of runoff per aliquot} = \frac{10668\ \text{L}}{10\ \text{aliquots}} = 1067\ \frac{\text{L}}{\text{aliquot}}$$

The largest storm that could be sampled would be 33,077 liters—0.78 inch storm.

3.5 Sampling Procedures

Clean sampling containers are placed in each sampler between storms, the equipment is reset, and debris is removed from the rain gauge. The day before an expected storm, an air blower is used to clear the gutter both upstream of the equipment to prevent flow obstruction, and downstream to prevent ponding. The tubing and strainer are checked and re-secured in the correct location if necessary. During storms, the sites are observed if possible and maintenance is performed to fix any problems.

After a storm event, lids were placed on the collected samples and the containers were exchanged. Post-collection, the samples were taken to the Lower Colorado River Authority lab in Austin for analysis. If the lab was closed, the samples were stored at CRWR in a 4°C room and delivered as soon as the lab was open. Table 3.2 contains the parameters and methods used by the lab for analyzing the samples. The practical quantification limit (PQL) represents the minimal limit at which concentrations can be accurately quantified. Concentrations less than these amounts are not detected and replaced with the PQL in the compiled data.

Table 3.2: Parameters and Methods

Parameter	Units	Method	Practical Quantification Limit
Total Suspended Solids	mg/L	E160.2	1.0
Total Kjeldahl Nitrogen (TKN)	mg/L	E351.2	0.40
Nitrate and Nitrite as N (NO_3+NO_2)	mg/L	E353.2	0.04
Total Phosphate as P	mg/L	E365.4	0.02
Dissolved Phosphate as P	mg/L	E365.4	0.02
Chemical Oxygen Demand (COD)	mg/L	E4104.4	7.0
Total Copper (Cu)	µg/L	E200.8	2.00
Dissolved Copper	µg/L	E200.8	1.02
Total Lead (Pb)	µg/L	E200.8	1.00
Dissolved Lead	µg/L	E200.8	1.02
Total Zinc (Zn)	µg/L	E200.8	5.00
Dissolved Zinc	µg/L	E200.8	4.08

3.6 Analytical Analysis

The water quality data from both the Camp Mabry and Camp Hubbard sites were compared to the data reported by Barrett et al. (1998) from Mopac. A Mann-Whitney test was conducted since the two groups are independent. The Mann-Whitney test was also selected over the two sample t-tests assuming unequal variance because it is nonparametric and avoided assumptions regarding the distribution. A confidence interval of 95% was used for this research, requiring a p-value less than 0.05 to indicate statistical significance. Observations below the reporting limit were replaced with the detection limit for all statistical procedures. This provides a conservative estimate of the differences between medians and minimizes the chances of detecting a significance that does not exist (Type 1 Error).

One focus of this study was to compare the water quality impacts of the two mix designs used at the sampling sites. Camp Mabry uses a PG 76 binder, and Camp Hubbard uses an A-R. A statistical comparison was also conducted between these two groups to determine if there was any significance between the water qualities at the two sites. The Wilcoxon signed rank test was selected for this analysis since the samples were paired. This test is also nonparametric and used a confidence interval of 95%.

The effect of a curb and gutter on PFC efficiency was evaluated by comparing the reductions of contaminants between this study and the previous Texas PFC study published by Eck et al. (2012b), which was conducted on uncurbed sections of Highways 360 and 620. Reductions for individual constituents were calculated for each of the five test sites based on the median concentration for the PFC and the corresponding conventional control. Median was selected over mean because it is a more robust parameter that minimizes the importance of extreme values. The pollutant reduction values were also compared to the reductions observed by the current standard BMP used in Austin, the slow sand filter.

3.7 Laboratory Aggregate Selection

In order to accurately model real-world conditions, the pavement used in the laboratory hydraulic experiments needed to exhibit properties similar to those of the pavement currently installed on Mopac. A standard PFC aggregate mix was obtained from Century Asphalt (Mix A) in San Antonio and tested along with a commercial mix from the company Porous Pave. The Porous Pave mix is 50% rubber chips and 50% coarse rock. Figure 3.7 shows the gradations of the two mixes plotted along with the upper and lower limits of the mixes used by TxDOT on the Mopac test sections. The grain sizes of the Porous Pave and Mix A aggregates fall within the ranges of those in the TxDOT specifications suggesting the porosities are similar.

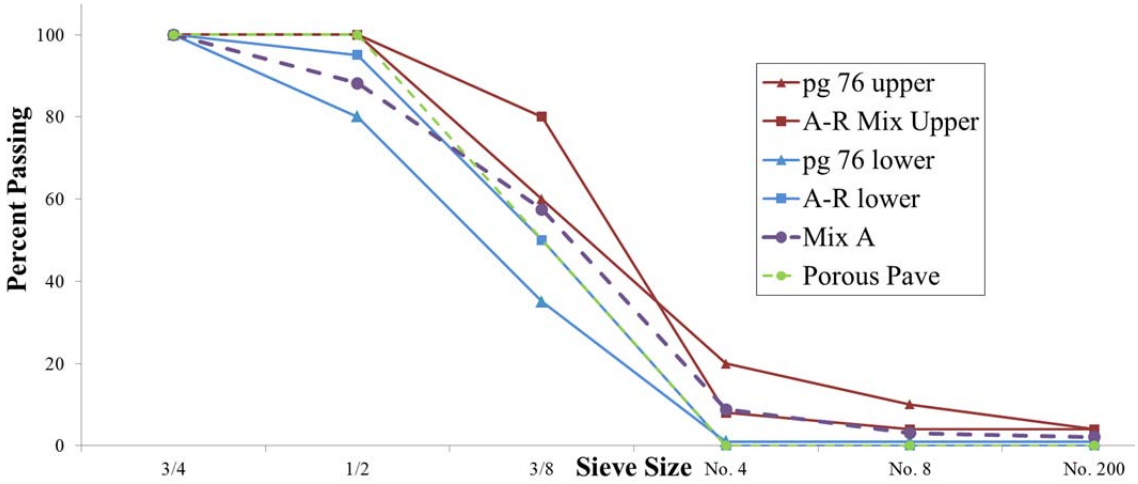

Figure 3.7: PFC gradation comparison

Working with hot asphalt indoors can be difficult and dangerous. Anderson et al. (1998) used a slow curing epoxy instead of asphalt binder to study the drainage of pavements. Liquid nails and epoxy were used as alternative binders on test slabs with Mix A. The Porous Pave Test slab was mixed with a polyurethane binder that came with the aggregate.

The slabs were tested to determine which combination of aggregate and binder had a hydraulic conductivity that most resembled the pavement on Mopac. The testing apparatus was an 18 in. by 24 in. box with reservoirs at the upstream and downstream ends of the pavement. Various flow rates were applied to the slabs using a peristaltic pump. The heads at both ends of the pavement were recorded using tape measurers. A weir was placed at the downstream end of the box to prevent sheet flow from occurring and petroleum jelly was applied to the edges of the box to minimize short-circuiting. The setup can be seen in Figure 3.8.

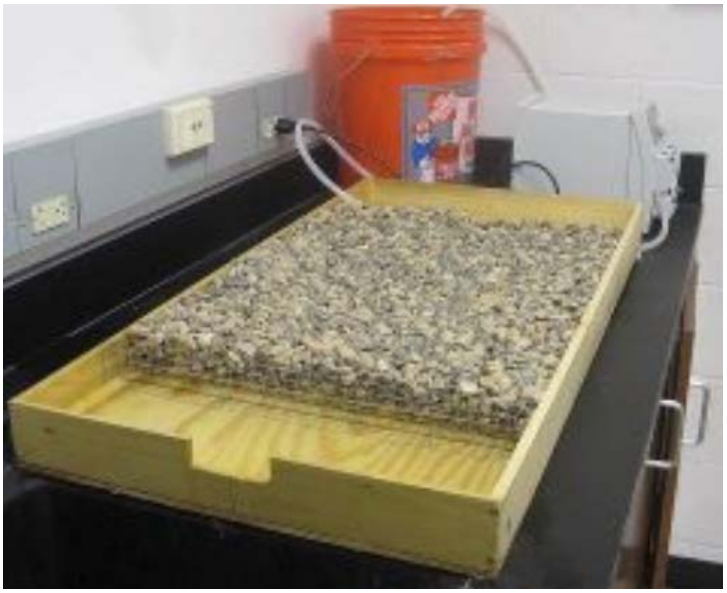

Figure 3.8: Hydraulic conductivity tests

The data gathered from the experiment was used in combination with the Dupuit equation shown in Equation 2 (originally shown in Chapter 2) to find the hydraulic conductivities of the various materials. Varying flow rates were run as triplicates for each slab. Table 3.3 provides the values determined.

$$Q = \frac{K}{2} * \frac{h_1^2 - h_2^2}{L} * w \qquad \text{(Eq. 2)}$$

Where:
Q = Flow Rate
H1= Upstream Head
H2= Downstream Head
L = Length (24 inches)
w= Width (18 inches)
k= Hydraulic Conductivity

Table 3.3: Hydraulic Conductivity results

	Mix A		**Porous Pave**
RPM	**Epoxy**	**Liquid Nails**	**Polyurethane**
600	22.51	8.24	6.10
400	22.22	9.16	6.46
200	19.07	8.91	6.97
Average k (in/s)	**21.27**	**8.77**	**6.51**

The resulting hydraulic conductivities were higher than expected, which could be due to the lack of compaction and potential for short circuiting. The Porous Pave/polyurethane combination was selected for the experiment since it exhibited the hydraulic conductivity closest to the two conductivities observed on Mopac.

3.8 Hydraulic Apparatus Design

An apparatus was constructed to run the hydraulic analysis on the PFC and underdrain combination. The frame consisted of an 8 ft. x 1 ft. wooden box to hold the pavement with 6 in. reservoirs at both ends. A 5 in. wide underdrain was installed two-thirds of the way down the PFC segment. A PVC pipe was cut horizontally in half and connected to the drain to collect the runoff. Polyurethane sealant was used to treat the wood and the joints were filled with silicone for waterproofing. The Porous Pave mix was installed 2 in. thick directly inside of the box and on top of the underdrain. A hole was drilled into the bottom of the downstream reservoir to allow for drainage of runoff that bypassed the underdrain. The described setup appears in Figure 3.9.

Figure 3.9: Initial setup with and without PFC overlay

To provide various flow rates to the system, tubes connecting three sinks in the lab were installed in the upstream reservoir along with a peristaltic pump for fine tuning. One side of the PVC drain channel was closed off with a rubber end cap and a bucket was placed below the second end to collect the flow. The influent end of the peristaltic pump was placed in the bucket to recycle some of the flow and the rest was piped to a nearby floor drain during operation. Figure 3.10 shows the final operational setup.

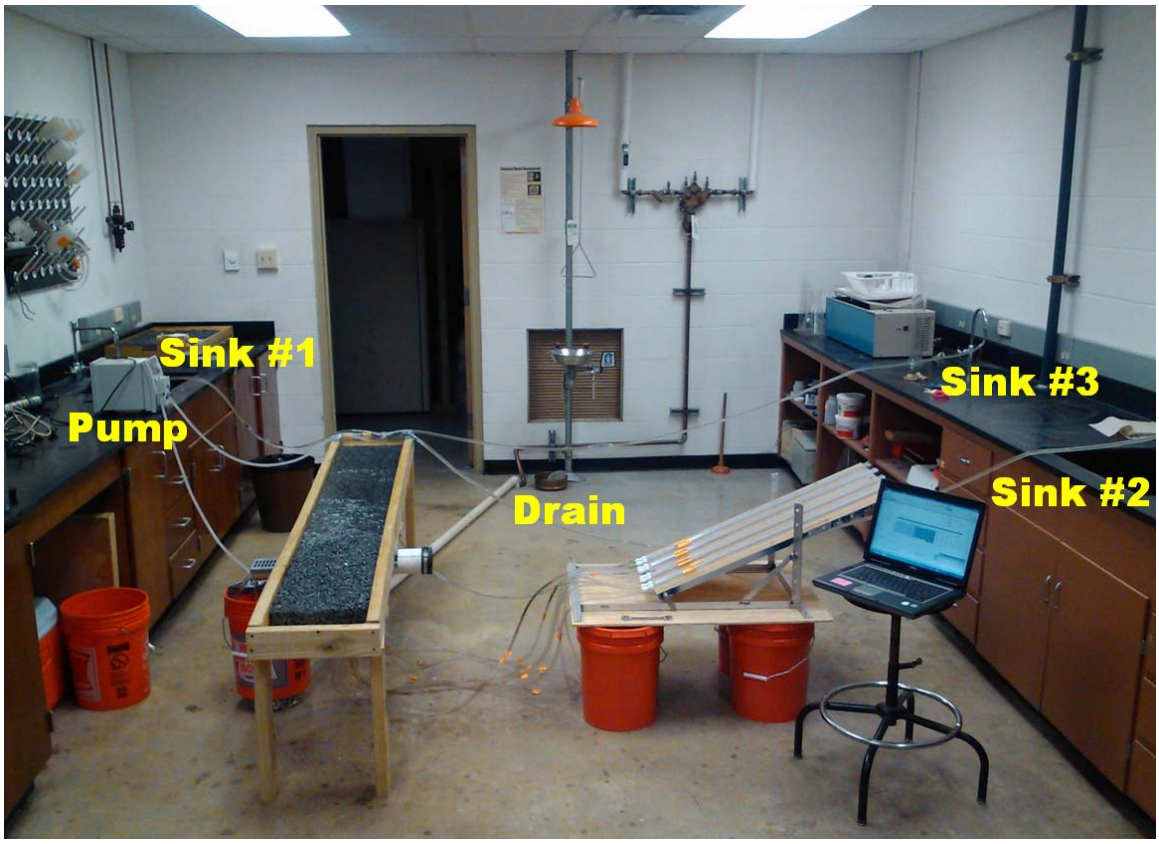

Figure 3.10: Operational sinks, pumps, and drains

A system of manometers was installed to monitor the water surface at various points within the pavement. The eight manometers were originally spaced logarithmically from the drain since the water height was expected to drop off exponentially approaching the drain. Holes were drilled into the bottom of the box and metal ports were hammered in at each sampling location. A connecting piece that was sealed into the monometer tubes could then screw into the ports or be moved to a new sampling location and replaced with a plug of the same size. This allowed for more data points to be collected than the original eight chosen locations. The final manometer locations are presented in Table 3.4. The tubes rested on a manometer board that could be adjusted to various angles for increased accuracy in the readings. A measuring tape was also placed at the upstream edge of the pavement to confirm the first value and calibrate the system. During operation the board was placed at an angle of 24.8 degrees. Figure 3.11 presents the ports and board.

Table 3.4: Manometer Locations

Manometer	Distance upstream of Drain (cm)
(Ruler)	143
7	88
2	46
8	25
3	14
4	8
5	6
6	1
1	6 (Downstream)

Figure 3.11: Manometer port and board

3.9 Apparatus Operation and Testing

During operation for all tests, water from the various sinks and the pump filled the upstream reservoir which then flowed through the pavement into the drain. During some experiments water also flowed on top of the pavement and reached the downstream reservoir. The experiments were run at each flow rate of interest until the system reached steady state and the manometer readings held constant. Baseline readings without flow were also taken at each slope before experimentation proceeded. Manometer readings were entered into Excel and converted into head data for all analysis.

Water surface profiles were modeled at slopes of 0%, 1.5%, and 2.5% to cover the range of typical PFC grades. The water depths were calculated in Excel by subtracting the baseline manometer readings at zero flow from the readings at each flow rate. The experiment was repeated at constant slope with increasing flow rates until the sheet flow carried over past the drain. The first flow rate to overload the drain was recorded along with the bypass flow rate to examine how drain efficiency changes with slope.

The apparatus was also used to determine if the flow was better represented by a linear model or a non-linear model. Hydraulic conductivities at different sections of the pavement were calculated and compared using various flow approximation equations. Hydraulic conductivity was analyzed at a slope of zero to meet the assumption of the Dupuit equation. The conductivity was also measured at a smaller flow rate that did not produce sheet flow. The pump was operated at 600 RPM, providing a flow rate of 35 cm^3/s. The furthest upstream manometer within the PFC overlay (#7) was used for the upstream head. The three manometers directly downstream of #7 were used as downstream heads in the analysis (#2, #3, #8).

Hydraulic conductivities from the Dupuit equation, which is derived from Darcy's Law, was used to test the linear model. Hydraulic conductivity was also analyzed using the Forcheimer equation for non-linear flow shown below (Equation 7). Porosity and gradation information was gathered from the supplier and used in conjunction with three different approximations for the linear (α) and non-linear (β) Forcheimer coefficients.

$$K = \frac{2Lq(1+\frac{q}{n})}{(h_1^2 - h_2^2)} \qquad \text{(Eq. 7)}$$

Where: n=α/β

While many coefficient approximation equations exist in the literature, they vary mostly in the extent that effective porosity (n_e) is taken into account. The coefficients used in the analysis are presented in Table 3.5. Using these equations, three non-linear models and one linear model were compared.

Table 3.5: Forcheimer Coefficients

Coefficient	Kadlec & Knight	Ergun	Ward
α	$\frac{255\mu(1-n_e)}{\rho g n_e^{3.7} D_p^2}$	$\frac{150\mu(1-n_e)^2}{\rho g n_e^3 D_p^2}$	$\frac{360\mu}{\rho g D_p^2}$
β	$\frac{2(1-n_e)}{g n_e^3 D_p}$	$\frac{1.75(1-n_e)}{g n_e^3 D_p}$	$\frac{10.44}{g D_p}$

Chapter 4. Results

This chapter will first discuss the results of the study, including the DOT survey, water quality data, and hydraulic modeling. The water quality evaluation will include an analysis of the compiled concentrations of all 12 constituents for each storm along the PFC test segment of Mopac. In addition, the water quality comparison between the conventional pavement and the new data is presented along with an analysis of the effect of binder composition and curb type. The removal efficiency is also compared to that of the current BMP standard: the Austin slow sand filter. The results of the hydraulic modeling study are presented later in the chapter. The hydraulic gradients for various slopes and flow rates are discussed in terms of trends that could assist future modeling efforts. The hydraulic conductivities calculated by each of the four flow equations mentioned earlier are used to discuss the applicability of Darcy's Law.

4.1 Survey Results

Figure 4.1 shows the states that currently use PFC based on a survey completed in 2011. It shows which DOTs use it on curb and gutter sections and in what configuration. Out of the 45 state DOTs that responded to the survey, 9 states (20%) currently use PFC from gutter to gutter or curb to curb on curbed sections of highway. Two states (4%) currently use PFC only on the travelled lanes of the highway. Twelve states (27%) use PFC but not on curb and gutter sections of their highways. The remaining 22 states (49%) do not currently use PFC.

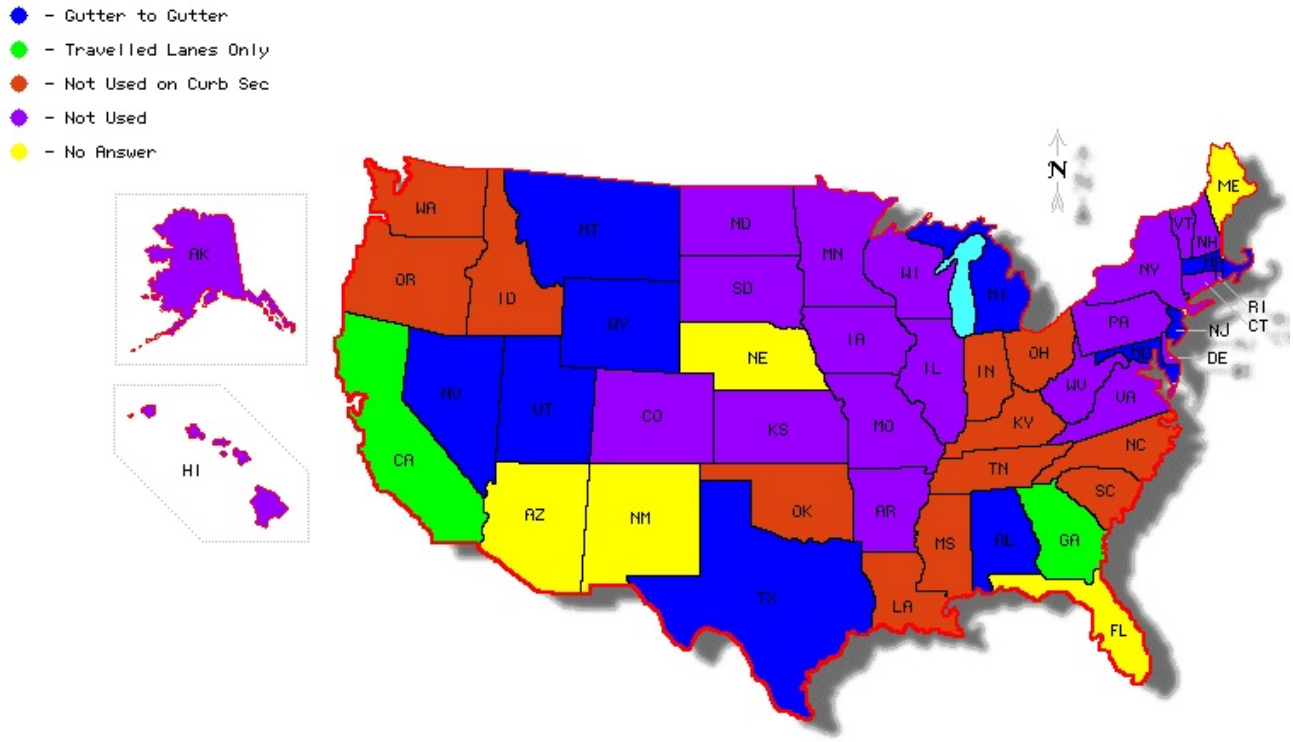

Figure 4.1: PFC use in the United States

4.2 Mopac Permeability Results

The falling head permeability test completed on both sides of the highway produced very different hydraulic conductivities. The Camp Mabry site uses a PG 76 binder, and the resulting hydraulic conductivity was 2.14 in/s. The Camp Hubbard site uses an A-R binder, and the resulting hydraulic conductivity was 0.76 in/s. The PG binder allowed water to flow into and through the pavement much quicker than the A-R binder did. The lower hydraulic conductivity at Camp Hubbard was also likely the results of the compaction occurring due to the low quality aggregate.

4.3 Stormwater Monitoring

Stormwater monitoring along Mopac occurred between January 9, 2011, and October 11, 2012. Over the course of the study, 30 storms were sampled and analyzed at Camp Mabry and 31 at Camp Hubbard. Individual concentrations for each storm can be found in Appendix B. The mean, median, and standard deviation and range for concentrations of each constituent monitored at Camp Mabry is presented in Table 4.1. The TSS data has a mean of 34 with a standard deviation of 47.2. The large range of TSS data is due to a period of sampling in 2011 where maintenance on the vegetated shoulder nearby may have caused increased debris. Time series graphs for concentrations of individual constituents at Camp Mabry can be found in Appendix C.

Table 4.1: Summary Statistics of the Concentrations at Camp Mabry

Constituent	Mean	Median	Standard Deviation	Range	Units
TSS	34	12	47.2	3.4–162	mg/L
TKN	1.50	0.99	1.946	0.228–10.9	mg/L
NO_3^-/NO_2^-	0.35	0.27	0.283	0.02–1.45	mg/L
P_{total}	0.17	0.09	0.310	0.02–1.7	mg/L
$P_{dissolved}$	0.07	0.02	0.58	0.02–0.812	µg/L
Cu_{total}	19	13	16.5	4.08–84.2	µg/L
$Cu_{dissolved}$	13	9	9.1	4.7–40.8	µg/L
Pb_{total}	3	2	3.92	1–19.1	µg/L
$Pb_{dissolved}$	1	1	0.58	1–4.1	µg/L
Zn_{total}	53	37	54	15.8–276	µg/L
$Zn_{dissolved}$	29	20	35	12–183	µg/L

The same statistics were calculated for each constituent at camp Hubbard and are presented in Table 4.2. The range of TSS at this site was also increased during the period of maintenance; however, since the maintenance was observed on the southbound side of the freeway, less debris may have ended up near Camp Hubbard. The range of heavy metal concentrations is similar at the two sites. A statistical comparison of the two sites is included later in the analysis. Time series graphs for concentrations of individual constituents at Camp Hubbard can be found in Appendix D.

Table 4.2: Summary Statistics of the Concentrations at Camp Hubbard

Constituent	Mean	Median	Standard Deviation	Range	Units
TSS	21	12	18.8	4.0–76.5	mg/L
TKN	1.34	0.94	1.188	0.305–6.32	mg/L
NO_3^-/NO_2^-	0.38	0.30	0.268	0.044–1.44	mg/L
P_{total}	0.11	0.06	0.114	0.02–0.457	mg/L
$P_{dissolved}$	0.05	0.02	0.31	0.02–0.3	µg/L
Cu_{total}	19	13	18.5	3.83–100	µg/L
$Cu_{dissolved}$	14	9	13.4	3.2–70.1	µg/L
Pb_{total}	3	2	2.56	1–9.57	µg/L
$Pb_{dissolved}$	1	1	0.31	1–2.7	µg/L
Zn_{total}	124	86	123	34.3–665	µg/L
$Zn_{dissolved}$	85	51	107	20.4–566	µg/L

The data were compared to the conventional pavement water quality data from Barrett et al. (1998) and reductions for each constituent were calculated based on the median concentration. The median was selected over the mean because the distribution of each constituent was skewed as a result of outliers. Table 4.3 provides the results of this comparison for both sites. The median concentrations for the conventional pavement site are also presented. Reductions of contaminants range between 56% and 99%. Values for the dissolved metals and TKN are not included in the study because conventional pavement concentrations were not available.

Table 4.3: Concentrations and Reductions at Both Sites

	Median Concentration			Percent Reduction	
Constituent	**Conventional**	**Camp Mabry**	**Camp Hubbard**	**Camp Mabry**	**Camp Hubbard**
TSS (mg/L)	152.0	12.0	12.0	92	92
NO_3^+/NO_2^- (mg/L)	0.7	0.3	0.3	61	56
Total P (mg/L)	0.5	0.1	0.1	81	86
Total Copper (µg/L)	50.0	13	13	75	74
Total Lead (µg/L)	130.0	2	2	99	98
Total Zinc (µg/L)	285.0	37	86	87	70

A Mann-Whitney test was performed to determine if the difference in the medians of each sites water quality data compared to the conventional data could be seen as statistically significant. The p-values calculated for each constituent at both sites were all 0.0001 or lower and all well below 0.05, indicating significance within a 95% confidence interval. The TSS value often used as a surrogate for all constituents of concern in highway runoff was found to be reduced by 92% at both sites. TSS is a constituent of particular concern because TCEQ requires

new land developments to remove 80% of the increase in TSS before discharging (Texas Administrative Code, 2005). This value easily exceeds the reduction requirement.

4.4 Site Comparison

One focus of this study was to compare the water quality impacts of the two mix designs used at the sampling sites. Camp Mabry uses a PG-76 binder, and Camp Hubbard uses an A-R binder. A statistical test was performed for all the constituents to see if there were any significant differences between the two sites. The Wilcoxon signed rank test was selected over the Mann-Whitney test because paired occurrences were present. Storms that were analyzed at only one site due to complications with one of the samplers were removed from the comparison. The p-values are shown in Table 4.4. Once again significance was indicated by p-values less than 0.05.

Table 4.4: Binder Comparison Results

Constituent	Median Concentration		P-Value
	Camp Mabry	Camp Hubbard	
TSS (mg/L)	12	12	0.4247
NO3+/NO2- (mg/L)	0.27	0.30	0.209
Total P (mg/L)	0.09	0.06	0.281
Total Copper (µg/L)	13	13	0.484
Total Lead (µg/L)	1.63	2.4	0.0869
Total Zinc (µg/L)	37	86	<0.0001
Dissolved P (mg/L)	0	0	0.3632
Dissolved Copper (µg/L)	9	9	0.352
Dissolved Lead (µg/L)	1	1	0.492
Dissolved Zinc (µg/L)	20	51	<0.0001

Out of the 10 constituents, only total and dissolved zinc showed a significant difference in concentration. Not only are the median concentrations higher at Camp Hubbard, but Figure 4.2 shows that the same is true for each individual storm event. One explanation for the higher zinc concentrations observed at Camp Hubbard is related to the asphalt binder used. The A-R binder used on the Camp Hubbard lanes contains recycled tires. Tires contain about 20 different types of metals. Zinc is present in particularly high amounts, since zinc oxide is used in the vulcanization process. Tire-tread material has a zinc content of about 1% by weight (ISS, 2008).

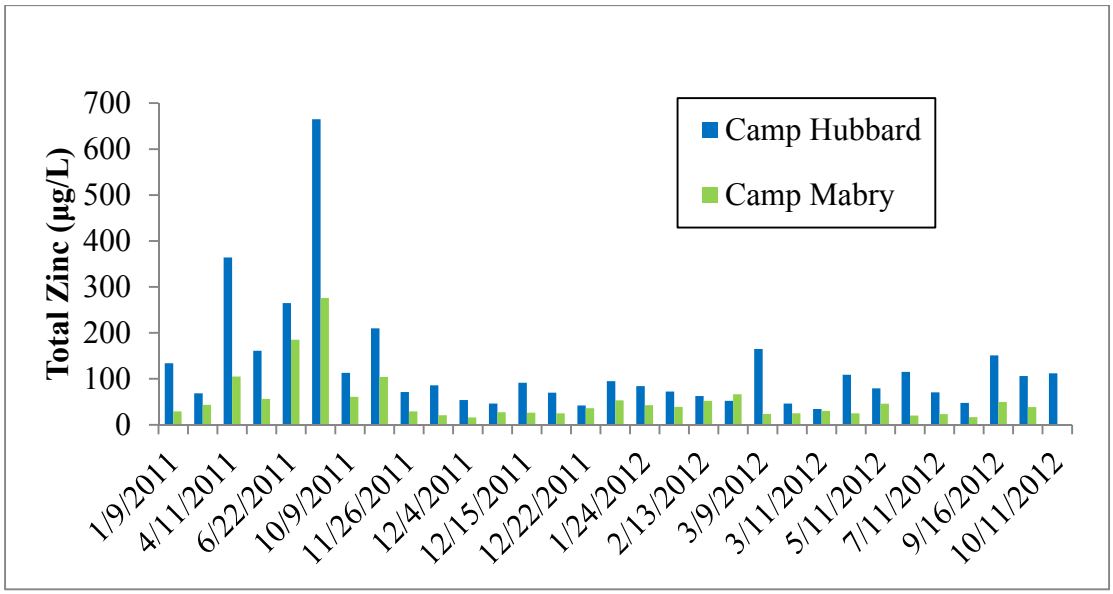

Figure 4.2: Individual concentrations of total zinc for all storm events

4.5 Comparison to Stormwater BMPs

Sand filters are the current standard treatment method for reducing TSS and other pollutants from runoff in Austin, Texas. The performance of five Austin sand filters was evaluated for TSS, total nitrate and nitrite, and many heavy metals by Barrett (2003). A comparison of the PFC along Mopac to the removal capabilities of the Austin sand filters is presented in Table 4.5.

Table 4.5: Comparison to Austin Sand Filter Reduction

Constituent	Sand Filter (%)	PFC (%)
TSS (mg/L)	89	92
NO3+/NO2- (mg/L)	17	59
Total P (mg/L)	59	84
Total Copper (µg/L)	72	74
Total Lead (µg/L)	86	98
Total Zinc (µg/L)	76	78

Sand filters are effective at treating runoff but require extra land and extended time. PFC is able to reach and exceed levels of treatment for the constituents monitored in this study but incorporates the treatment into the roadway surface without additional right of way or construction. Maintenance is also limited only to the resurfacing that would already occur on traditional roadways.

Recently, TCEQ has approved the use of PFC as a BMP on uncurbed roadways. This decision was supported by past water quality studies of PFC, which were typically completed on roadway segments with vegetated strips along the shoulder. This study investigated a section of

Mopac with a curb and gutter system, which addresses the concern that curbs contribute to accumulation of debris affecting water quality. The reduction values from this study are repeated in Table 4.6 along with the values obtained from a similar study published by Eck et al. (2012b). Eck's research was conducted along highways 360 and 620 in Austin, Texas. Both these highways have vegetated shoulders instead of curbs and gutter systems. The values in the table are averages from the three sites studied by Eck et al. and the two sites from this study.

Table 4.6: Reductions Comparison for Curb Types

Constituent	Average Reduction	
	Vegetated Shoulder	Curb and Gutter
TSS (mg/L)	93	92
NO_3/NO_2 (mg/L)	-28	59
Total P (mg/L)	71	84
Total Copper (µg/L)	62	74
Total Lead (µg/L)	92	98
Total Zinc (µg/L)	87	78

The reduction values for NO_3/NO_2, total phosphorus, total copper, and total lead are higher for the curb and gutter system. The TSS reduction is just slightly lower than the reduction from the previous study. Total zinc is the only constituent that shows any real decrease in efficiency and this could be due to the asphalt rubber binder used at Camp Hubbard. Total zinc at Camp Mabry was reduced by 87%, the exact amount reduced on average at the vegetated shoulder sites. While these studies were conducted for different storms and traffic loads, the results suggest that a curb and gutter system does not hinder the ability of PFC to improve water quality.

4.6 Hydrograph Analysis

A runoff hydrograph for the PFC pavement at both sites were created for each rain event. The hydrograph shows the rainfall, the measured flow rate, the modeled flow rate, and the time at which the samples were taken. An example storm hydrograph for Camp Mabry is presented in Figure 4.3. The storm on October 9, 2011, was a large rain event (1.43 in.). Since this storm exceeds the largest storm event possible (0.78 in.), only the front end of the storm could be sampled—about 72%. The delay in peak runoff from peak rainfall was approximately 3 minutes. The smaller rain events had peak lags up to 14 minutes. These values are very comparable to the 5–15 minutes calculated from Eck et al. (2010). The hydrographs for all the monitored rain events for Camp Mabry are presented in Appendix E.

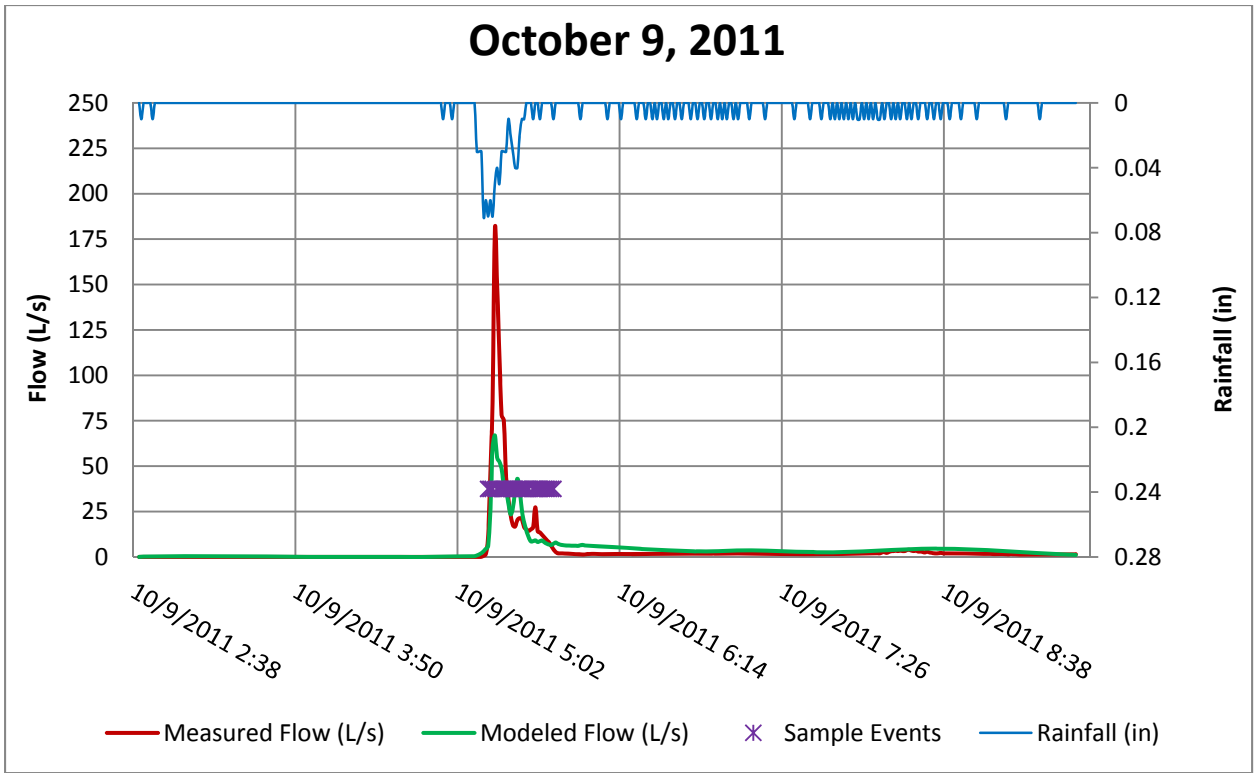

Figure 4.3: Hydrograph from sampled rain event on October 9, 2011, at Camp Mabry

Some of the events could not be included because errors occurred in the data collection. Rainfall errors occurred due to clogging from bugs and leaves in the rain gauge and the wire between the flow meter and rain gauge being cut. This happened for three of the sampled events, so rain data from the NWS gauge located at Camp Mabry was used (NOAA). The Flowlink software calculated the total flow from a sample event. Figure 4.4 shows the relationship between rainfall and runoff at Camp Mabry. The slope of the linear trend line can be interpreted as the runoff coefficient for the overlay. The PFC at Camp Mabry produced a runoff coefficient of 0.99.

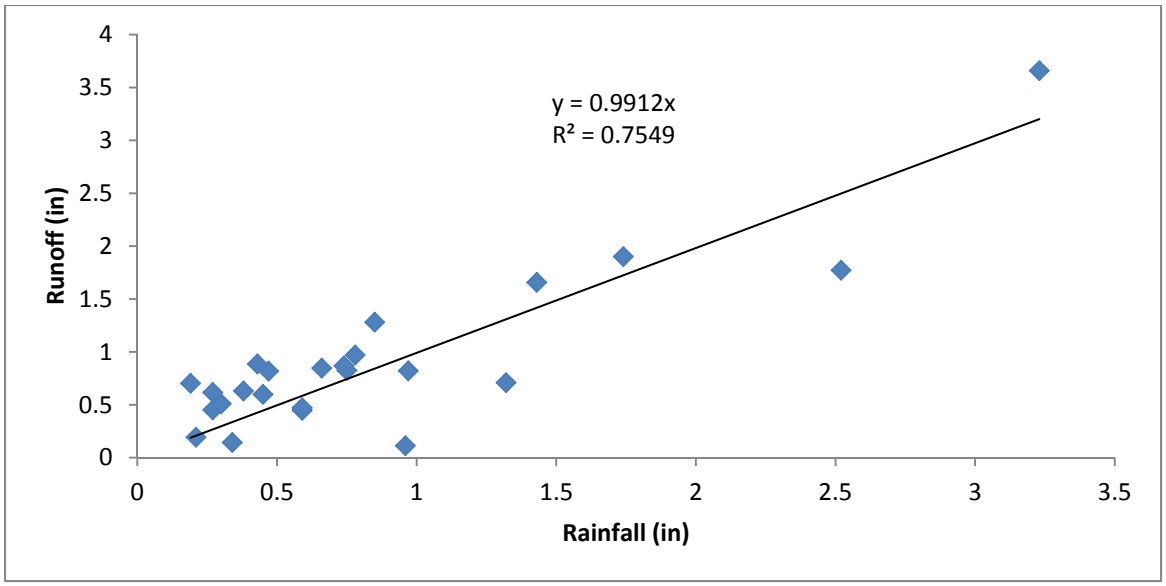

Figure 4.4: Rainfall-runoff relationship for Camp Mabry

A hydrograph for Camp Hubbard is shown in Figure 4.5. The storm on October 9, 2011, was a large rain event (1.43 in.). Ninety-six percent of this storm was able to be sampled at the Camp Hubbard site, unlike the 72% from the Camp Mabry site. This increase is due to the larger runoff coefficient at Camp Mabry site for this storm. The delay in peak runoff from peak rainfall was approximately 3 minutes. The smaller rain events had peak lags up to 25 minutes. The 25 minutes is much larger than the Eck et al. (2010) values and could be due to the smaller hydraulic conductivity associated with the Camp Hubbard site. The hydrographs for all the monitored rain events for Camp Hubbard are presented in Appendix E. Like Camp Mabry, some of the events could not be included because of errors occurring in the data.

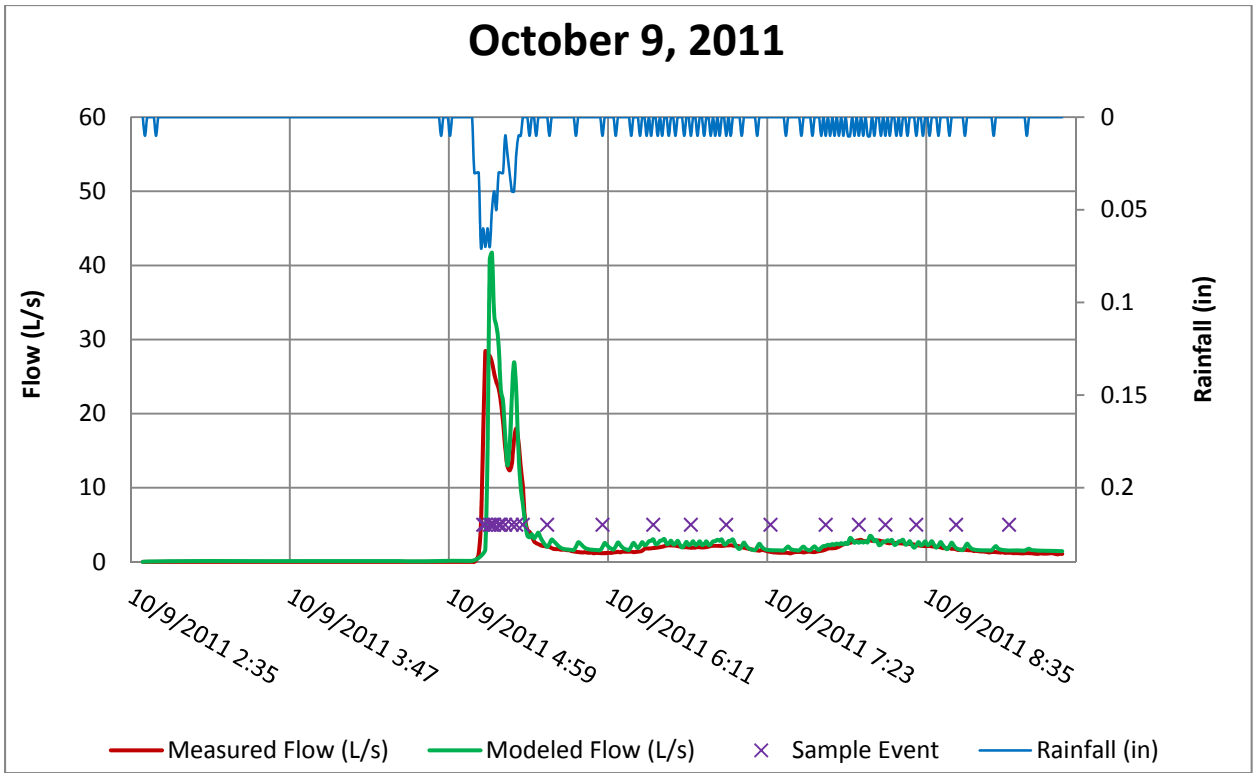

Figure 4.5: Hydrograph from a sampled rain event on October 9, 2011, at Camp Hubbard

Figure 4.6 shows the relationship between rainfall and runoff at Camp Hubbard. The slope of the linear trend line can be interpreted as the runoff coefficient for the overlay. Camp Hubbard showed a lower runoff coefficient than Camp Mabry with a value of 0.79.

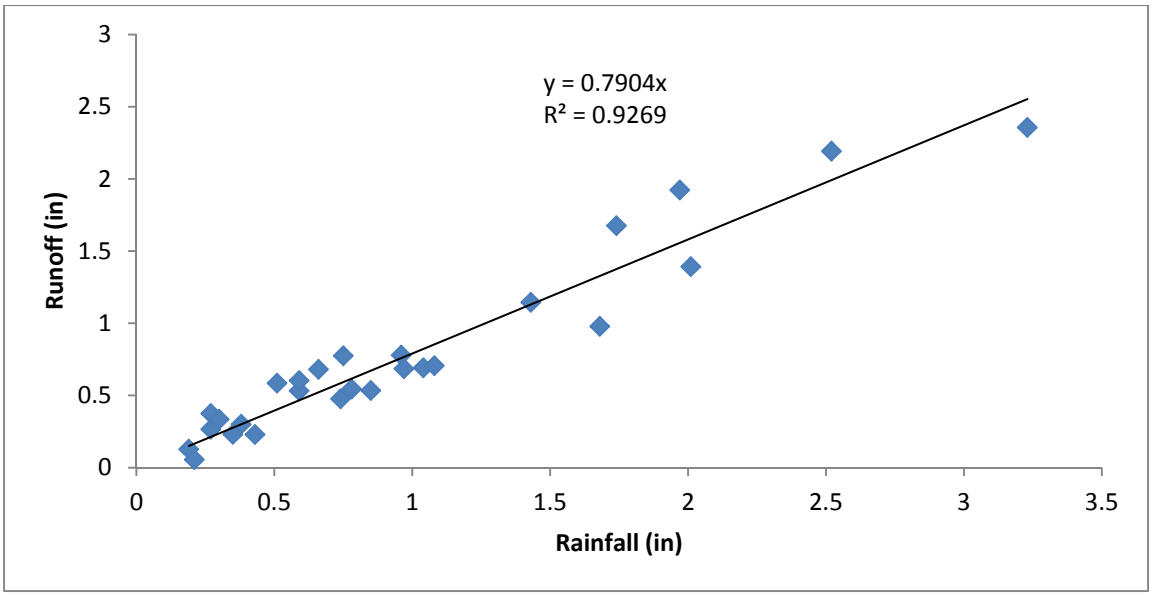

Figure 4.6: Rainfall-runoff relationship from Camp Hubbard

4.7 Pollutant Removal Mechanism

Barrett and Shaw (2007) relate two theories on the mechanism for pollutant removal in PFC. First, PFC reduces the amount of surface water, which reduces the amount of splash and spray. By limiting the amount of spray, fewer pollutants are washed off from the bottom of vehicles and engine compartments. Secondly, PFC also may act to filter the stormwater. As the water flows through the pores of the surface overlay, pollutants can be filtered out.

PERFCODE (Eck et al. 2012c) was used to test these hypotheses. This computer model calculates the fraction of the road surface where runoff is present on the surface (η). A value of zero means there is no surface water on the road, and a value of 1 means the entire road is covered in water. The value picked for η for this study was greater than or equal to 0.38—this value put sheet flow from the curb and gutter to the middle of the first driving lane, so that at least some cars would be driving through the surface water. Figure 4.7 shows TSS concentrations at Camp Mabry and Camp Hubbard versus the percent of a storm sample that η was greater than or equal to 0.38. From this graph you can see there is no correlation between the TSS concentration at either site or the amount of surface flow during the sample event. From this, the conclusion can be made that the pavement is primarily acting to retain pollutants with the pores of the overlay. This analysis was conducted over the first-year stormwater monitoring.

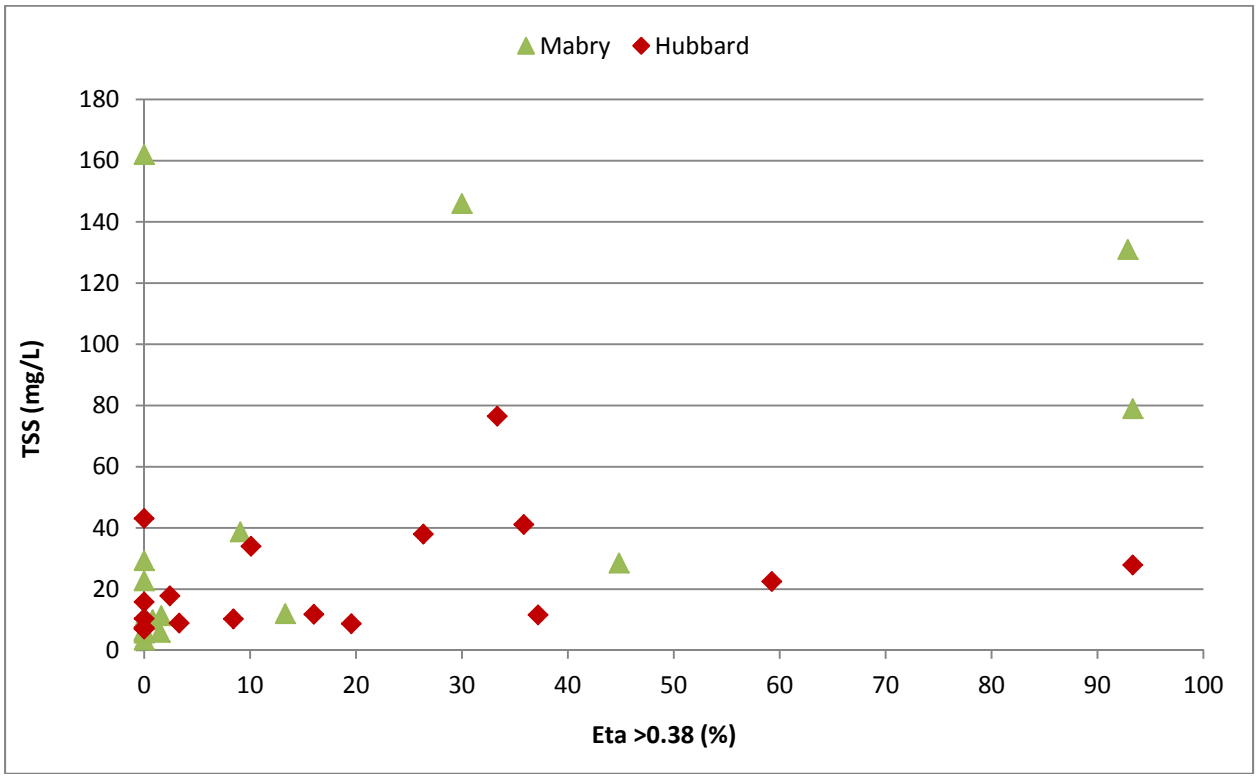

Figure 4.7: TSS concentrations at Camp Hubbard and Camp Mabry versus surface flow during sample event

4.8 Hydraulic Modeling

The next two sections of the report discuss the results of the hydraulic modeling experiments. First, the water surface elevations that were determined from the water depths measured by the manometers are presented. A similar shape was observed for all flow rates across all slopes. The water surface in the pavement remains relatively flat until nearing the drain; at that point it decreases rapidly and levels off at the lip of the drain. When flow rate is increased the water level inside the pavement is also increased, shifting the curve up on the graphed models. The points shown past the drain represent the water level on the other side of the drain when the flow overloaded the system. The results for several flows at each slope are shown in Figures 4.8 through 4.10. The water depth calculations are included in Appendix F.

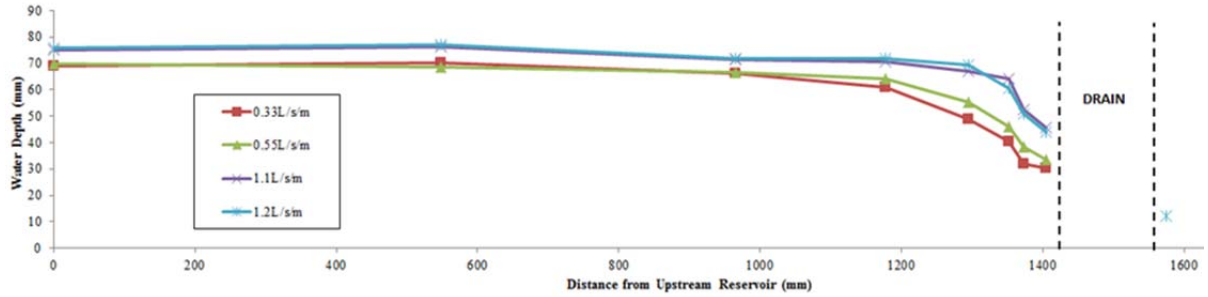

Figure 4.8: Water surface profiles for 0% slope

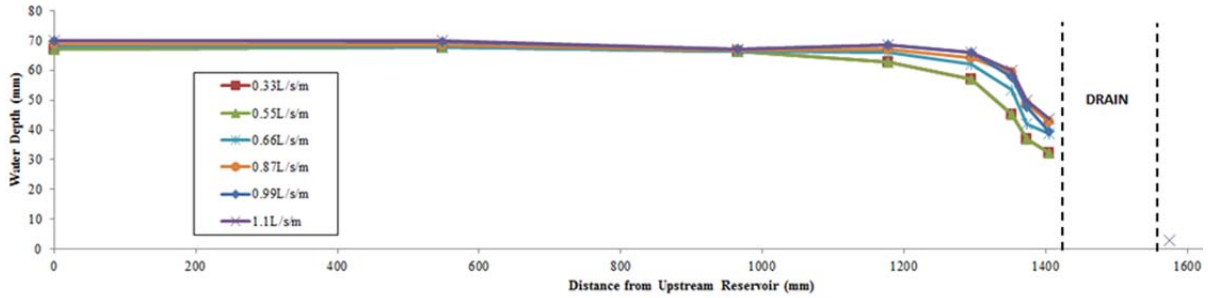

Figure 4.9: Water surface profiles for 1.5% slope

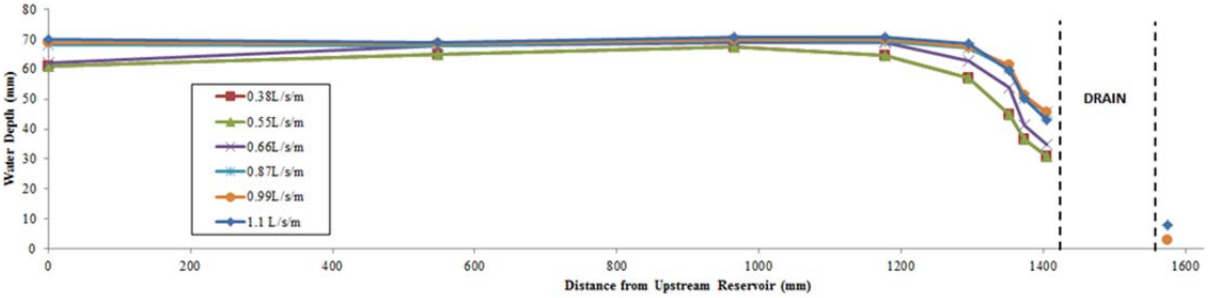

Figure 4.10: Water surface profiles for 2.5% slope

When slope is held constant as seen in Figures 4.8–4.10, the behavior near the reservoir behaves similarly independent of flow rate, only shifting up when sheet flow occurs. When

gradients from the same flow rate are graphed for each slope, a different pattern occurs. Figure 4.11 shows the water surface profiles for a flow rate of 0.55 L/s/m across all three slopes. When the flow rate is held constant the water depth near the upstream reservoir varies but converges as it approaches the drain. This trend could be useful in future modeling endeavors.

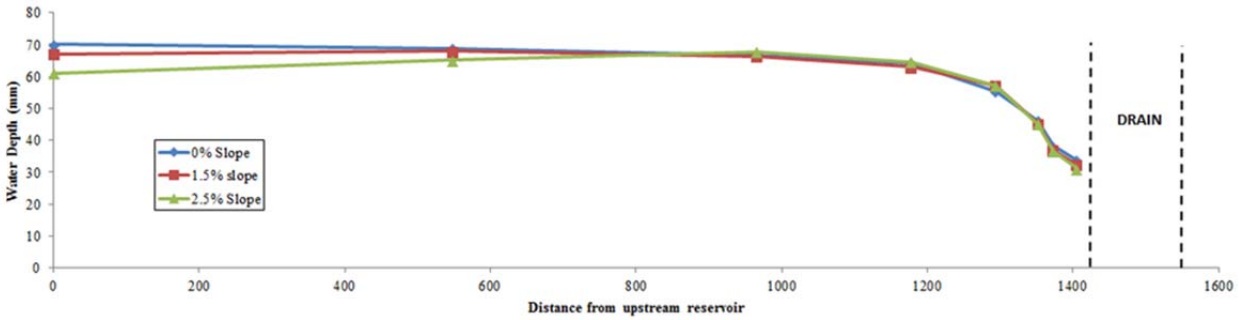

Figure 4.11: Water surface elevations for constant flow

Drain efficiency was evaluated by determining how much flow per meter of length the drain could handle before the underdrain was bypassed. The runoff reaching the downstream end was measured and the bypass flow rate was calculated. The overloading flow was operated until runoff began to reach the downstream reservoir at a constant rate. Table 4.7 shows the overloading flow rate at each slope and the flow of water bypassing the channel.

Table 4.7: Drain Efficiency Results

	0%	1.5%	2.5%
Max q (L/s/m)	1.2	1.1	0.99
q bypassed (L/s/m)	0.00151	0.00164	0.0011
% of total flow	0.13%	0.15%	0.11%

The simulation ran at the same flow rate for more than 3 hours before any of the runoff reached the downstream reservoir at the above flow rates. These flows represent the point at which runoff barely trickles past the drain. The efficiency of the drain decreases with increasing slope. These results are specific to the drain used in the experiment and could be repeated in the future for a specific TxDOT preferred drain.

4.9 Comparison of Linear and Non-Linear Relationships for Flow

Hydraulic conductivities based on linear flow were calculated using the Dupuit-Forcheimer equation. Conductivities were found for three stretches of the pavement to test consistency and evaluate validity of the linear assumption. The resulting conductivities were very close together supporting the use of the equation. The average hydraulic conductivity found was 2.77 in/s which compares well with the conductivity at Camp Mabry of 2.14 in/s. The parameters used in the linear analysis and resulting conductivities are presented in Table 4.8.

Table 4.8: Linear Conductivities and Parameters

	cm				cm^3/s	cm/s	in/s
	L	**W**	**H1**	**H2**	**Q**	**K**	**k**
7 to 2	41.8	45.72	4.82	3.73	35.00	6.88	**2.71**
7 to 8	63	45.72	4.82	3.15	35.00	7.21	**2.84**
7 to 3	74.7	45.72	4.82	2.64	35.00	7.02	**2.76**

Three forms on the non-linear Forcheimer equation were also used to calculate the hydraulic conductivities for the three stretches of pavement. The resulting hydraulic conductivities were consistent for each equation, and across the non-linear equations. In addition they were also close to the range of the linear values. The non-linear conductivities are shown along with the linear values below in Table 4.9. These results suggest that even with an underdrain, inertial effects are negligible compared to viscous forces and Darcy's Law is applicable.

Table 4.9: Linear and Non Linear Hydraulic Conductivities

		Non Linear (in/s)		
Ports	**Linear (in/s)**	**K & K**	**Ergun**	**Ward**
7 to 2	2.71	2.71	2.71	2.70
7 to 8	2.84	2.84	2.85	2.84
7 to 3	2.76	2.74	2.75	2.74
Average:	2.77	2.76	2.77	2.76

Chapter 5. Conclusions

PFC is used throughout the United States and overseas for sidewalks, parking lots, and roadways. While traditionally installed for safety reasons, the environmental benefits are becoming better understood and appreciated. The two main objectives of this research were to 1) determine if the removal efficiency of pollutants observed on uncurbed highways would be observed on curbed sections as well, and 2) conduct preliminary tests that could facilitate TxDOT guidance on the spacing and configuration of underdrains, improving stormwater conveyance and further reducing standing water on roadways with PFC.

Over a period of 2 years, 32 storms were monitored at Camp Mabry and Camp Hubbard. The results show a reduction in the concentration of TSS, NO3+/NO2- , total phosphorus, zinc, lead, and copper. The median TSS removal observed on Mopac was 92%, easily exceeding the expectations as a BMP for highway treatment of stormwater runoff in the Austin area. Two different binders were used in the mixes at the test site along Mopac. The performance-graded binder had a higher hydraulic conductivity, allowing water to move more easily into and through it, while the asphalt-rubber binder produced more sheet flow. The only statistically significant difference in water quality between the binders is that the runoff from the asphalt-rubber binder contained higher concentrations of total and dissolved zinc. This result likely arises from the zinc composition of the binder itself.

Most previous studies on the effects of water quality with PFC installation investigated highways with vegetated shoulders. This study was conducted at sites with a curb and gutter between the roadway and vegetation. The presence of a curb and gutter did not hinder overall pollutant removal when compared to previous studies. However, debris accumulation is more likely when curbs are in place, which can cause pollutant buildup if the roadway is not properly maintained. Data from both curbed and uncurbed sections of highways in Austin met and exceeded the pollutant reduction values from the Austin sand filter.

Using computer modeling, the fraction of the road surface where runoff is present at the surface was monitored. From this modeling, it was able to be determined that there was no correlation between surface water and pollutant concentration. Therefore, the primary mechanism for pollutant removal is PFC acting as a filter—as the water flows through the pores of the surface overlay, pollutants can be filtered out.

The environmental and safety benefits provided through PFC are related to the prevention of surface ponding. It is possible that combining the pavement with underdrains could remove even more runoff from the roadway especially in areas with a vertical sag or superelevation transition. Water flowing within pavement behaves differently than traditional sheet flow runoff. Before placing underdrains on roadways with porous media, laboratory experiments could be used to develop a calibrated model to provide guidance to TxDOT on their size, configuration, and spacing.

The hydraulic research conducted has identified an alternative material to hot mix asphalt for use in laboratory hydraulic testing of porous overlays. The results demonstrate that water levels within the pavement can be accurately measured at various slopes and flow rates. The water levels at selected points were used to model the depth of flow within the entire length of pavement and showed a repeated shape under different conditions. The profiles plotted show that changing flow rates controls the hydraulic gradient in the region near the underdrain while changing slope affects the water depths at the upstream end. Hydraulic conductivity tests showed that Darcy's Law is applicable for modeling flow through PFC.

A method of identifying the maximum amount of flow that a specific drain can handle has been developed by monitoring downstream of the channel. While the drain and experimental set up used in these tests are not representative of real-world conditions, the work shows that future evaluation on a larger scale with more complex geometry is feasible. The results of additional experimentation and modeling could allow TxDOT to further improve stormwater conveyance and reduce standing water on roadways.

Despite the safety and water quality benefits of PFC, many agencies throughout the US are cautious about installing PFC on highways. Test sections, such as the sites along Mopac, are being used to address these concerns and further understand the benefits. Continued research on the effects of various shoulder types and binder compositions on water quality can help TCEQ know which conditions are necessary to meet environmental regulations. Future modeling efforts on the ideal configurations of underdrains based on roadway geometry could assist TxDOT in improving stormwater conveyance and providing safer roadway conditions.

References

Anderson, D.A., Huebner, R.S., Reed, J.R., Warner, J.C., Henry, J. J. (1998): Improved Surface Drainage of Pavements," NCHRP Web Document #16 Web Site: http://www.nap.edu/catalog.php?record_id=6357

Barrett, M., Irish, Lyn B., Malina, Joseph F., Jr., and Charbeneau, Randall J. (1998): "Characterization of highway runoff in Austin, Texas area," American Society of Civil Engineers Journal of Environmental Engineering, Vol. 124, No. 2, pp. 131–137.

Barrett, M. E. (2003): "Performance, cost, and maintenance requirements of Austin sand filters." J. Water Resour. Plann. Management, 129(3), 234–242

Bear, J. (1972): Dynamics of Fluids in Porous Media, American Elsevier Publishing Company, Inc., New York.

Bendtsen, H. and B. Andersen (2005): "Report 141: Noise Reducing Pavements – State of the Art in Denmark," Road Directorate, Danish Road Institute, Denmark Ministry of Transport.

Berbee, R., Rijs, G., de Brouwer, R., and van Velzen, L. (1999): "Characterization and Treatment of Runoff from highways in the Netherlands Paved with Impervious and Pervious Asphalt." Water Environment Research, Vol. 71, No. 2, pp. 183–190.

Burch, C.W., Johnson, F., and Maestri, B., (1985): Management Practices for Mitigation of Highway Runoff Pollution: Volume II, Literature Review, FHWA/RD-85-002, Versar Inc., Springfield, VA.

Charbeneau, R.J. (2000): Groundwater Hydraulics and Pollutant Transport, Prentice-Hall, Upper Saddle River, NJ.

Charbeneau, R.J. and M.E. Barrett (2008): "Drainage Hydraulics of Permeable Friction Courses," Water Resources Research, Vol. 44, W04417.

Collins, R.E. (1961): Flow of Fluids through Porous Materials, Reinhold, New York.

Darcy, H. (1856): The Public Fountains of the City of Dijon, English Translation by Patricia Bobeck (2004), Kendall/Hunt Publishing Company, Dubuque, Iowa.

Eck, Bradley J., Klenzendorf, J. Brandon, Charbeneau, Randall J., and Barrett, M. (2010) Investigation of Stormwater Quality Improvements Utilizing Permeable Friction Course (PFC), Center for Transportation Research Report 0-5220-2, University of Texas at Austin. Accessed at URL: http://www.utexas.edu/research/ctr/pdf_reports/0_5220_2.pdf

Eck, B.J; Barrett, M.E ; Charbeneau, R.J. (2012a): "Forchheimer flow in gently sloping layers: Application to drainage of porous asphalt," Water Resources Research, Vol. 48, W01530

Eck, B.; R. Winston; W. Hunt; M. Barrett (2012b): "Water Quality of Drainage from Permeable Friction Course." Journal of Environmental Engineering, 138 (2), pp. 174–181

Eck, Bradley, Barrett, M., and Charbeneau, Randall, (2012c): Coupled surface-subsurface model for simulating drainage from permeable friction course highways, American Society of Civil Engineers Journal of Hydraulic Engineering, 138, (1), pp. 13–22,

Ergun, S. (1952): "Fluid Flow Through Packed Columns," Chemical Engineering Progress, Vol. 48, No. 2, pg. 89–94.

Forchheimer, P. (1901): "Wasserbewegung dur Bodem," Zeitschrift des Verbundes der deutschen Ingenieurs, Vol. 45, pg. 1782–1788.

Fwa, T.F., S.A. Tan, and C.T. Chuai (1998): "Permeability Measurement of Base Materials Using Falling-Head Test Apparatus," Transportation Research Record, No. 1615, pg. 94–99.

Fwa, T.F., S.A. Tan, and Y.K Guwe (1999): "Laboratory Evaluation of Clogging Potential of Porous Asphalt Mixtures," Transportation Research Record, No. 1681, pg. 43–49.

Hassanizadeh, S.M. and W.G. Gray (1987): "High Velocity Flow in Porous Media," Transport in Porous Media, Vol. 2, pg. 521–531.

Izbash, S. (1931): O Filtracii Kropnozernstom Materiale, Leningrad, USSR.

Isenring, T., H. Koster and I. Scazziga (1990): "Experiences with Porous Asphalt in Switzerland," Transportation Research Record, No. 1265, pg. 41–53

International Surfacing Systems (ISS). (2008): Material Safety Data Sheet. Retrieved October 16, 2011 from International Surfacing Systems Web Site: http://www.asphaltrubber.com/

Jackson, T.J. and R.M. Ragan (1974): "Hydrology of Porous Pavement Parking Lots," Journal of the Hydraulic Division, Vol. 100, HY 12, pg. 1739–1752.

Kadlec, H.R. and L.R. Knight (1996): Treatment Wetlands, CRC Press Lewis Publishers, Boca Raton, Florida.

Kovacs, G. (1981): Seepage Hydraulics, Elsevier Scientific Publishing Company, Amsterdam.

Klenzendorf, J.B., Eck, B.J., Charbeneau, R. J., and Barrett, M. (2012), Quantifying the behavior of porous asphalt overlays with respect to drainage hydraulics and runoff water quality, Environmental and Engineering Geoscience, Vol. XVIII, No. 1, pp. 99–111.

Klenzendorf, J. B. (2010): Hydraulic Conductivity Measurement of Permeable Friction Course (PFC) Experiencing Two-Dimensional Nonlinear Flow Effects. Dissertation. University of Texas at Austin.

Legret, M., Nicollet, M., Miloda, P., Colandini, V. and Raimbault, G. (1999): "Simulation of Heavy Metal Pollution from Stormwater Infiltration through a Porous Pavement with Reservoir Structure." Water Science and Technology, Vol. 39, No. 2, pp. 119–125.

Loaiciga, H.A. (2005): "Steady State Phreatic Surfaces in Sloping Aquifers," Water Resources Research, Vol. 41, W08402.

National Cooperative Highway Research Program (NCHRP) Report 640, (2009): "Construction and Maintenance Practices for Permeable Friction Courses." Transportation Research Board, Washington, D.C.

National Oceanic and Atmospheric Administration (NOAA). Weather observations for the past three days. Gauge: Camp Mabry/Austin City. http://www.srh.noaa.gov/

Pagotta, C., M. Legret, and Le Cloirec, P. (2000): "Comparison of the Hydraulic Behaviour and the Quality of Highway Runoff Water According to the Type of Pavement." Water Resources, Vol. 34, No. 18, pp. 4446–4454.

Ranchet, J. (1995): "Impacts of porous pavements on the hydraulic behaviour and the cleansing of water." Techniques Sciences et Méthodes 11, pp. 869–871.

Rand, D. (2006): TxDOT's Use of Permeable Friction Courses (PFC). Retrieved September 30, 2011 from Arkansas Asphalt Pavement Association Web Site: http://www.arasphalt.com/

Ranieri, V. (2002): "Runoff Control in Porous Pavements," Transportation Research Record, No. 1789, pg. 46–55.

Sartor, J.D., and Boyd, G.B., (1972): Water Pollution Aspects of Street Surface Contaminants, URS Research Company for the U.S. EPA, Office of Research and Monitoring, Environmental Protection Series EPA-R2-72-081.

Scheidegger, A. E. (1963): The physics of flow through porous media. University of Toronto Press, Toronto, Canada.

Stotz, G., (1987): "Investigations of the Properties of the Surface Water Runoff from Federal Highways in the FRG," The Science of the Total Environment, Vol. 59, pp. 329–337.

Stotz, G. and K. Krauth (1994): "The Pollution of Effluents from Pervious Pavements of an Experimental Highway Section: First Results," The Science of the Total Environment, Vol. 146–147, pg. 465–470.

Tan, S.A., T.F. Fwa, and C.T. Chuai (1997): "A New Apparatus for Measuring the Drainage Properties of Porous Asphalt Mixes," Journal of Testing and Evaluation, Vol. 25, No. 4, pg. 370–377.

Tan, S.A., T.F. Fwa, and C.T. Chuai (1999): "Automatic Field Permeameter for Drainage Properties of Porous Asphalt Mixes," Journal of Testing and Evaluation, Vol. 27, No. 1, pg. 57–62.

Texas Administration Code (TAC). (2005) Title 30, Environmental Quality, Chapter 213, Edwards Aquifer. Retrieved March 20, 2012 from the TCEQ Web Site: http://info.sos.state.tx.us/pls/pub/readtac$ext.ViewTAC.

Texas Department of Transportation (TxDOT). (2004): Item 342 Permeable Friction Course (PFC) Standard Specifications for Construction and Maintenance of Highways, Streets, Bridges, Austin, Texas. pp. 312–328. Web Site: http://www.dot.state.tx.us/business/specifications.htm

Venkataraman, P. and P. Rama Mohan Rao (2000): "Validation of Forchheimer's Law for Flow Through Porous Media with Converging Boundaries," Journal of Hydraulic Engineering, Vol. 126, No. 1, pg. 63–71.

Van der Zwan, J., Goeman, T., Gruis, H., Swart, J. and Oldenburger, R. (1990): "Porous Asphalt Wearing Courses in the Netherlands: State of the Art Review," Journal of the Transportation Research Board, No. 1265, TRB, National Research Council, Washington D.C., pp. 95–110.

Ward, J.C. (1964): "Turbulent Flow in Porous Media," Journal of the Hydraulic Division, Vol. 90, HY 5, pg. 1–12.

White, F.M. (1999): Fluid Mechanics, Fourth Edition. WCB/McGraw-Hill.

Wilkins, J. K. (1955). "Flow of water through rockfill and its application to the design of dams." New Zealand Engineering.

Yates, S.R., A.W. Warrick, and D.O. Lomen (1985): "Hillside Seepage: An Analytical Solution to a Nonlinear Dupuit-Forchheimer Problem," Water Resources Research, Vol. 21, No. 3, pg. 331–336.

Appendix A: DOT Survey Contacts

State DOT	*DOT Contact*	*Email*	*Phone Number*
Alabama	Cathy Cox	coxc@dot.state.al.us	334-353-6554
Alaska	Stephan Saboundjian	steve.saboundjian@alaska.gov	907-269-6214
Arizona	—	—	—
Arkansas	Phil McConnell	Phil.McConnell@arkansashighways.com	501-569-2301
California	Terrie Bressette	terrie_bressette@dot.ca.gov	
Colorado	James Zufall	James.Zufall@dot.state.co.us	303-398-6501
Connecticut	Nelio Rodrigues	Nelio.Rodrigues@po.state.ct.us	860-258-0399
Delaware	Jim Pappas	James.Pappas@state.de.us	
Florida	Bruce Dietrich	bruce.dietrich@dot.state.fl.us	
Georgia	Peter Wu	Peter.Wu@dot.state.ga.us	404-608-4840
Hawaii	JoAnne Nakamura	JoAnne.Nakamura@hawaii.gov	
Idaho	Mike Dehlin	Mike.Dehlin@itd.idaho.gov	
Illinois	James Trepanier	James.Trepanier@illinois.gov	217-782-9607
Indiana	Becky McDaniel	rsmcdani@purdue.edu	765-463-2317 ext. 226
Iowa	Scott Schram	scott.schram@dot.iowa.gov	515-239-1604
Kansas	Andy Gisi	Agisi@ksdot.org	785-291-3856
Kentucky	Allen H. Myers	Allen.Myers@ky.gov	502-564-7034
Louisiana	Chad Winchester	chad.winchester@la.gov	225-379-1048
Maine	Brian Luce	Brian.Luce@maine.gov	
Maryland	Geoff Hall	GHall1@sha.state.md.us	443-572-5067
Massachusetts	Ed Naras	Edmund.Naras.state.ma.us	617-973-8269
Michigan	Curtis Bleech	BleechC@michigan.gov	
Minnesota	John Garrity	john.garrity@dot.state.mn.us	
Mississippi	Jeremy Robinson	wjrobinson@mdot.state.ms.us	601-359-9770
Missouri	John Donahue	John.Donahue@modot.mo.gov	573-526-4334
Montana	Dan Hill	dahill@mt.gov	406-444-3424
Nebraska	Moe Jamshidi	mjamshid@dor.state.ne.us	
Nevada	Reid G. Kaiser	rkaiser@dot.state.nv.us	775-888-7520

State DOT	*DOT Contact*	*Email*	*Phone Number*
New Hampshire	Denis Boisvert	Dboisvert@dot.state.nh.us	
New Jersey	Eileen C. Sheehy	eileen.sheehy@dot.state.nj.us	609-530-2307
New Mexico	Jeffery Mann	JeffreyS.Mann@state.nm.us	
New York	Russell Thielke	rthielke@dot.state.ny.us	518-457-4585
North Carolina	Todd W Whittington	twhittington@ncdot.gov	919-329-4060
North Dakota	Ron Horner	rhorner@state.nd.us	
Ohio	Aric Morse	Aric.Morse@dot.state.oh.us	614-995-5994
Oklahoma	Jeff Dean	jdean@odot.org	405-522-0988
Oregon	Justin G. Moderie	Justin.G.MODERIE@odot.state.or.us	503-986-3122
Pennsylvania	John Hocker	johnhocker@state.pa.us	717-783-3161
Rhode Island	Bryan Engstrom	bengstrom@dog.ri.gov	401-222-2524 ext. 4144
South Carolina	Andy Johnson	johnsonam@scdot.org	803-737-6683
South Dakota	Rick Rowen	rick.rowen@state.sd.us	605-773-3427
Tennessee	Mark Woods	Mark.Woods@state.tn.us	615-350-4149
Utah	Howard J. Anderson	handerson@utah.gov	801-965-4065
Vermont	Michael Pologruto	Mike.Pologruto@state.vt.us	
Virginia	Trenton M. Clark	Trenton.Clark@VDOT.Virginia.gov	
Washington	Jeff Uhlmeyer	UhlmeyJ@wsdot.wa.gov	360-709-5485
West Virginia	Thomas J. Medvick	Thomas.J.Medvick@wv.gov	304-558-9887
Wisconsin	Steven Krebs	steven.krebs@dot.state.wi.us	
Wyoming	Rick Harvey	Rick.Harvey@dot.state.wy.us	307-777-4070
Washington, DC	Wasi Khan	Wasi.Khan@dc.gov	

Appendix B: Concentrations of Constituents for All Storm Events

Constituent Concentrations at Camp Mabry

Date	Rainfall	TSS	TKN	NO_3^-/NO_2^-	P_{total}	$P_{dissolved}$	Cu_{total}	$Cu_{dissolved}$	Pb_{total}	$Pb_{dissolved}$	Zn_{total}	$Zn_{dissolved}$
	(in)	(mg/L)	(mg/L)	(mg/L)	(µg/L)	(µg/L)	(µg/L)	(µg/L)	(µg/L)	(µg/L)	(µg/L)	(µg/L)
1/9/2011	1.78	11.3	0.785	0.206	0.085	0.041	11.2	8.3	1.73	1	29	16.5
1/14/2011	1.25	11.9	0.974	0.451	0.02	0.02	12.1	8.2	1.6	1	43.3	21.6
5/12/2011	2.86	145.0	2.77	0.48	0.384	0.114	36.9	19.8	11.1	1	105	37.5
5/20/2011	0.51	28.5	2.1	0.611	0.11	0.02	26.4	19.2	3.19	1	56.4	34.1
6/22/2011	1.74	131.0	3.77	0.676	0.537	0.197	52.6	40.8	9.86	1.9	185	120
10/8/2011	0.38	162.0	10.9	1.45	1.7	0.812	84.2	37.2	19.1	4.1	276	183
10/9/2011	1.43	79.0	1.26	0.072	0.189	0.041	15.6	9	5.54	1	60.8	19
11/15/2011	0.78	146.0	2.61	0.563	0.254	0.067	36.5	27	5.97	1	104	51.1
11/26/2011	0.96	10.0	0.679	0.138	0.039	0.02	13.2	10.5	1.12	1	29.1	18.9
12/4/2011	0.75	5.9	0.435	0.128	0.042	0.02	6.61	6.5	1	1	20.6	13.4
12/5/2011	0.59	3.4	0.228	0.193	0.02	0.02	4.08	5.4	1	1	15.8	12
12/15/2011	0.39	6.5	0.674	0.192	0.046	0.02	12.2	9.5	1	1	27.5	17.3
12/16/2011	0.27	5.7	0.43	0.212	0.026	0.02	7.83	5.9	1.66	1	26.3	15.9
12/22/2011	0.97	6.2	0.39	0.106	0.038	0.027	5.53	4.7	1	1	25	15.5
1/9/2012	0.74	29.3	1	0.405	0.081	0.033	10.6	7.8	2.63	1	36.2	14
1/24/2012	3.23	38.7	0.987	0.365	0.093	0.02	16.3	11.9	3.03	1	53.3	20.3
2/4/2012	0.19	22.7	1.08	0.134	0.098	0.02	17.8	11.5	1.72	1	42.8	17
2/13/2012	0.21	10.5	1.27	0.557	0.084	0.02	12	9.3	1.13	1	38.7	21.8
2/17/2012	1.97	12.0	0.636	0.441	0.034	0.02	14.2	9.9	2.4	1	52	23.7
3/9/2012	0.27	32.6	1.65	0.605	0.152	0.07	27.5	23.2	3.78	1	66.2	31.6
3/10/2012	0.27	8.1	0.569	0.412	0.056	0.02	7.47	8.2	1.38	1	23.7	19.6
3/11/2012	0.3	3.5	0.461	0.287	0.028	0.02	5.61	6.1	1	1	24.9	23.8
3/20/2012	2.52	10.9	0.812	0.212	0.12	0.068	10	8.2	1.54	1	30.3	20.5
5/11/2012	1.68	11.1	1.23	0.134	0.103	0.02	8.11	4.9	1	1	25.1	12.9
7/10/2012	0.85	14.7	1.53	0.39	0.2	0.104	25.1	19.2	2.51	1	45.8	22.9
7/11/2012	0.34	8.1	1.07	0.186	0.099	0.045	19.3	14.1	1	1	20.1	10.1
7/16/2012	1.04	17.9	0.806	0.246	0.077	0.027	10.9	6.6	1.08	1	23.3	10.6
9/16/2012	1.32	8.4	0.599	0.034	0.041	0.02	9.58	7.6	1	1	16.7	8.9
9/29/2012	0.47	27.7	1.98	0.02	0.163	0.028	23.1	16.4	3.37	1	49.7	25.1
10/11/2012	0.43	15.7	1.19	0.581	0.128	0.04	21.7	17.2	1.23	1	38.6	22.1

Constituent Concentrations at Camp Hubbard

Date	Rainfall	TSS	TKN	NO_3^-/NO_2^-	P_{total}	$P_{dissolved}$	Cu_{total}	$Cu_{dissolved}$	Pb_{total}	$Pb_{dissolved}$	Zn_{total}	$Zn_{dissolved}$
	(in)	(mg/L)	(mg/L)	(mg/L)	(µg/L)	(µg/L)	(µg/L)	(µg/L)	(µg/L)	(µg/L)	(µg/L)	(µg/L)
1/9/2011	1.78	11.6	1.23	0.302	0.059	0.023	17.6	12.2	3.46	1	134	96.8
1/14/2011	1.25	8.0	0.754	0.181	0.02	0.02	9.19	6	1.26	1	68.3	43.5
4/11/2011	0.25	42.0	3.5	0.762	0.349	0.3	49.3	39.9	6.49	1.3	364	306
5/20/2011	0.51	22.5	2.18	0.609	0.119	0.02	29.7	19.9	6.82	1	161	103
6/22/2011	1.74	27.9	2.14	0.408	0.243	0.124	33.8	28.6	4.82	1.0	265	210
10/8/2011	0.38	43.1	6.32	1.41	0.457	0.169	100	70.1	8.3	2.7	665	566
10/9/2011	1.43	38.0	0.891	0.1	0.102	0.02	14.7	9.3	8.98	1	113	57.7
11/15/2011	0.78	76.5	2.22	0.46	0.188	0.045	37.7	25.6	5.75	1	210	126
11/26/2011	0.96	11.8	0.967	0.18	0.057	0.02	11.1	9.4	1.85	1	71.3	51.3
12/2/2011	0.59	7.0	0.937	0.581	0.042	0.02	14	10.6	1.66	1	85.8	61.5
12/4/2011	0.75	10.3	0.386	0.246	0.038	0.02	6.19	4.8	2.4	1	53.7	31.3
12/5/2011	0.59	8.9	0.305	0.281	0.02	0.02	4.57	3.7	1.22	1	46.1	30
12/15/2011	0.39	15.8	0.803	0.301	0.06	0.02	14.9	8.8	2.61	1	91.3	51.9
12/16/2011	0.27	10.4	0.514	0.295	0.037	0.02	9.33	5.7	1.92	1	69.7	42.1
12/22/2011	0.97	8.7	0.414	0.086	0.032	0.023	5.69	3.2	1	1	42	21.7
1/9/2012	0.74	17.8	1.34	0.585	0.057	0.02	12.5	9.3	2.05	1	95	58.9
1/24/2012	3.23	34.0	0.798	0.197	0.064	0.02	10.3	5.1	3.23	1	84.2	27.3
2/4/2012	0.19	7.4	0.657	0.274	0.066	0.02	12.5	9.6	1	1	72.3	48.1
2/13/2012	0.21	7.1	1.07	0.675	0.04	0.02	10.6	8.3	1.25	1	62.4	44.8
2/17/2012	1.97	12.0	0.636	0.441	0.034	0.02	14.2	9.9	2.4	1	52	23.7
3/9/2012	0.27	27.5	2.13	0.668	0.168	0.068	29.9	21	6.1	1	165	78.7
3/10/2012	0.27	8.3	0.666	0.292	0.03	0.02	6.14	5.3	1.25	1	46.1	32
3/11/2012	0.3	4.0	0.357	0.389	0.02	0.02	3.83	4.4	1	1	34.3	31.5
3/20/2012	2.52	5.8	0.705	0.218	0.068	0.047	8.16	7.3	1.24	1	109	85.5
5/11/2012	1.68	35.5	0.982	0.103	0.137	0.02	10.6	3.6	4.95	1	79.3	20.4
7/10/2012	0.85	16.5	1.86	0.395	0.202	0.101	27.4	20.5	2.67	1	115	86.1
7/11/2012	0.34	8.6	1.17	0.37	0.096	0.02	18.4	13.4	1.52	1	70.5	50.8
7/16/2012	1.04	12.6	0.849	0.269	0.064	0.03	11.9	6.6	1.78	1	47.5	28.7
9/16/2012	1.32	76.0	2.48	0.574	0.407	0.183	30.2	11.9	9.57	1	151	42.4
9/29/2012	0.47	4.0	0.746	0.253	0.071	0.043	13.1	12.2	1	1	106	93.2
10/11/2012	0.43	25.6	1.42	0.0447	0.199	0.097	20.9	15.9	2.86	1	112	71.2

Appendix C: Time Series of Constituents at Camp Mabry

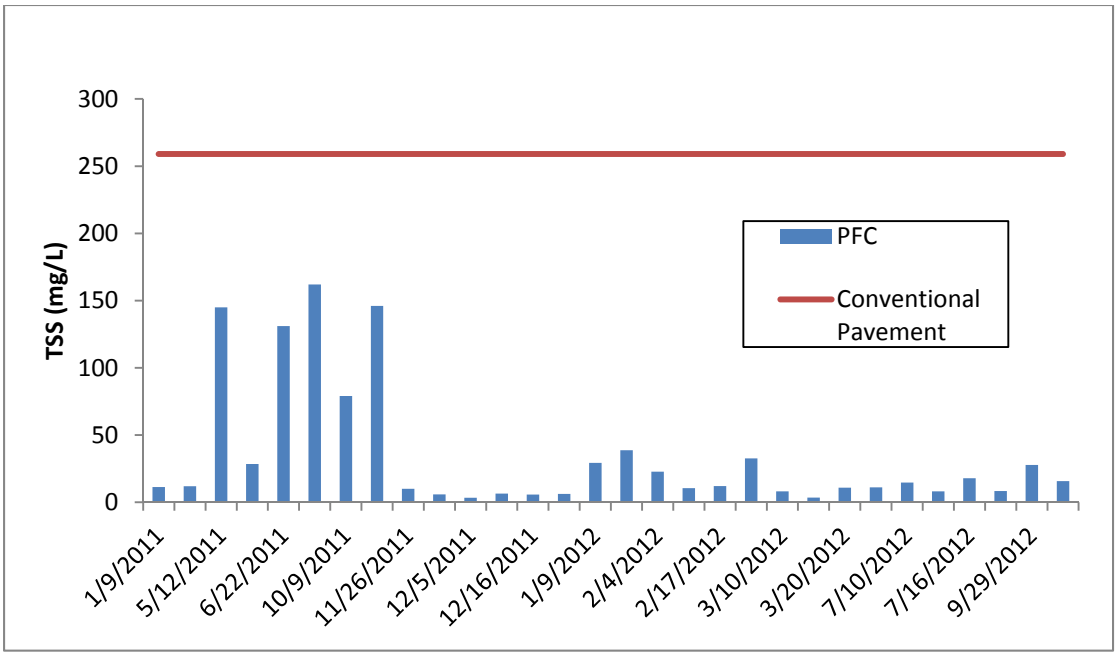

Figure C1. TSS at Camp Mabry

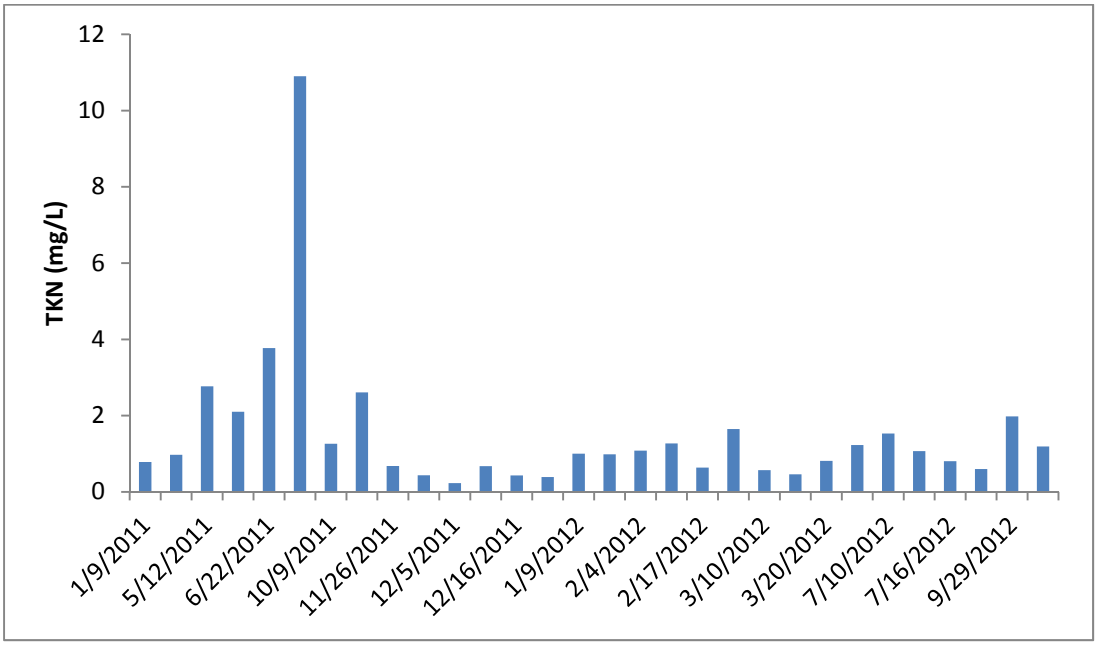

Figure C2. TKN at Camp Mabry

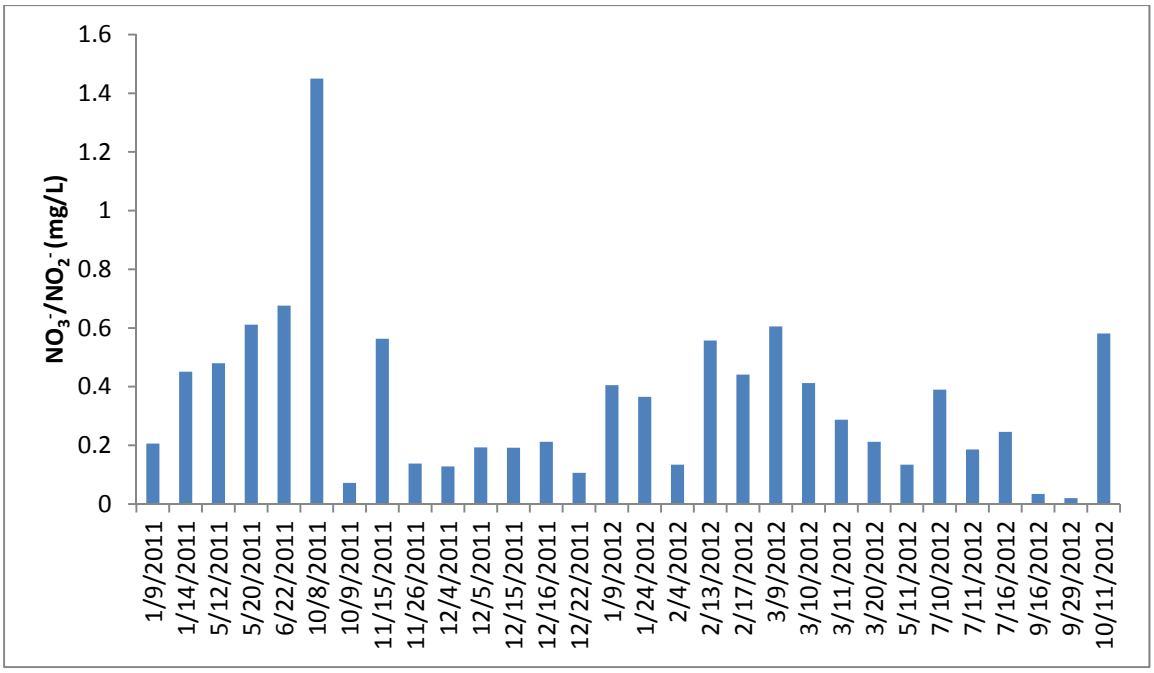

Figure C3. N03/N02 at Camp Mabry

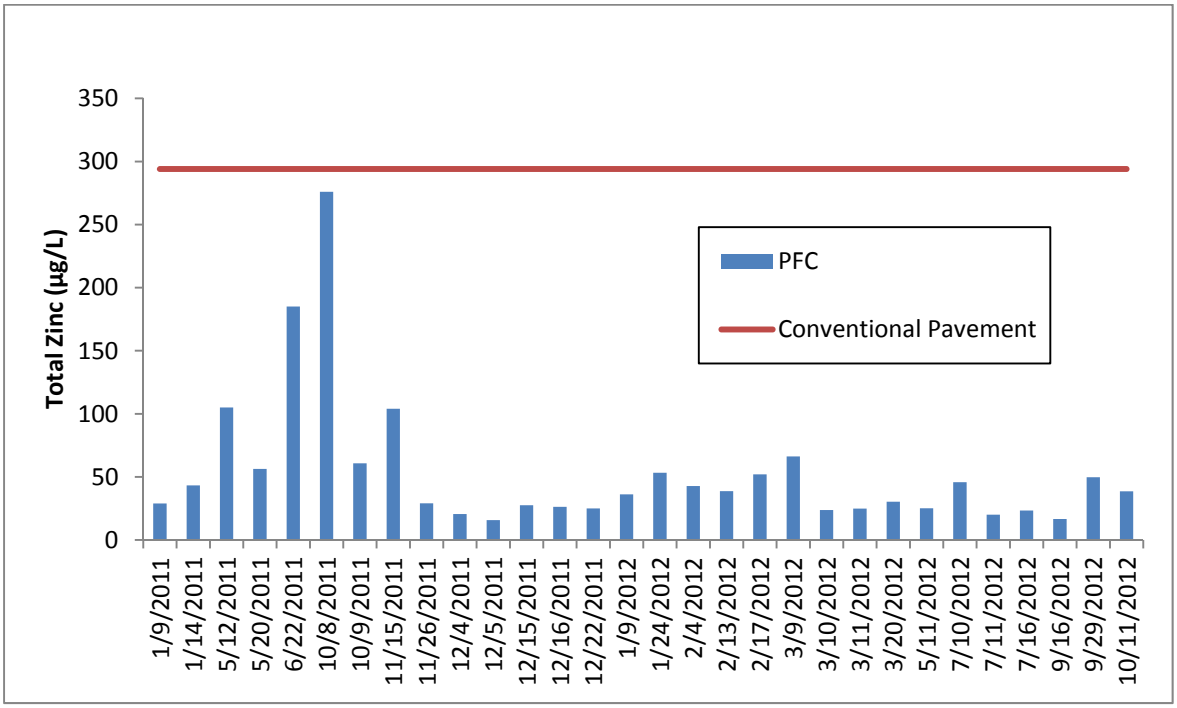

Figure C4. Total Zinc at Camp Mabry

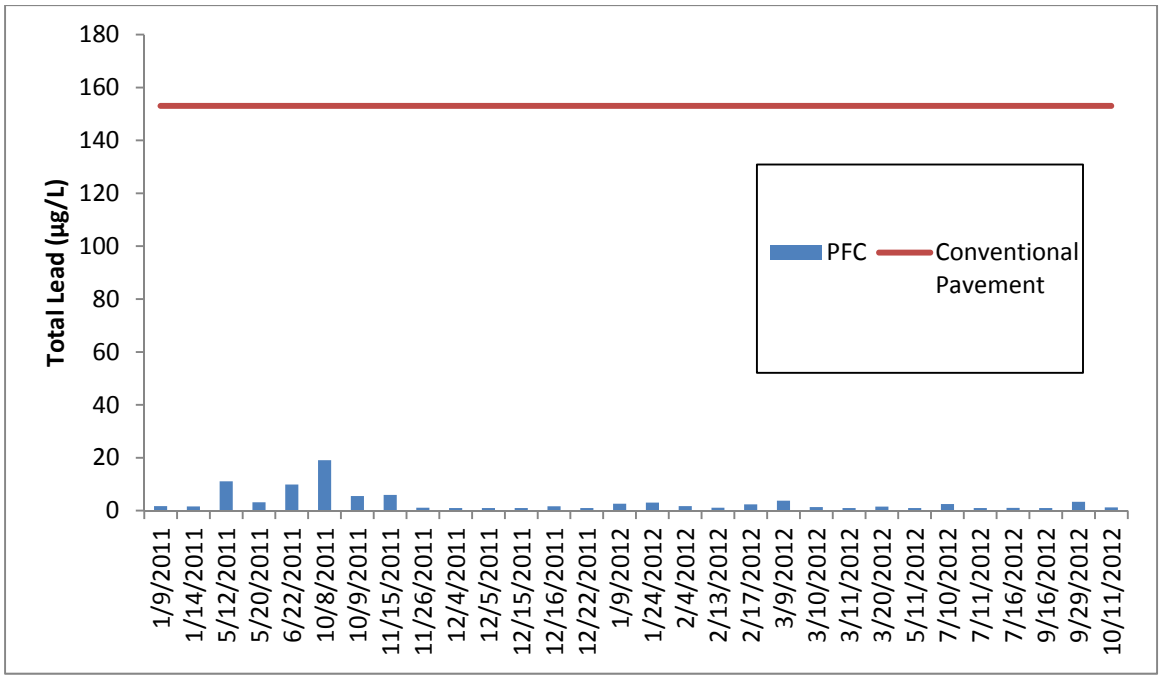

Figure C5. Total Lead at Camp Mabry

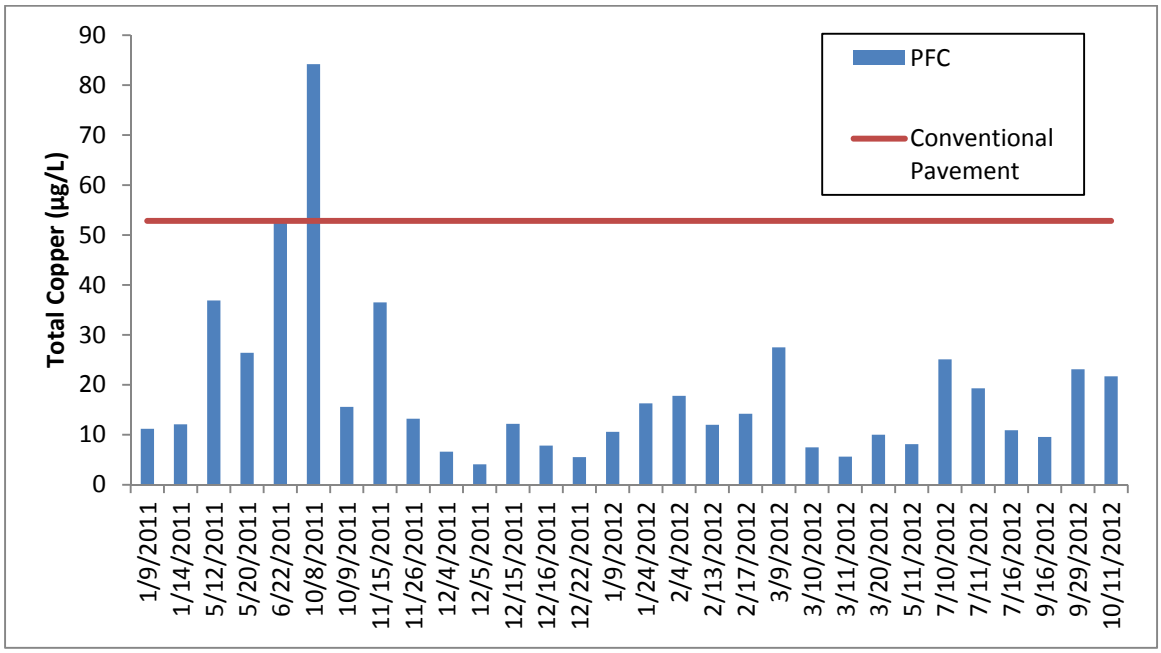

Figure C6. Total Copper at Camp Mabry

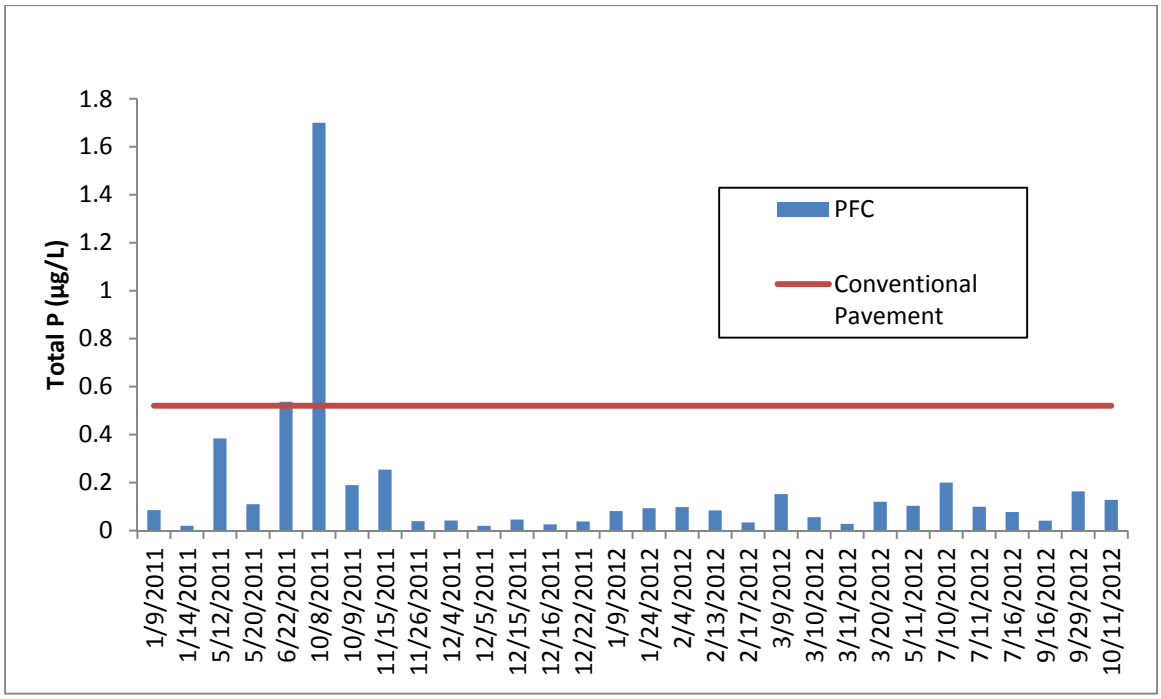

Figure C7. Total P at Camp Mabry

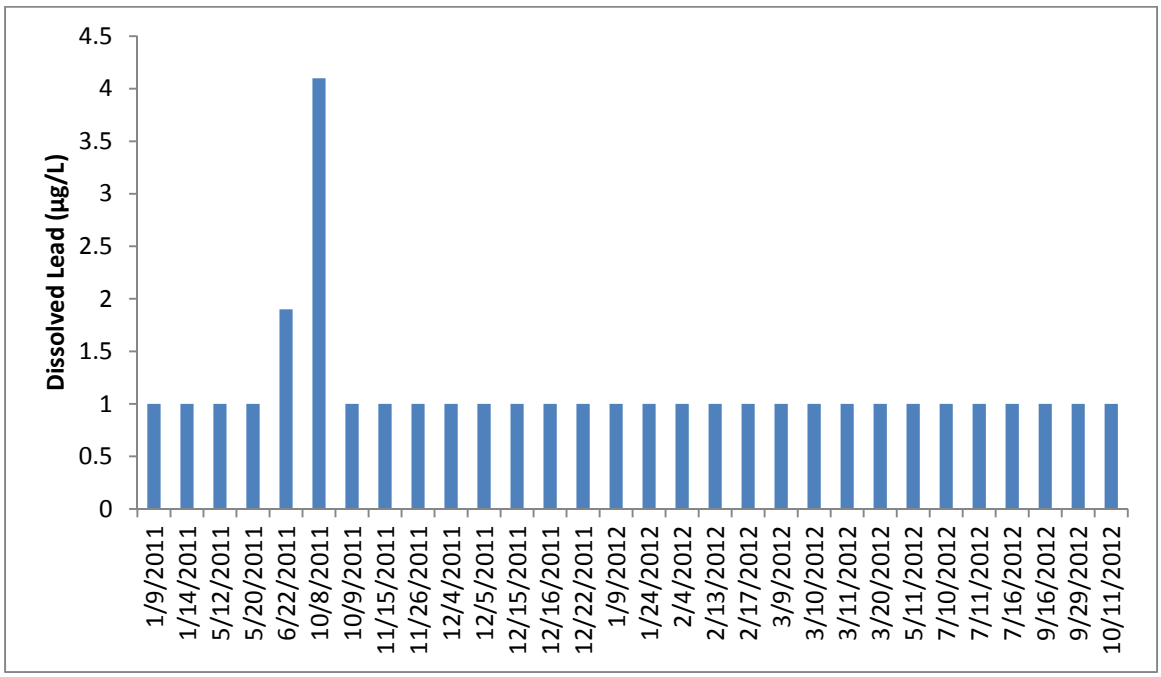

Figure C8. Dissolved Lead at Camp Mabry

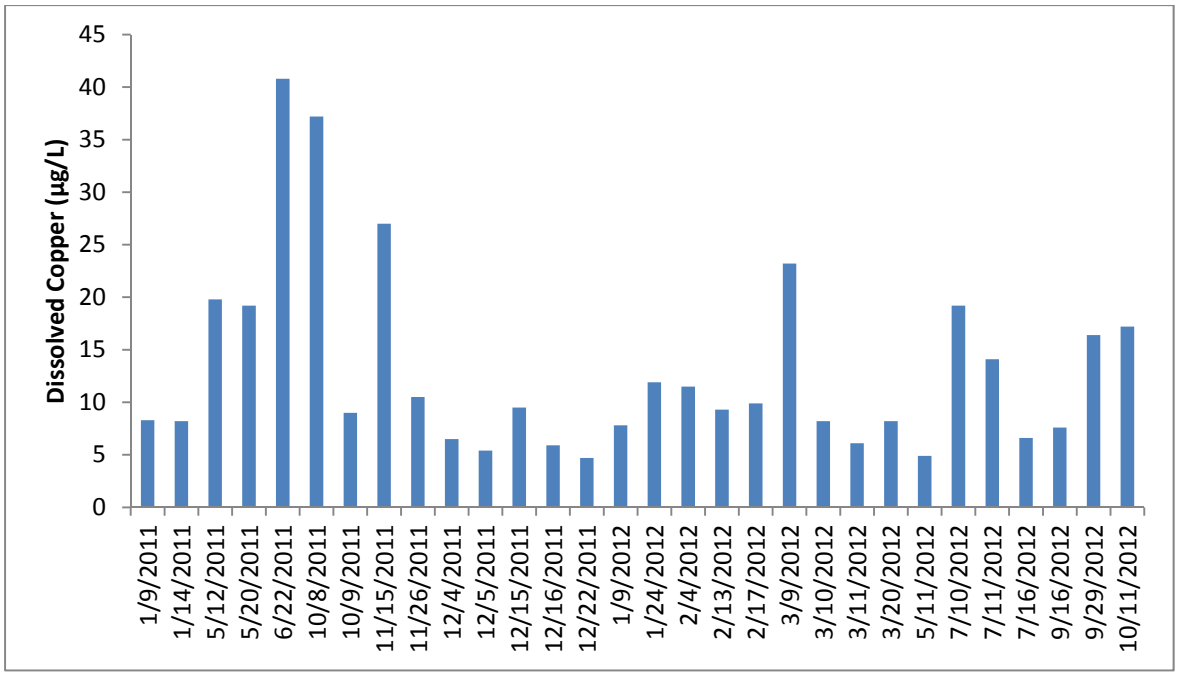

Figure C9. Dissolved Copper at Camp Mabry

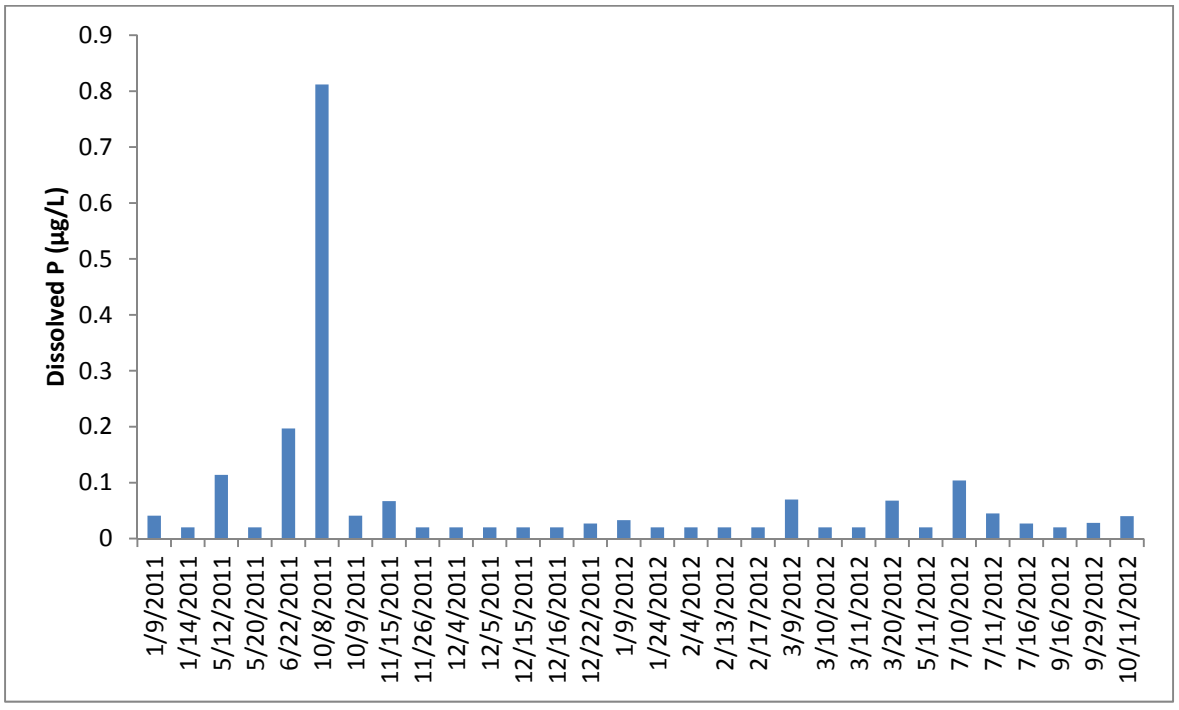

Figure C10. Dissolved P at Camp Mabry

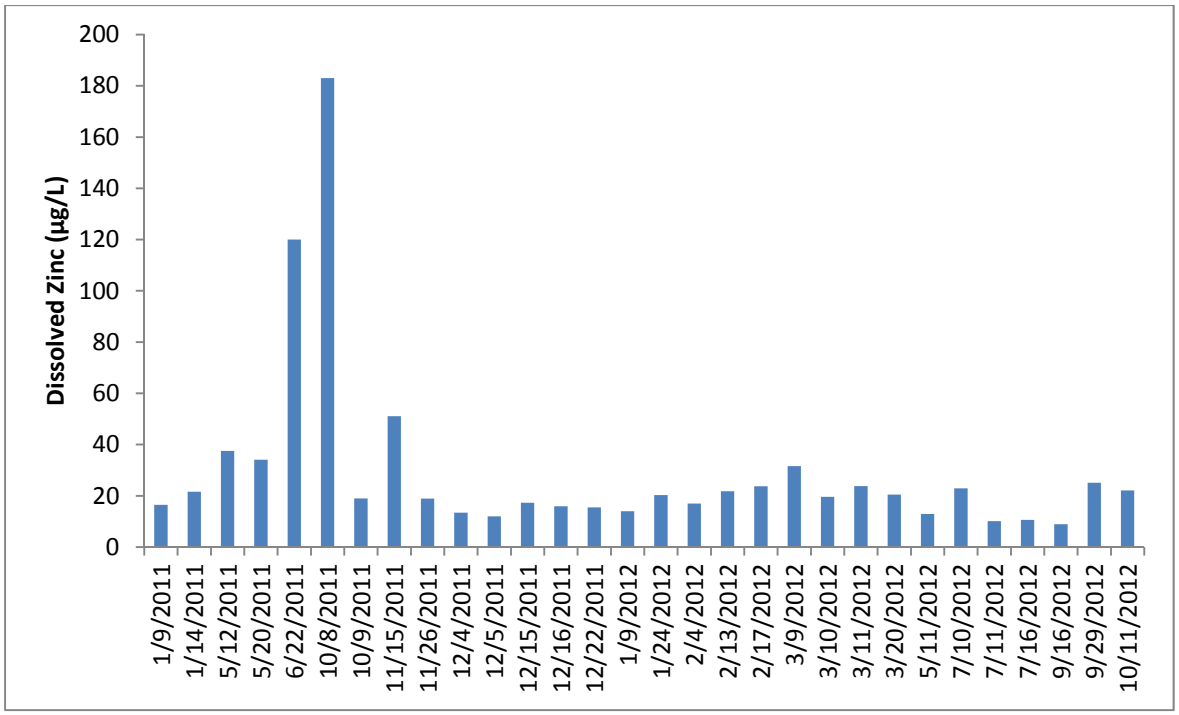

Figure C11. Dissolved Zinc at Camp Mabry

Appendix D: Time Series of Constituents at Camp Hubbard

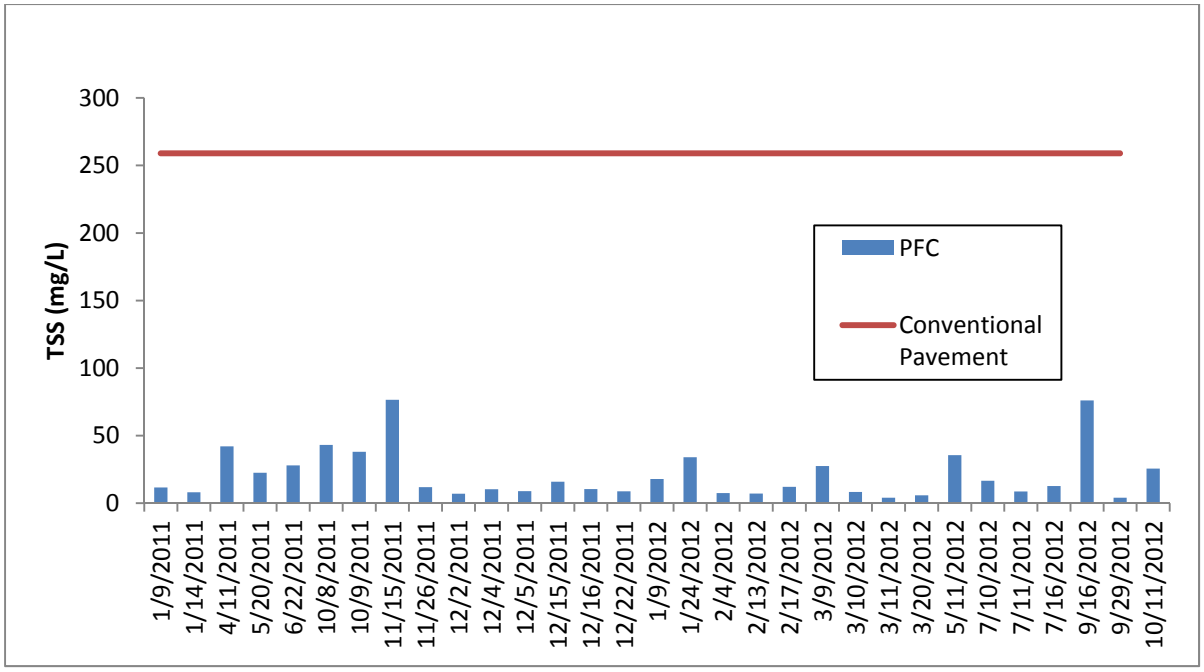

Figure D1. TSS at Camp Hubbard

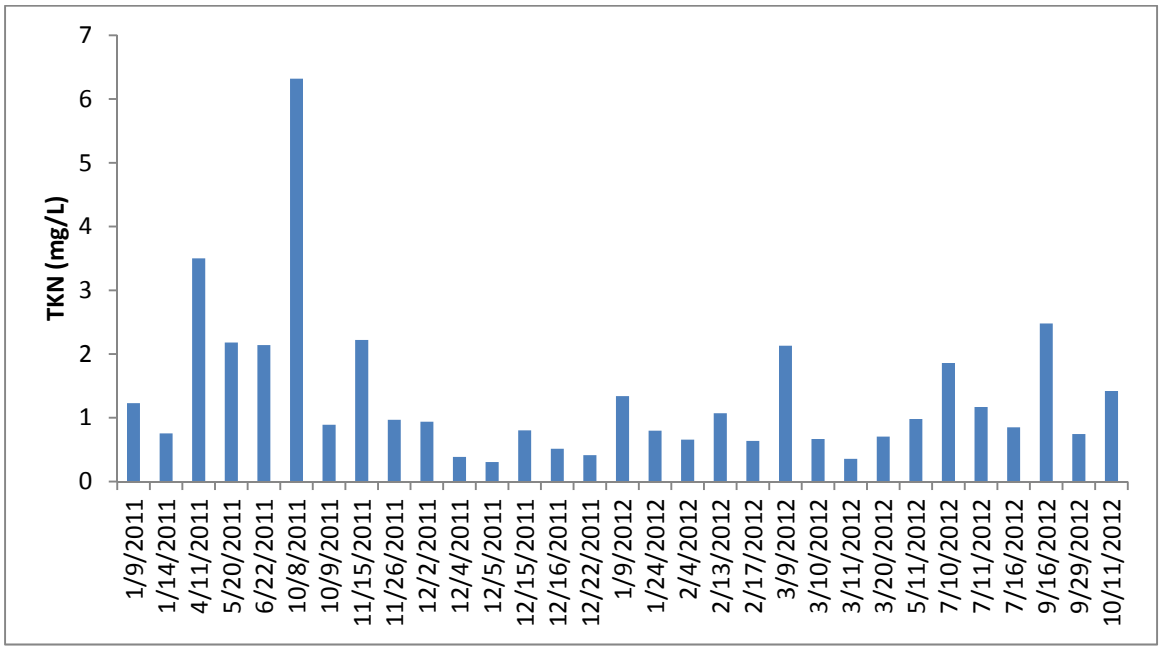

Figure D2. TKN at Camp Hubbard

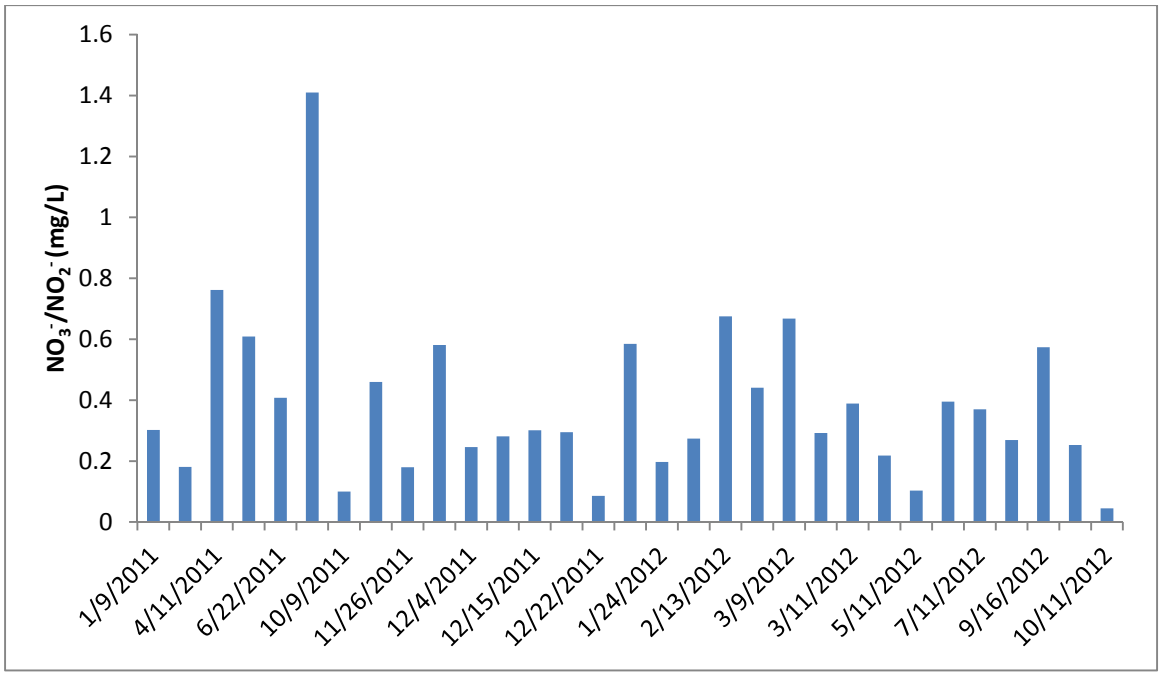

Figure D3. N03/N02 at Camp Hubbard

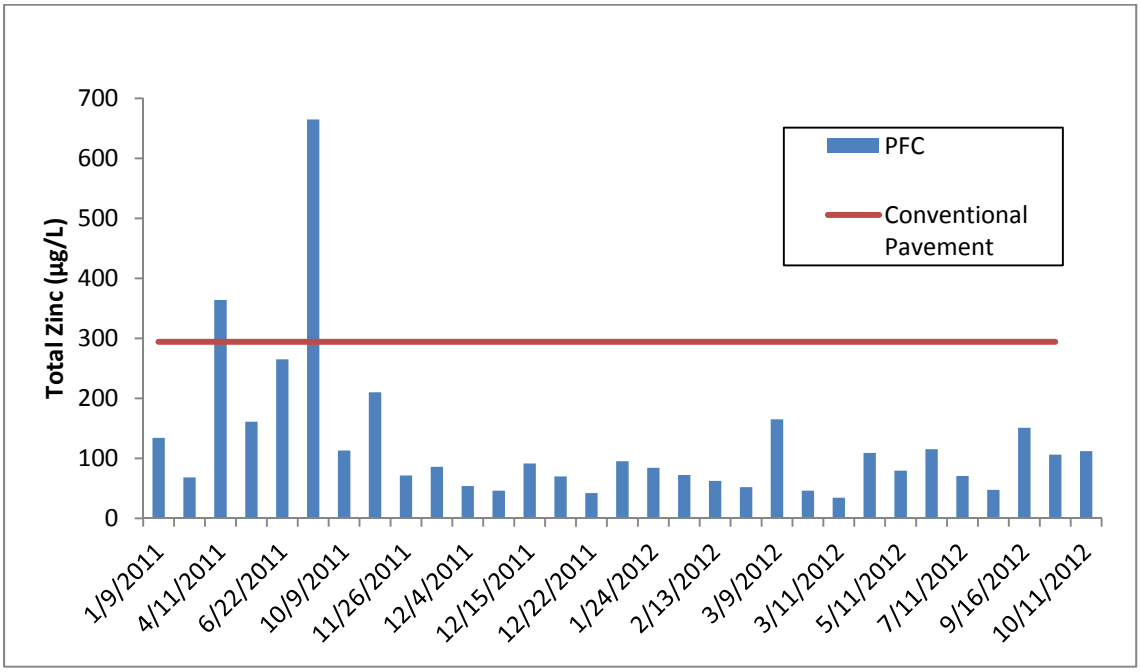

Figure D4. Total Zinc at Camp Hubbard

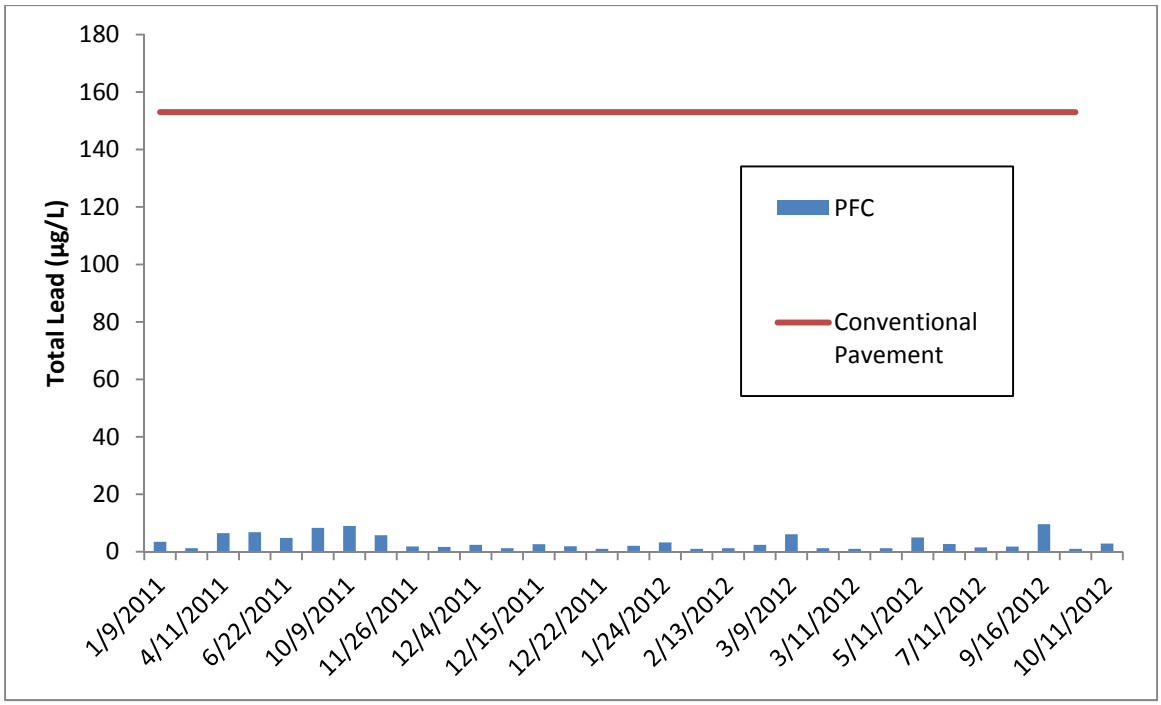

Figure D5. Total Lead at Camp Hubbard

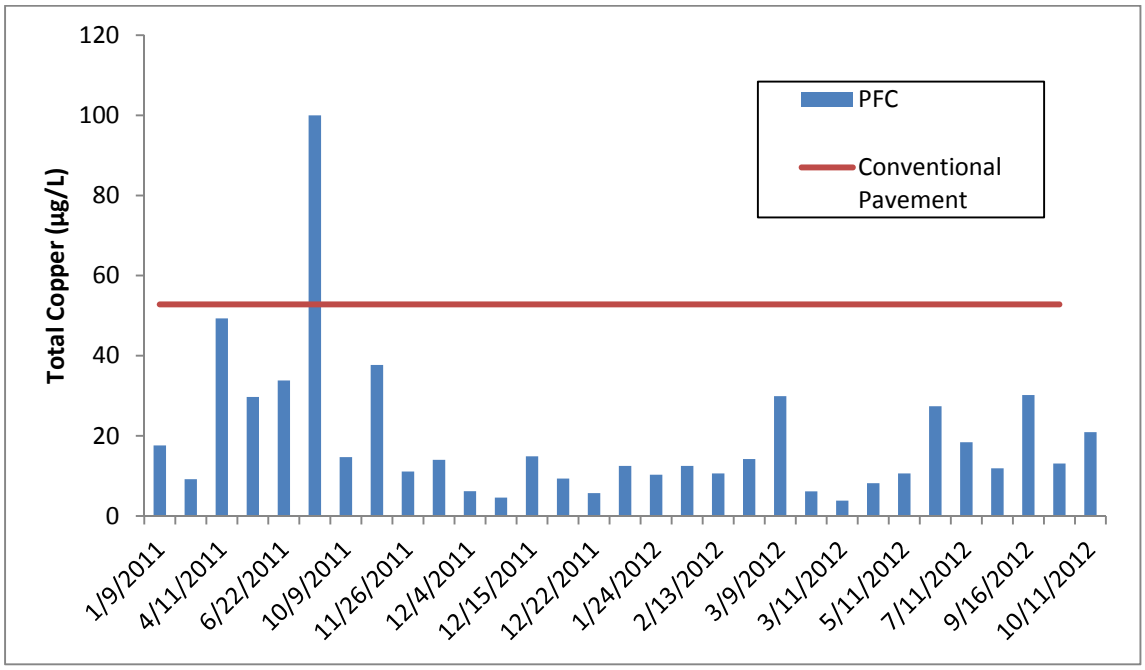

Figure D6. Total Copper at Camp Hubbard

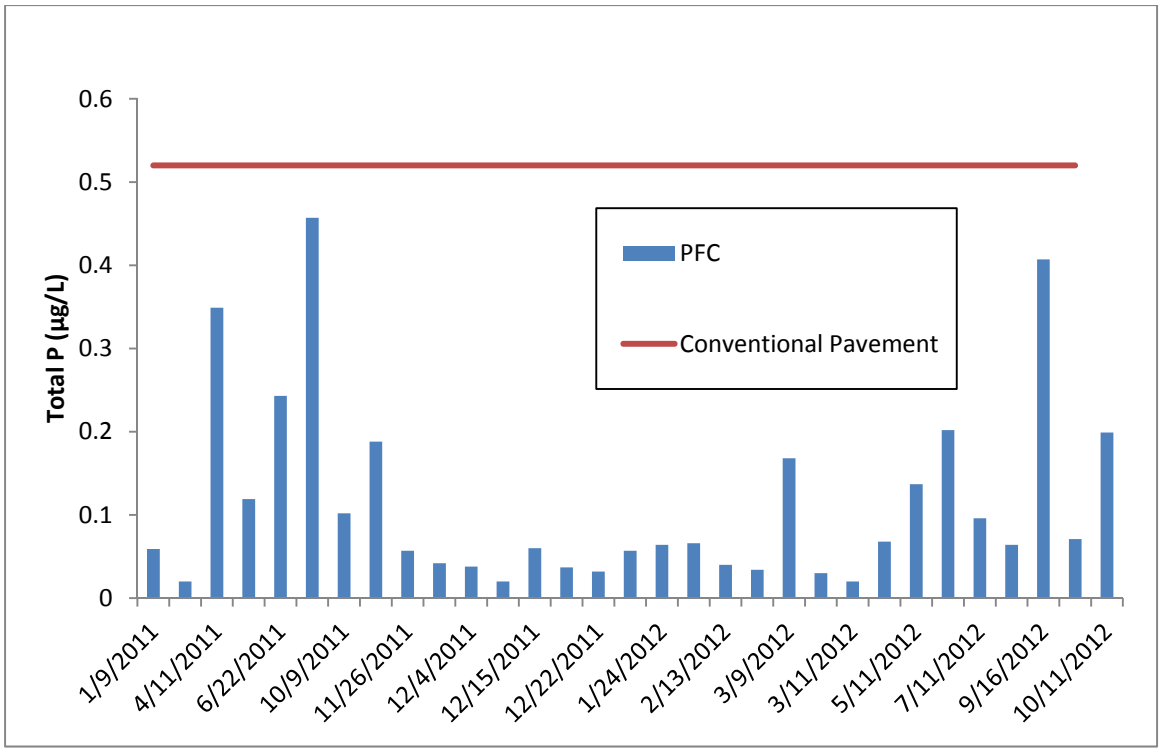

Figure D7. Total P at Camp Hubbard

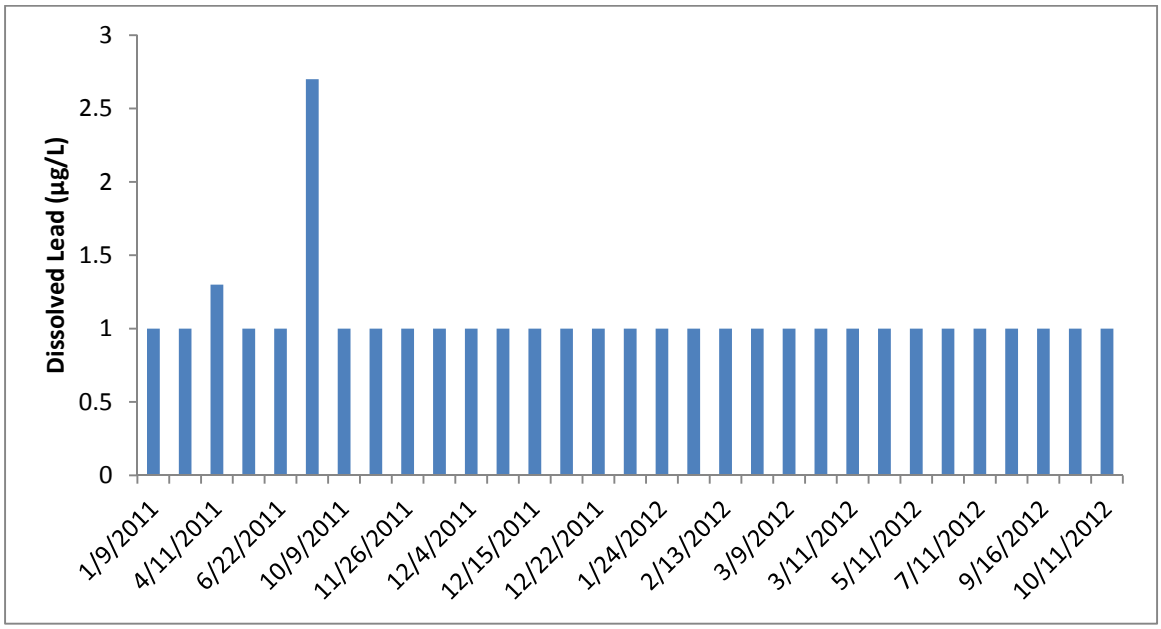

Figure D8. Dissolved Lead at Camp Hubbard

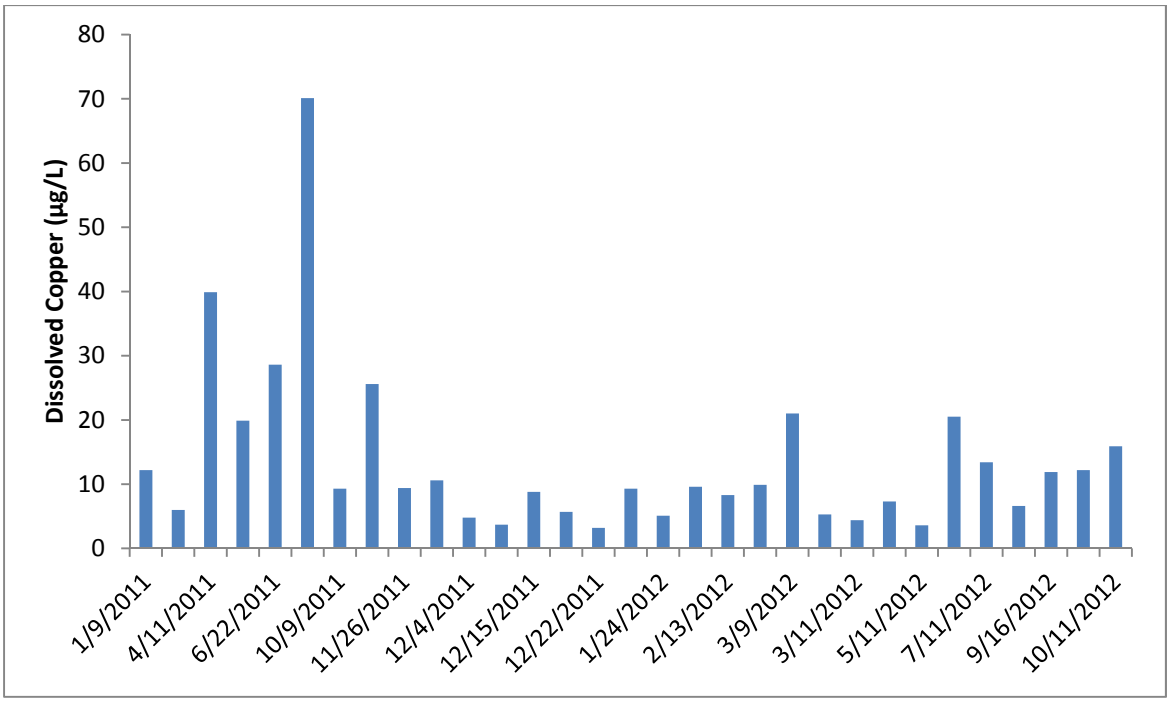

Figure D9. Dissolved Copper at Camp Hubbard

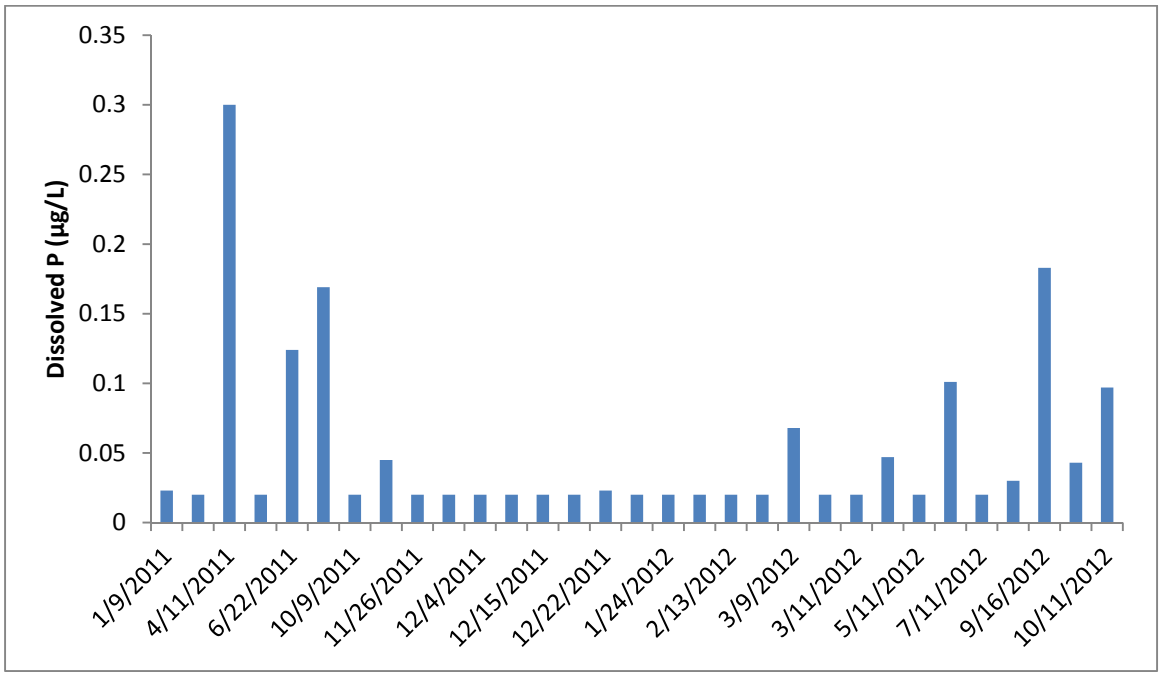

Figure D10. Dissolved P at Camp Hubbard

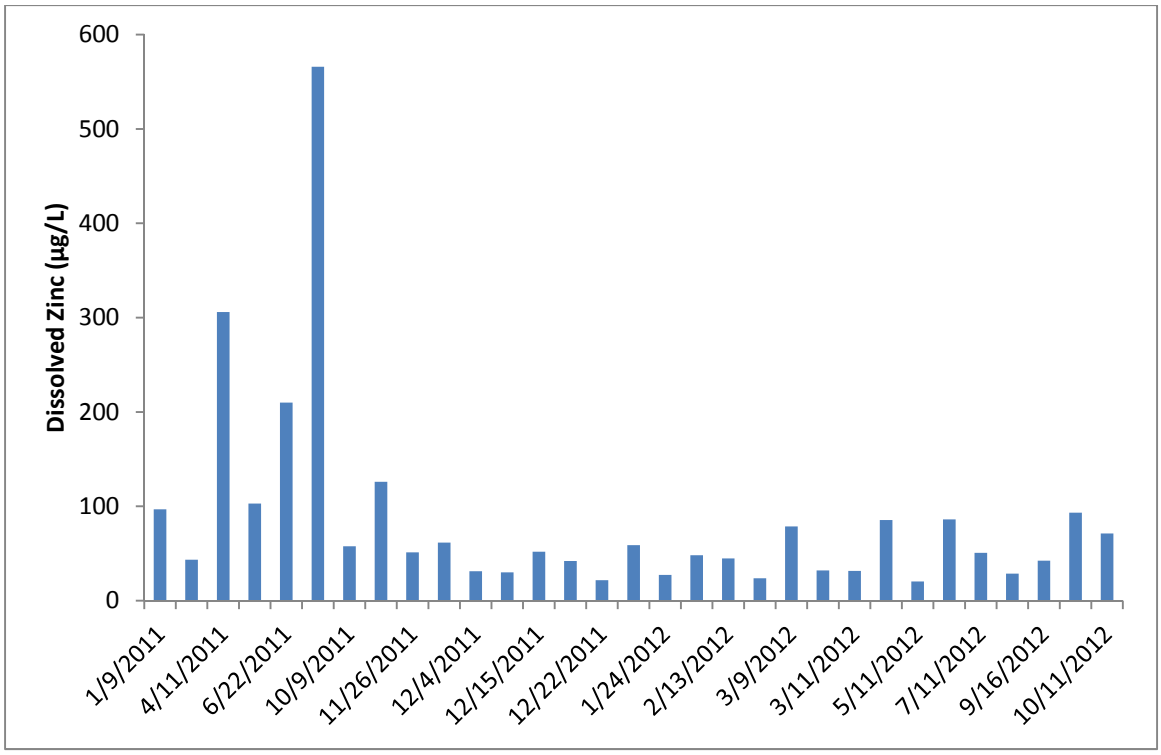

Figure D11. Dissolved Zinc at Camp Hubbard

Appendix E: Hydrographs for Each Monitored Rain Event

Camp Mabry Hydrographs

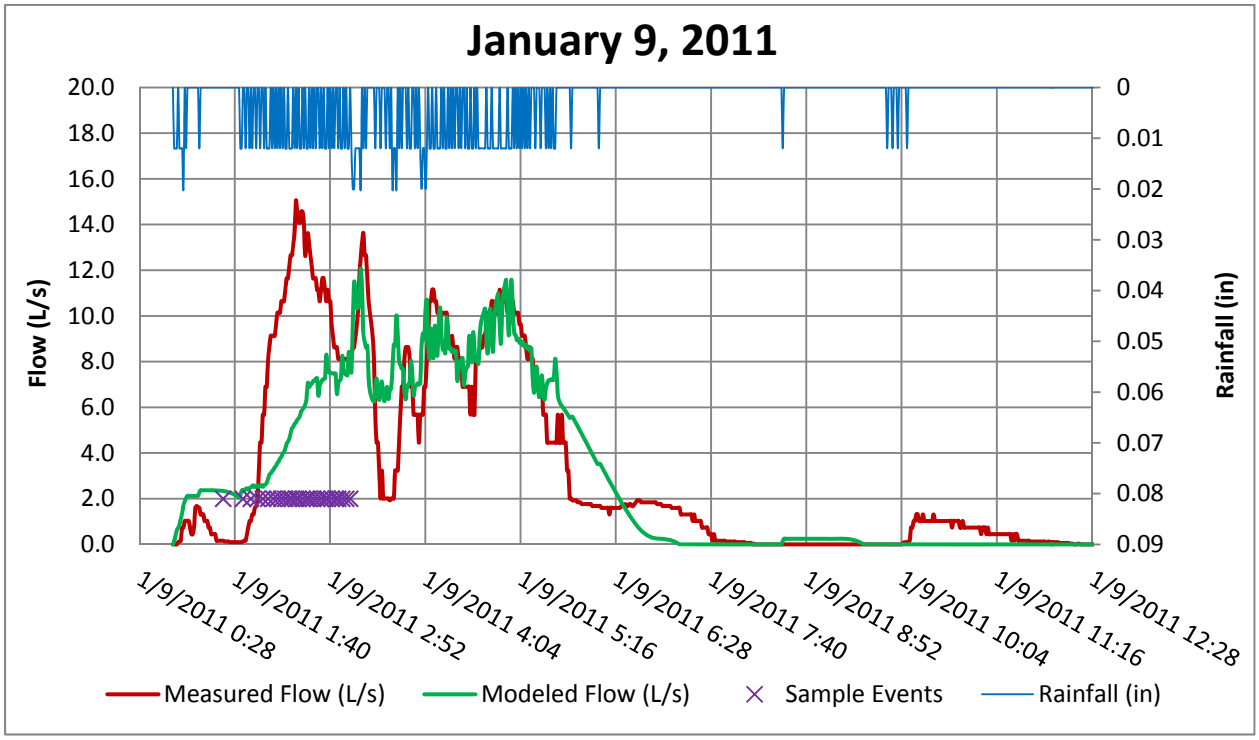

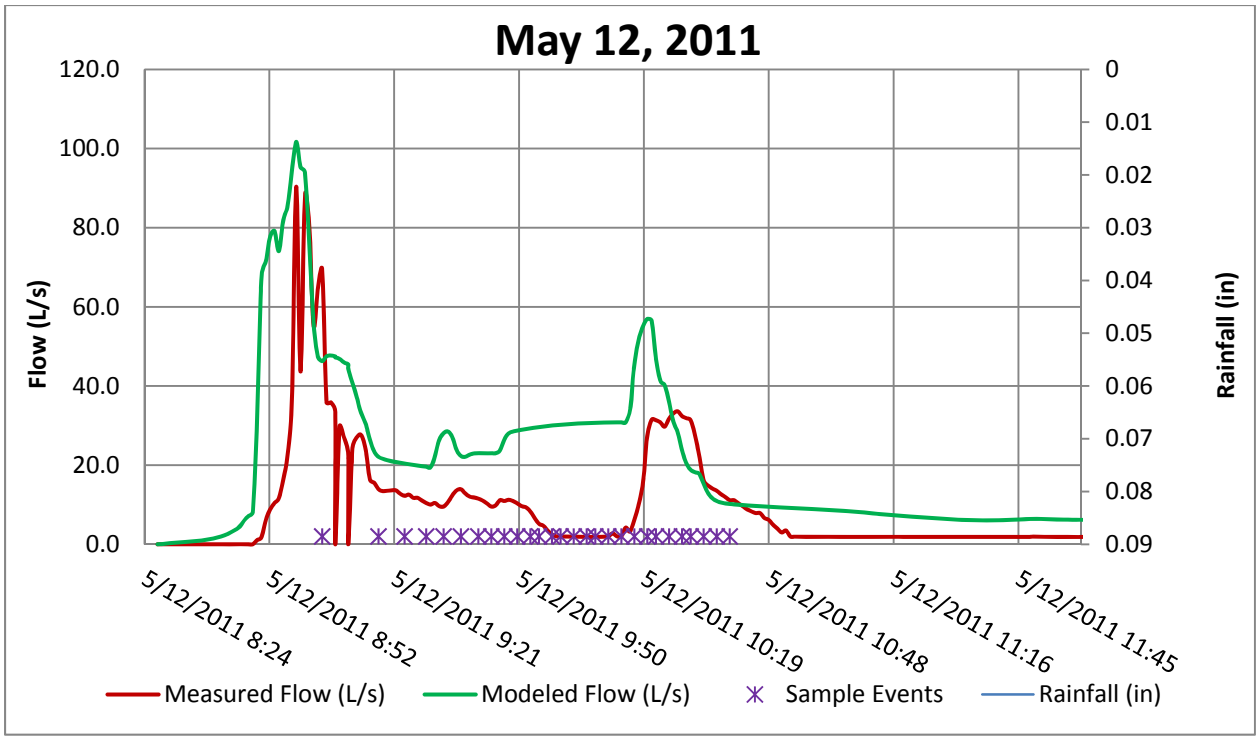
May 12, 2011
120.0
100.0
80.0
60.0
40.0
20.0
0.0
Flow (L/s)
0
0.01
0.02
0.03
0.04
0.05
0.06
0.07
0.08
0.09
Rainfall (in)
5/12/2011 8:24
5/12/2011 8:52
5/12/2011 9:21
5/12/2011 9:50
5/12/2011 10:19
5/12/2011 10:48
5/12/2011 11:16
5/12/2011 11:45
Measured Flow (L/s)
Modeled Flow (L/s)
Sample Events
Rainfall (in)

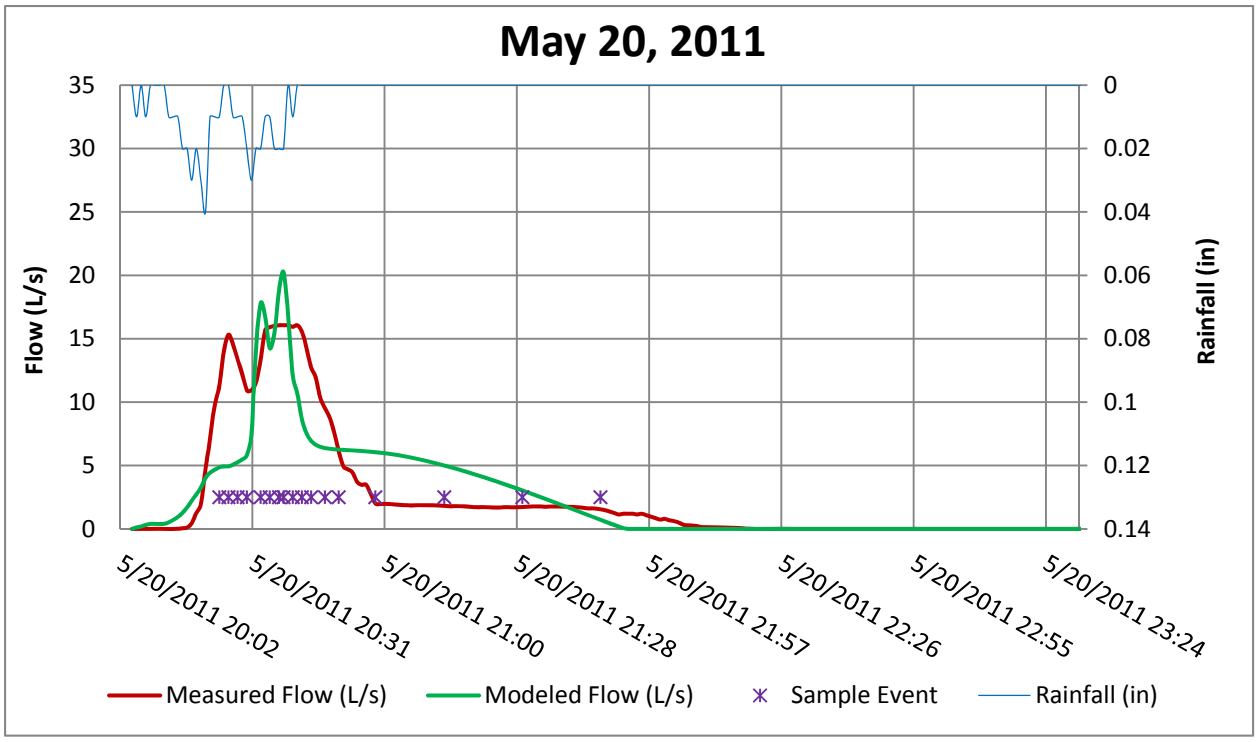
May 20, 2011
35
30
25
20
15
10
5
0
Flow (L/s)
0
0.02
0.04
0.06
0.08
0.1
0.12
0.14
Rainfall (in)
5/20/2011 20:02
5/20/2011 20:31
5/20/2011 21:00
5/20/2011 21:28
5/20/2011 21:57
5/20/2011 22:26
5/20/2011 22:55
5/20/2011 23:24
Measured Flow (L/s)
Modeled Flow (L/s)
Sample Event
Rainfall (in)

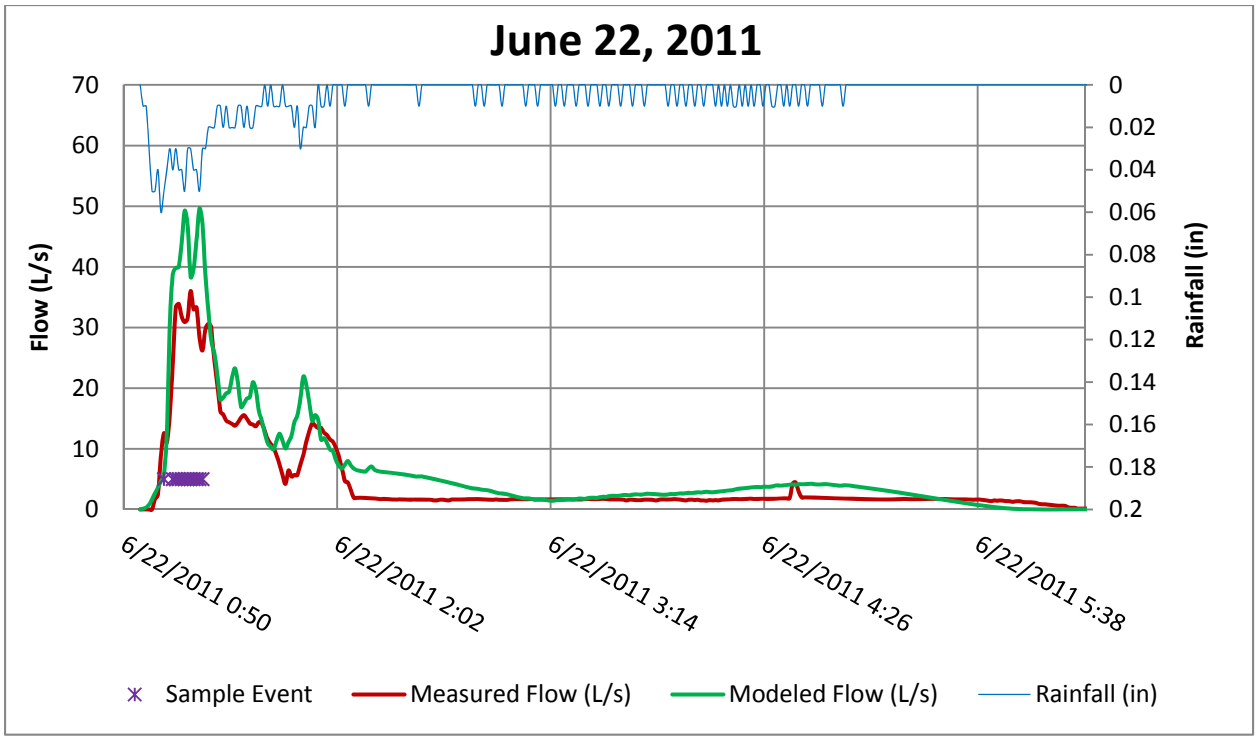
June 22, 2011
Flow (L/s)
Rainfall (in)
70
60
50
40
30
20
10
0
0
0.02
0.04
0.06
0.08
0.1
0.12
0.14
0.16
0.18
0.2
6/22/2011 0:50
6/22/2011 2:02
6/22/2011 3:14
6/22/2011 4:26
6/22/2011 5:38
Sample Event
Measured Flow (L/s)
Modeled Flow (L/s)
Rainfall (in)

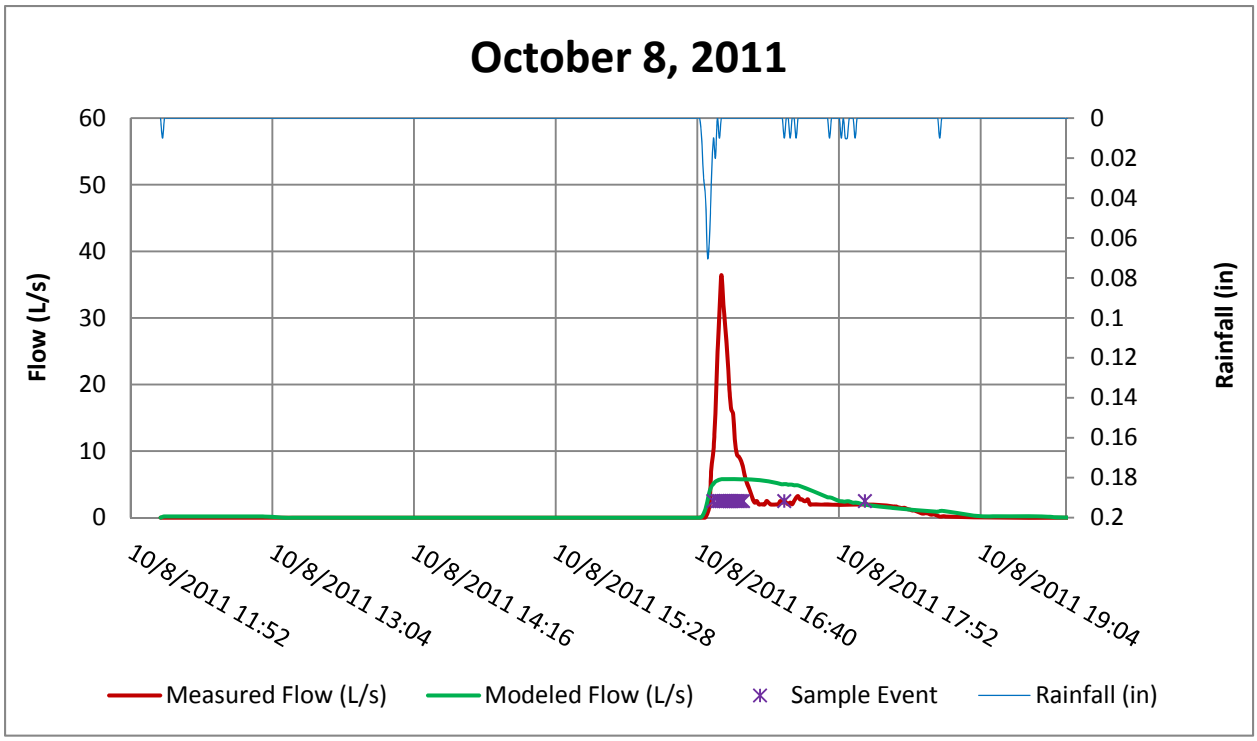
October 8, 2011
Flow (L/s)
Rainfall (in)
60
50
40
30
20
10
0
0
0.02
0.04
0.06
0.08
0.1
0.12
0.14
0.16
0.18
0.2
10/8/2011 11:52
10/8/2011 13:04
10/8/2011 14:16
10/8/2011 15:28
10/8/2011 16:40
10/8/2011 17:52
10/8/2011 19:04
Measured Flow (L/s)
Modeled Flow (L/s)
Sample Event
Rainfall (in)

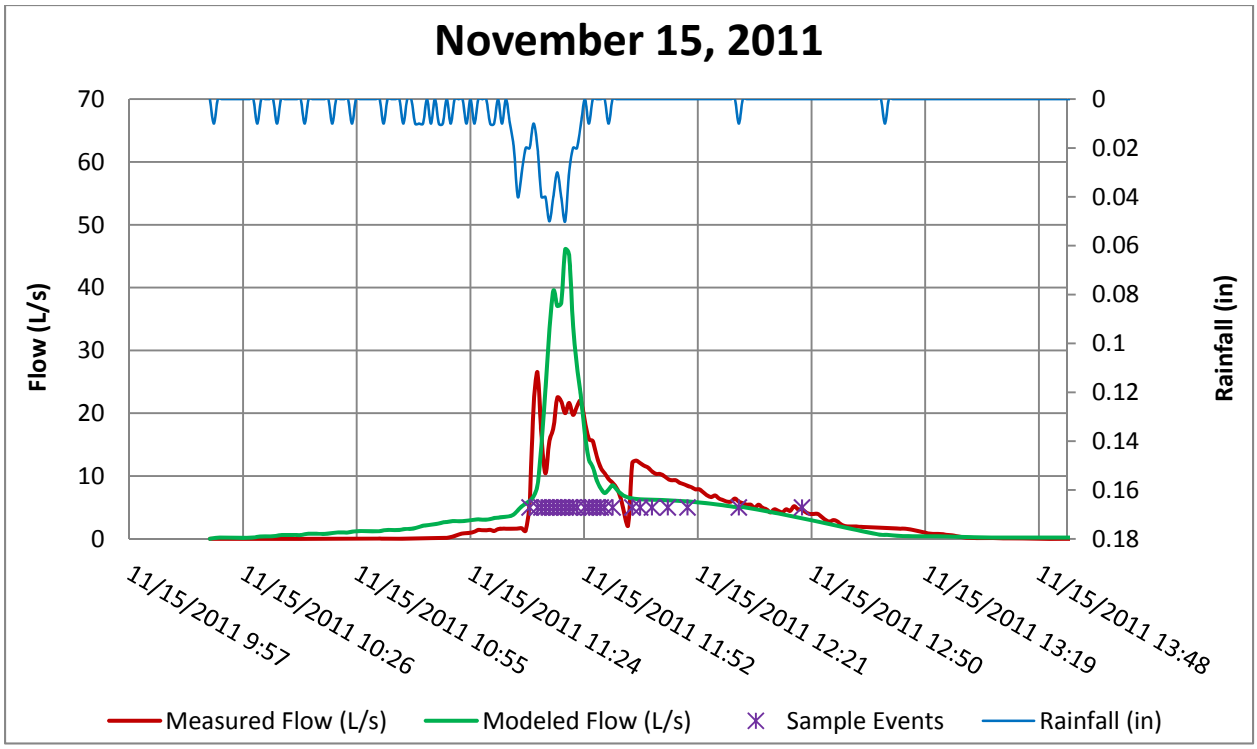
November 15, 2011
Flow (L/s)
Rainfall (in)
70
60
50
40
30
20
10
0
0
0.02
0.04
0.06
0.08
0.1
0.12
0.14
0.16
0.18
11/15/2011 9:57
11/15/2011 10:26
11/15/2011 10:55
11/15/2011 11:24
11/15/2011 11:52
11/15/2011 12:21
11/15/2011 12:50
11/15/2011 13:19
11/15/2011 13:48
Measured Flow (L/s)
Modeled Flow (L/s)
Sample Events
Rainfall (in)

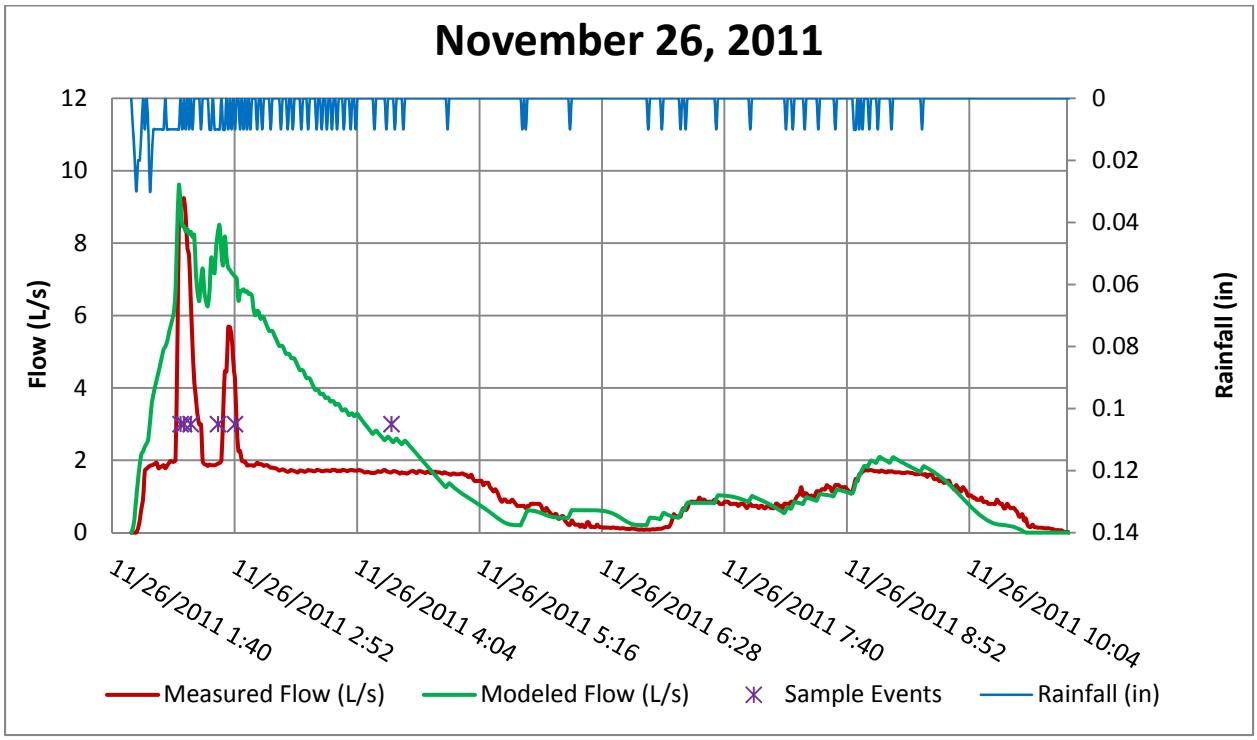
November 26, 2011
Flow (L/s)
Rainfall (in)
12
10
8
6
4
2
0
0
0.02
0.04
0.06
0.08
0.1
0.12
0.14
11/26/2011 1:40
11/26/2011 2:52
11/26/2011 4:04
11/26/2011 5:16
11/26/2011 6:28
11/26/2011 7:40
11/26/2011 8:52
11/26/2011 10:04
Measured Flow (L/s)
Modeled Flow (L/s)
Sample Events
Rainfall (in)

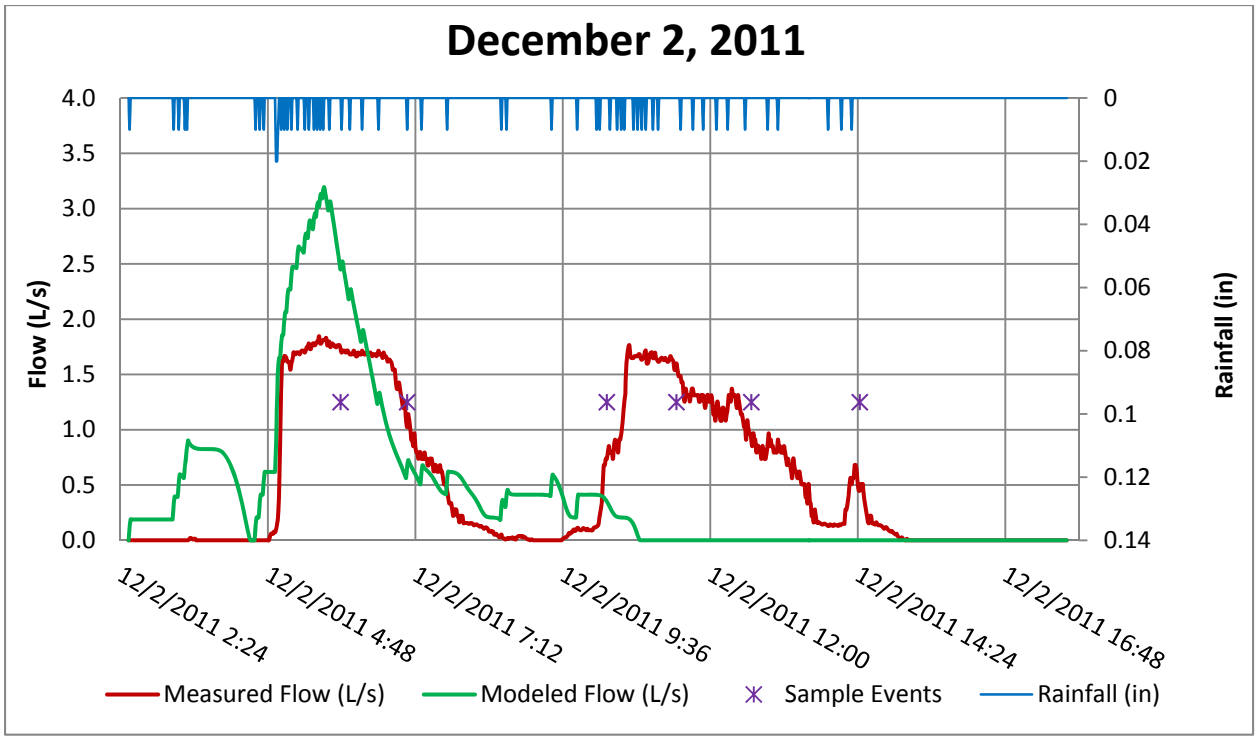
December 2, 2011
Flow (L/s)
Rainfall (in)
4.0
3.5
3.0
2.5
2.0
1.5
1.0
0.5
0.0
0
0.02
0.04
0.06
0.08
0.1
0.12
0.14
12/2/2011 2:24
12/2/2011 4:48
12/2/2011 7:12
12/2/2011 9:36
12/2/2011 12:00
12/2/2011 14:24
12/2/2011 16:48
Measured Flow (L/s)
Modeled Flow (L/s)
Sample Events
Rainfall (in)

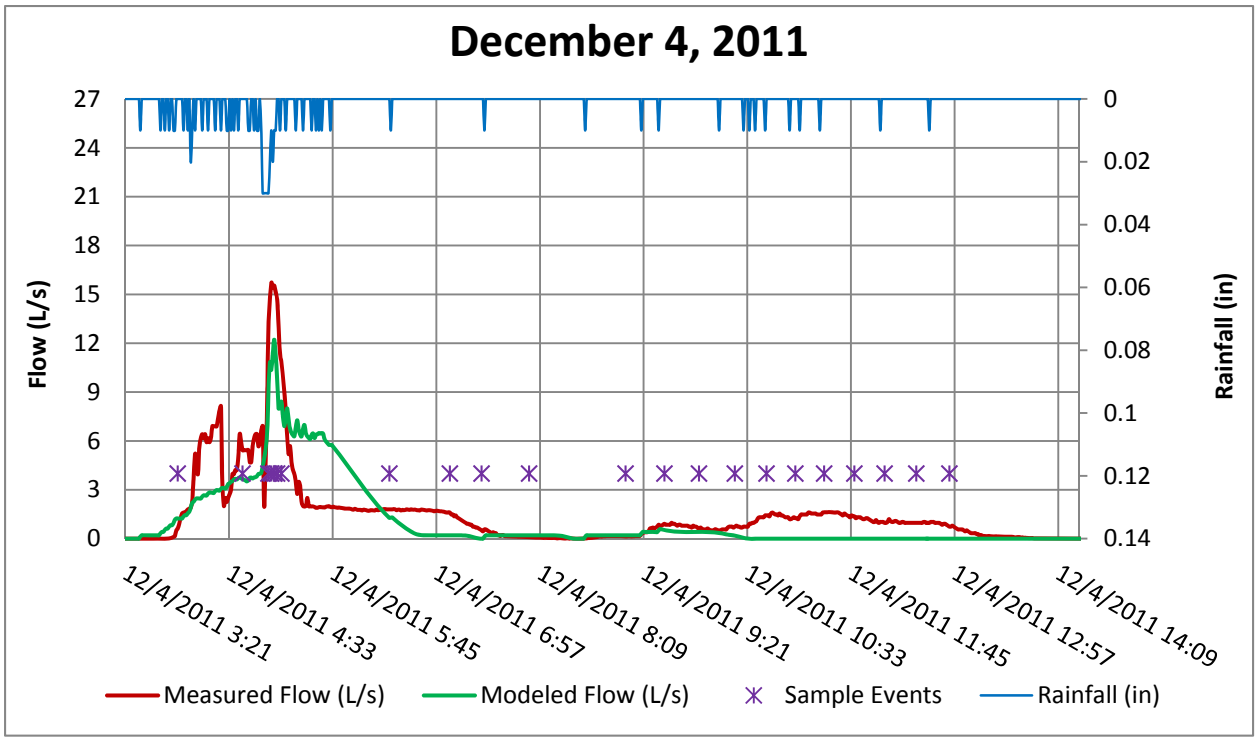
December 4, 2011
Flow (L/s)
Rainfall (in)
27
24
21
18
15
12
9
6
3
0
0
0.02
0.04
0.06
0.08
0.1
0.12
0.14
12/4/2011 3:21
12/4/2011 4:33
12/4/2011 5:45
12/4/2011 6:57
12/4/2011 8:09
12/4/2011 9:21
12/4/2011 10:33
12/4/2011 11:45
12/4/2011 12:57
12/4/2011 14:09
Measured Flow (L/s)
Modeled Flow (L/s)
Sample Events
Rainfall (in)

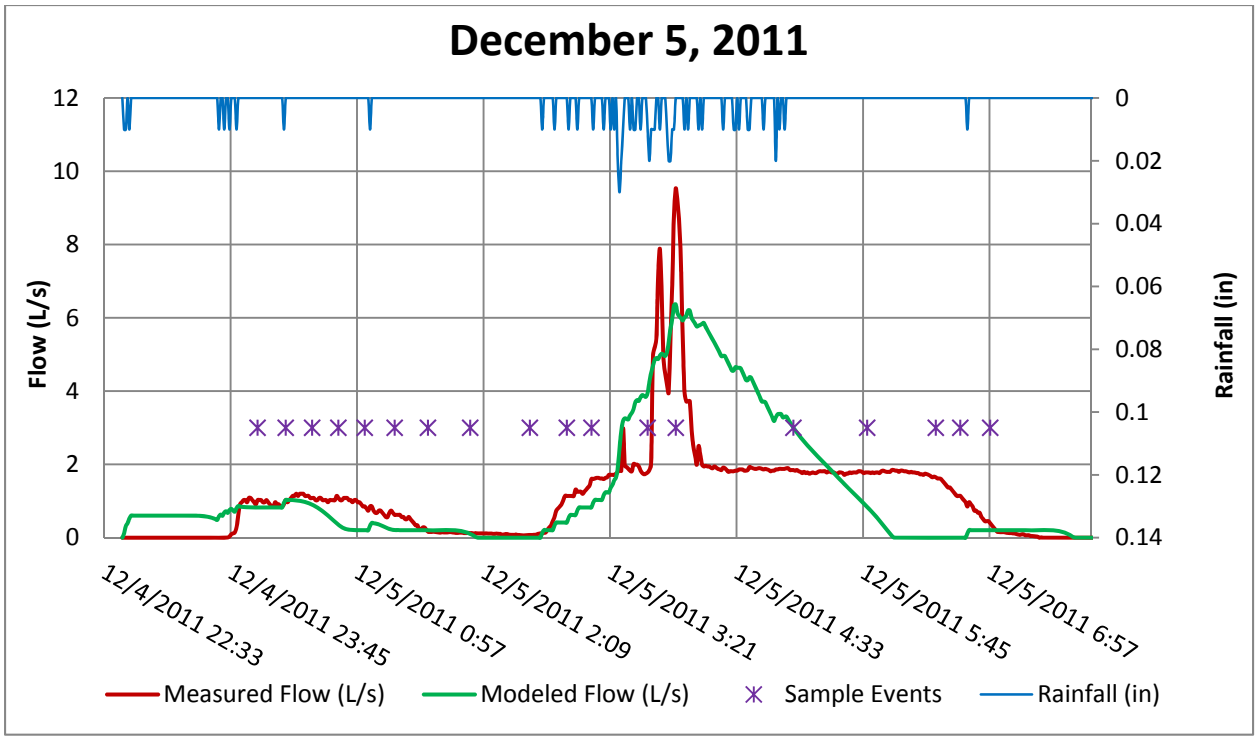
December 5, 2011
Flow (L/s)
Rainfall (in)
12
10
8
6
4
2
0
0
0.02
0.04
0.06
0.08
0.1
0.12
0.14
12/4/2011 22:33
12/4/2011 23:45
12/5/2011 0:57
12/5/2011 2:09
12/5/2011 3:21
12/5/2011 4:33
12/5/2011 5:45
12/5/2011 6:57
Measured Flow (L/s)
Modeled Flow (L/s)
Sample Events
Rainfall (in)

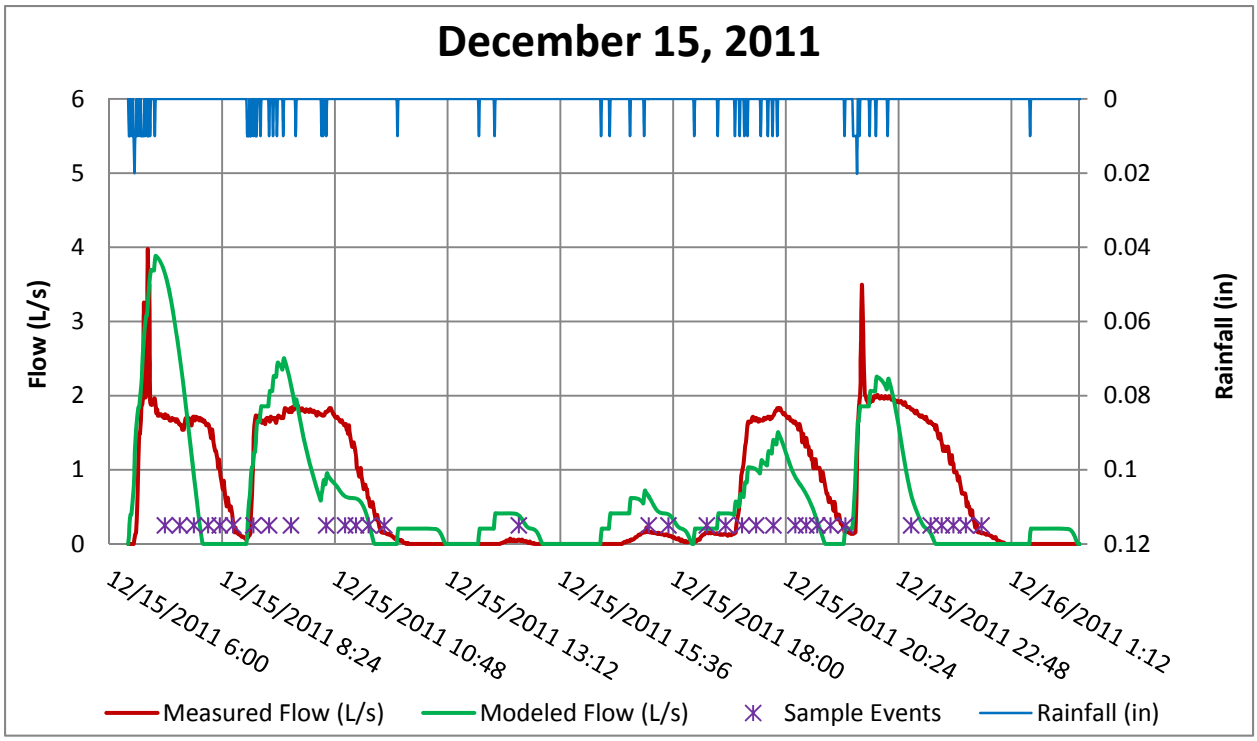
December 15, 2011
Flow (L/s)
Rainfall (in)
6
5
4
3
2
1
0
0
0.02
0.04
0.06
0.08
0.1
0.12
12/15/2011 6:00
12/15/2011 8:24
12/15/2011 10:48
12/15/2011 13:12
12/15/2011 15:36
12/15/2011 18:00
12/15/2011 20:24
12/15/2011 22:48
12/16/2011 1:12
Measured Flow (L/s)
Modeled Flow (L/s)
Sample Events
Rainfall (in)

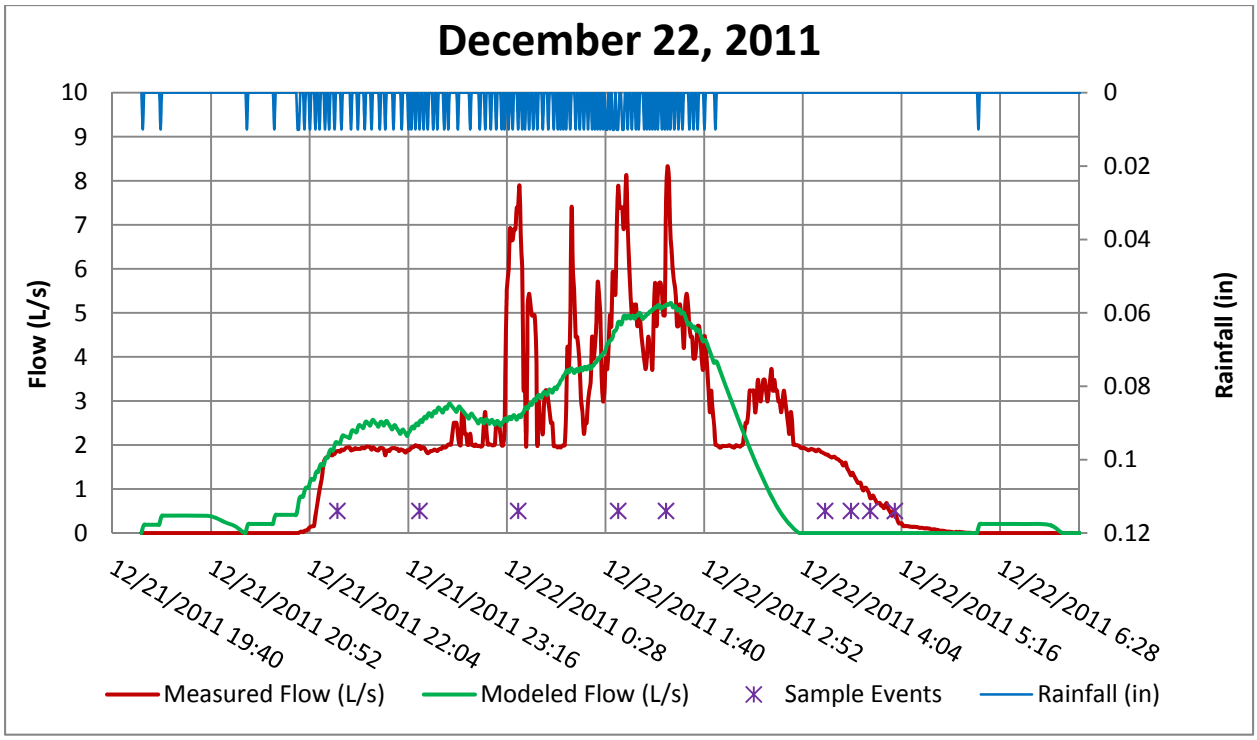
December 22, 2011
Flow (L/s)
Rainfall (in)
10
9
8
7
6
5
4
3
2
1
0
0
0.02
0.04
0.06
0.08
0.1
0.12
12/21/2011 19:40
12/21/2011 20:52
12/21/2011 22:04
12/21/2011 23:16
12/22/2011 0:28
12/22/2011 1:40
12/22/2011 2:52
12/22/2011 4:04
12/22/2011 5:16
12/22/2011 6:28
Measured Flow (L/s)
Modeled Flow (L/s)
Sample Events
Rainfall (in)

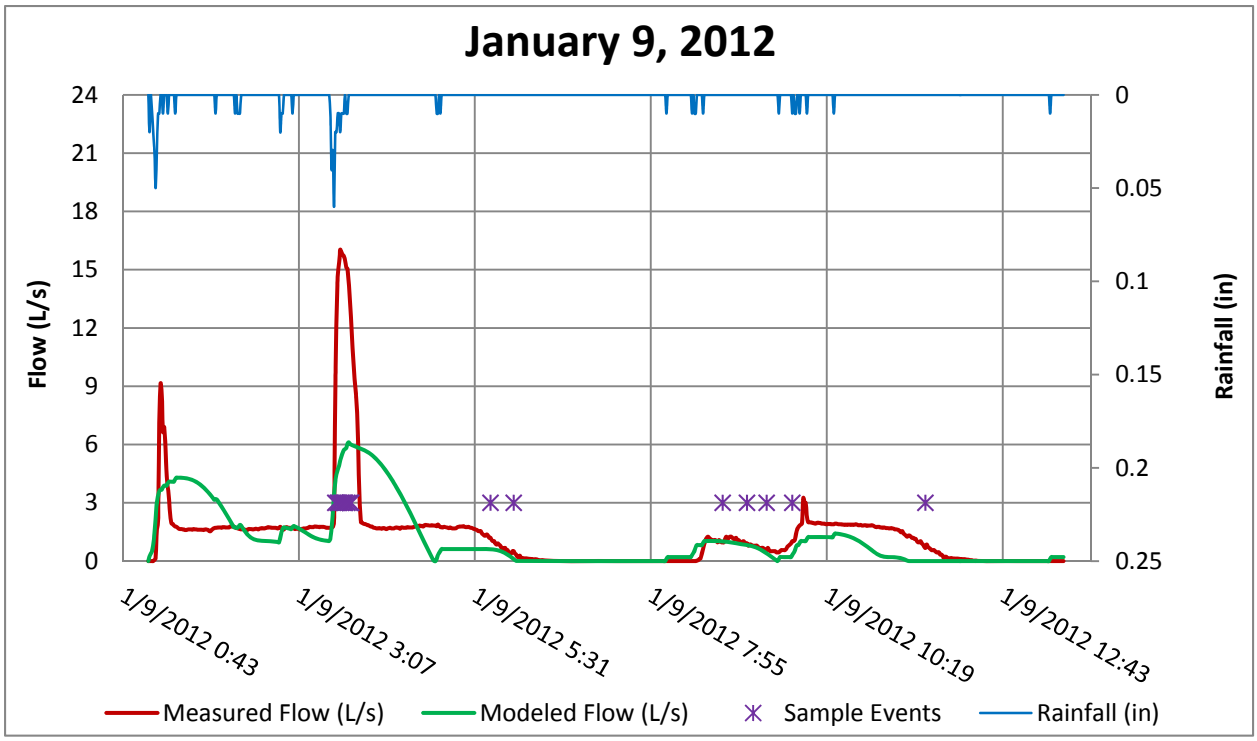
January 9, 2012
Flow (L/s)
Rainfall (in)
24
21
18
15
12
9
6
3
0
0
0.05
0.1
0.15
0.2
0.25
1/9/2012 0:43
1/9/2012 3:07
1/9/2012 5:31
1/9/2012 7:55
1/9/2012 10:19
1/9/2012 12:43
Measured Flow (L/s)
Modeled Flow (L/s)
Sample Events
Rainfall (in)

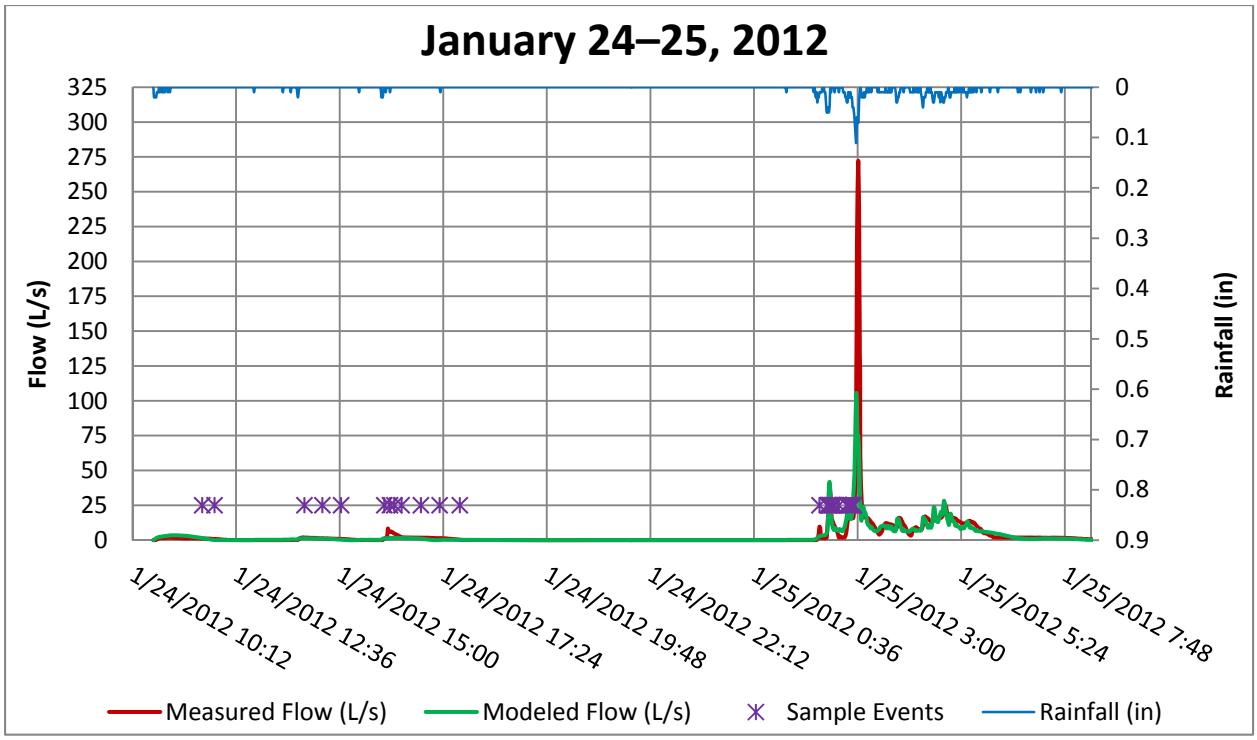
January 24–25, 2012
Flow (L/s)
Rainfall (in)
325
300
275
250
225
200
175
150
125
100
75
50
25
0
0
0.1
0.2
0.3
0.4
0.5
0.6
0.7
0.8
0.9
1/24/2012 10:12
1/24/2012 12:36
1/24/2012 15:00
1/24/2012 17:24
1/24/2012 19:48
1/24/2012 22:12
1/25/2012 0:36
1/25/2012 3:00
1/25/2012 5:24
1/25/2012 7:48
Measured Flow (L/s)
Modeled Flow (L/s)
Sample Events
Rainfall (in)

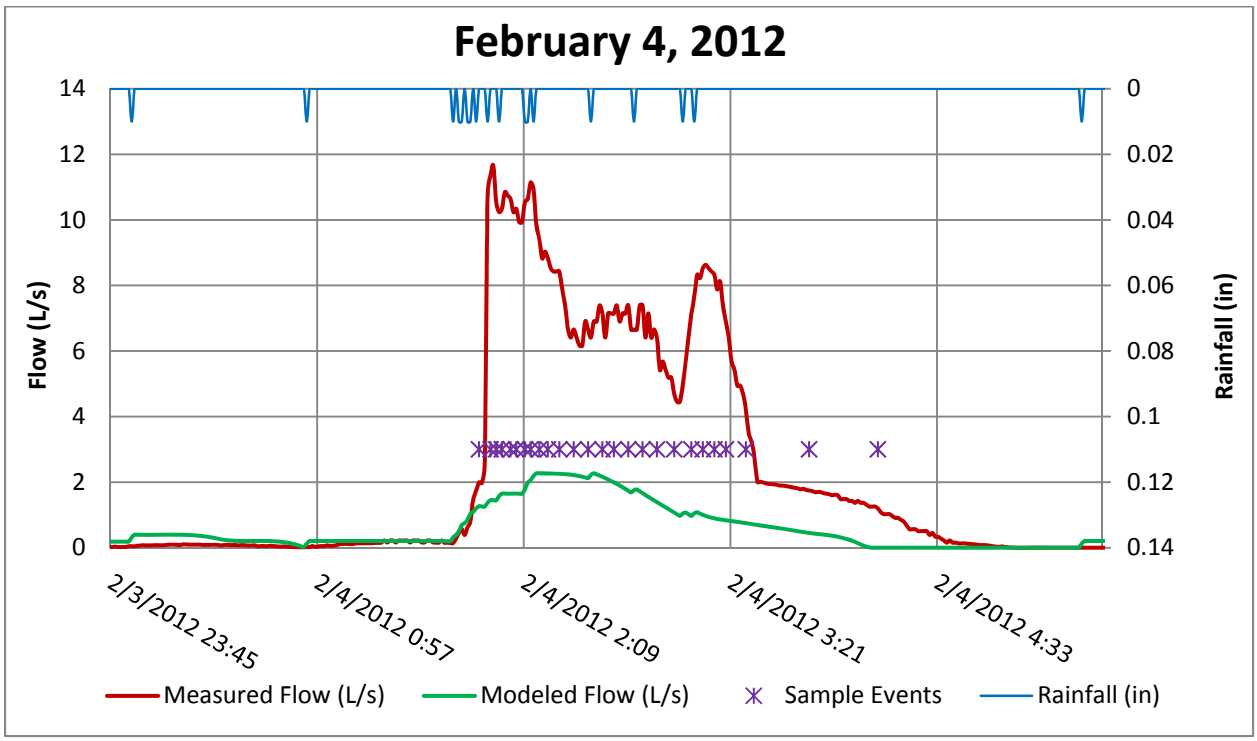
February 4, 2012
Flow (L/s)
Rainfall (in)
14
12
10
8
6
4
2
0
0
0.02
0.04
0.06
0.08
0.1
0.12
0.14
2/3/2012 23:45
2/4/2012 0:57
2/4/2012 2:09
2/4/2012 3:21
2/4/2012 4:33
Measured Flow (L/s)
Modeled Flow (L/s)
Sample Events
Rainfall (in)

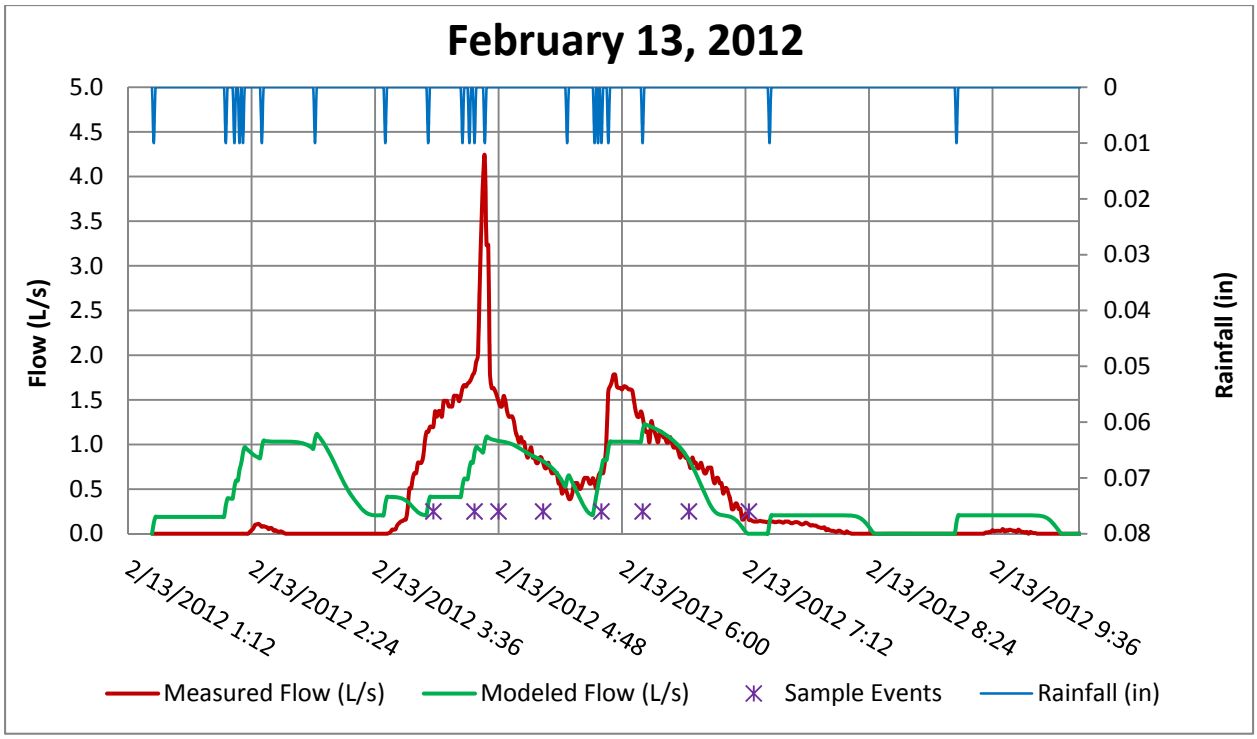
February 13, 2012
Flow (L/s)
Rainfall (in)
5.0
4.5
4.0
3.5
3.0
2.5
2.0
1.5
1.0
0.5
0.0
0
0.01
0.02
0.03
0.04
0.05
0.06
0.07
0.08
2/13/2012 1:12
2/13/2012 2:24
2/13/2012 3:36
2/13/2012 4:48
2/13/2012 6:00
2/13/2012 7:12
2/13/2012 8:24
2/13/2012 9:36
Measured Flow (L/s)
Modeled Flow (L/s)
Sample Events
Rainfall (in)

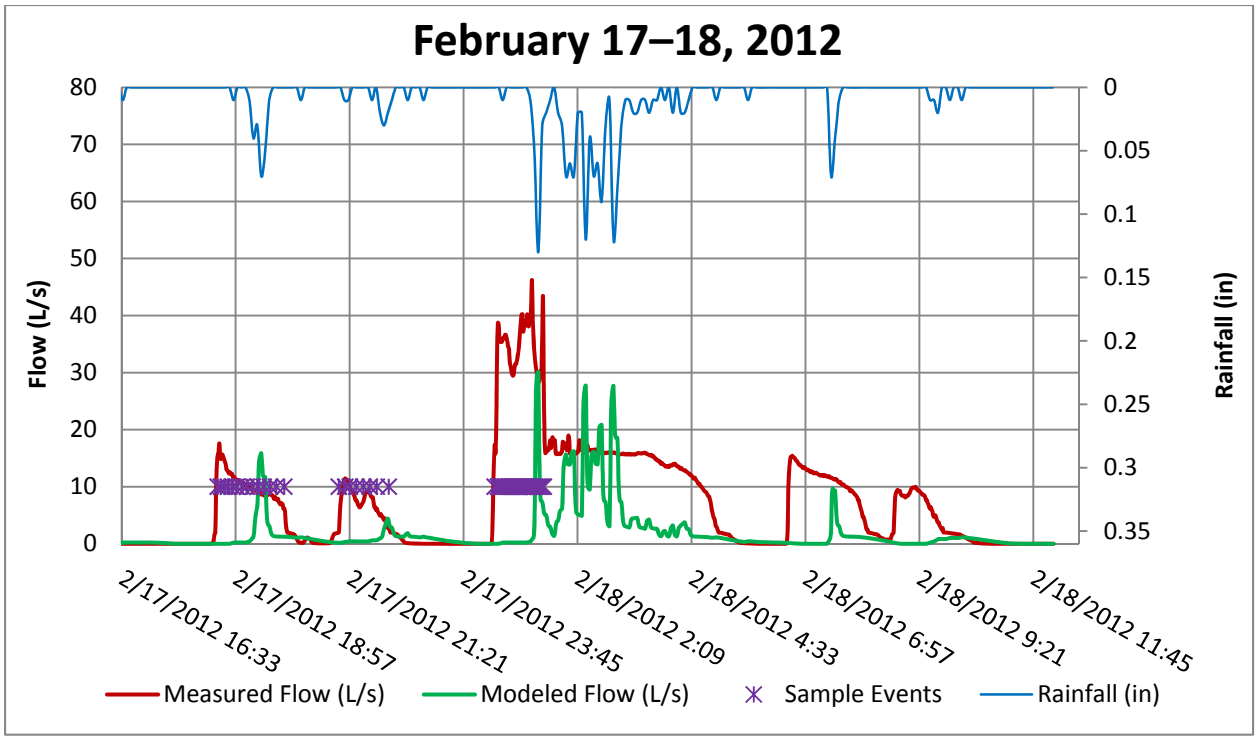
February 17–18, 2012
Flow (L/s)
Rainfall (in)
80
70
60
50
40
30
20
10
0
0
0.05
0.1
0.15
0.2
0.25
0.3
0.35
2/17/2012 16:33
2/17/2012 18:57
2/17/2012 21:21
2/17/2012 23:45
2/18/2012 2:09
2/18/2012 4:33
2/18/2012 6:57
2/18/2012 9:21
2/18/2012 11:45
Measured Flow (L/s)
Modeled Flow (L/s)
Sample Events
Rainfall (in)

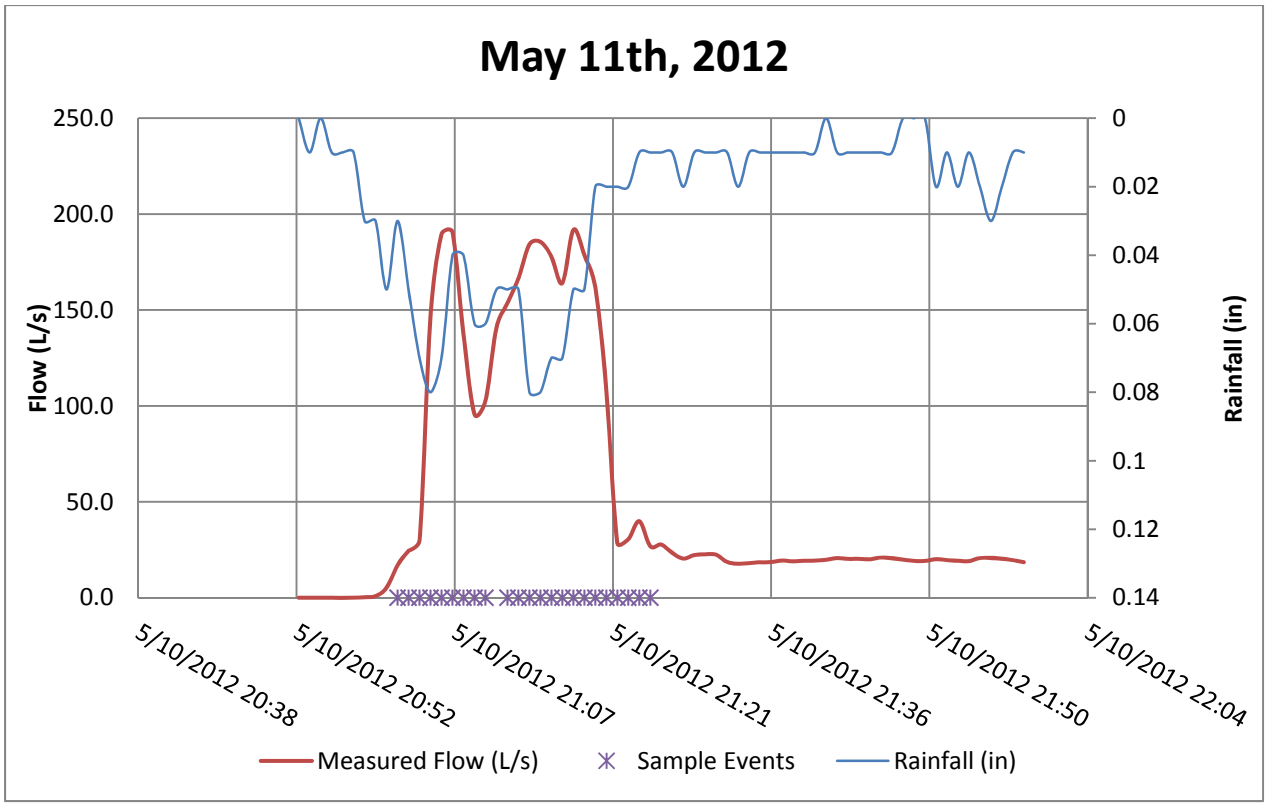
May 11th, 2012
250.0
200.0
150.0
100.0
50.0
0.0
Flow (L/s)
0
0.02
0.04
0.06
0.08
0.1
0.12
0.14
Rainfall (in)
5/10/2012 20:38
5/10/2012 20:52
5/10/2012 21:07
5/10/2012 21:21
5/10/2012 21:36
5/10/2012 21:50
5/10/2012 22:04
Measured Flow (L/s)
Sample Events
Rainfall (in)

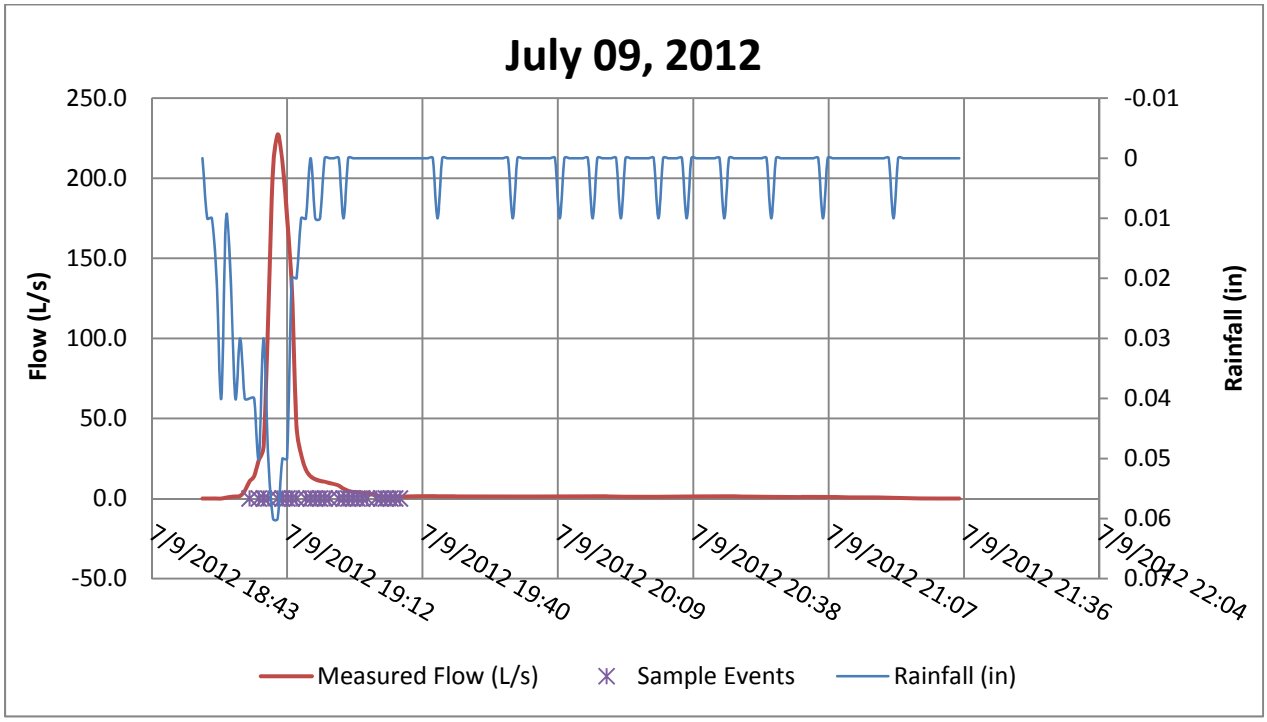
July 09, 2012
250.0
200.0
150.0
100.0
50.0
0.0
-50.0
Flow (L/s)
-0.01
0
0.01
0.02
0.03
0.04
0.05
0.06
0.07
Rainfall (in)
7/9/2012 18:43
7/9/2012 19:12
7/9/2012 19:40
7/9/2012 20:09
7/9/2012 20:38
7/9/2012 21:07
7/9/2012 21:36
7/9/2012 22:04
Measured Flow (L/s)
Sample Events
Rainfall (in)

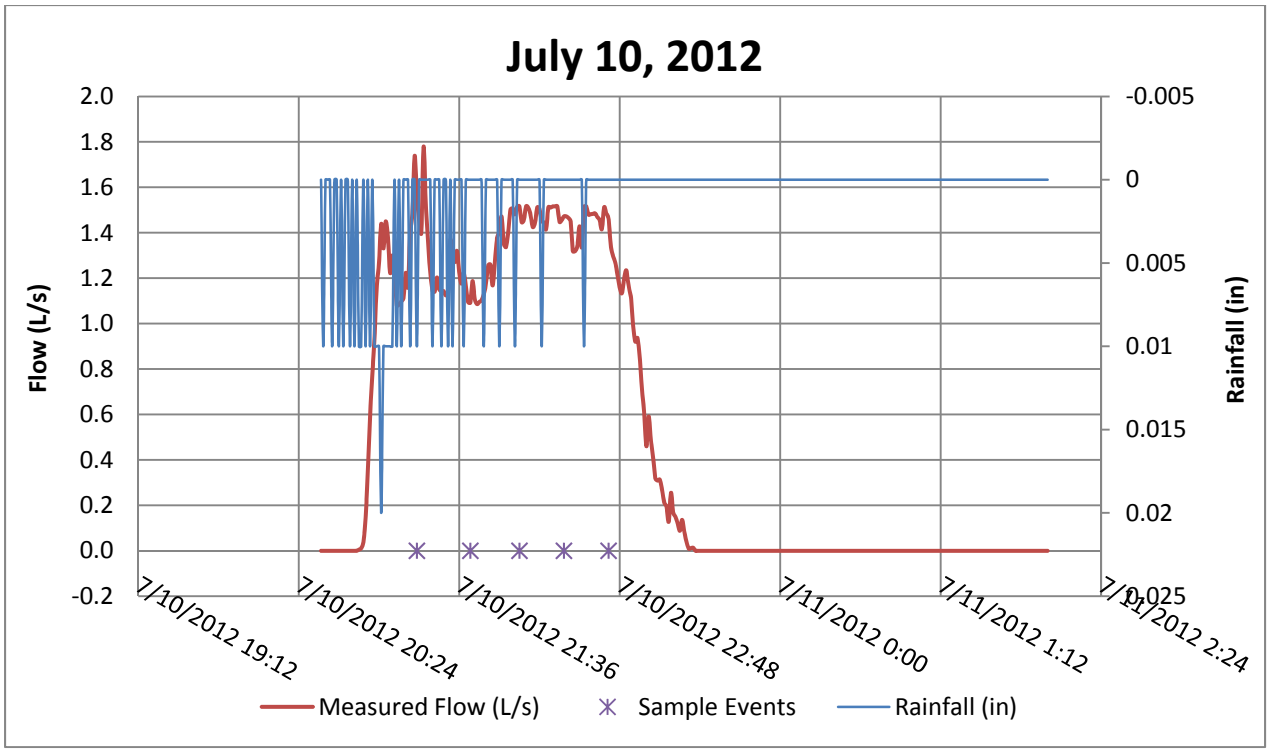
July 10, 2012
Flow (L/s)
Rainfall (in)
2.0
1.8
1.6
1.4
1.2
1.0
0.8
0.6
0.4
0.2
0.0
-0.2
-0.005
0
0.005
0.01
0.015
0.02
0.025
7/10/2012 19:12
7/10/2012 20:24
7/10/2012 21:36
7/10/2012 22:48
7/11/2012 0:00
7/11/2012 1:12
7/11/2012 2:24
Measured Flow (L/s)
Sample Events
Rainfall (in)

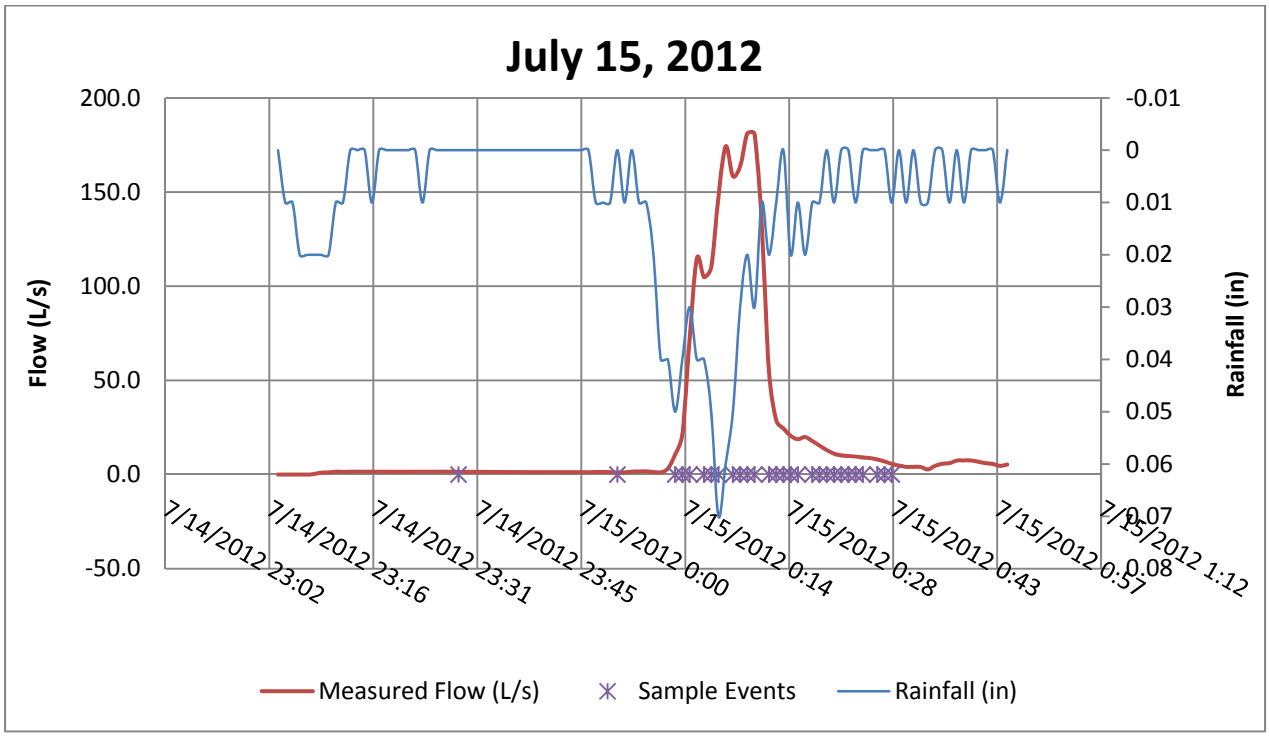
July 15, 2012
Flow (L/s)
Rainfall (in)
200.0
150.0
100.0
50.0
0.0
-50.0
-0.01
0
0.01
0.02
0.03
0.04
0.05
0.06
0.07
0.08
7/14/2012 23:02
7/14/2012 23:16
7/14/2012 23:31
7/14/2012 23:45
7/15/2012 0:00
7/15/2012 0:14
7/15/2012 0:28
7/15/2012 0:43
7/15/2012 0:57
7/15/2012 1:12
Measured Flow (L/s)
Sample Events
Rainfall (in)

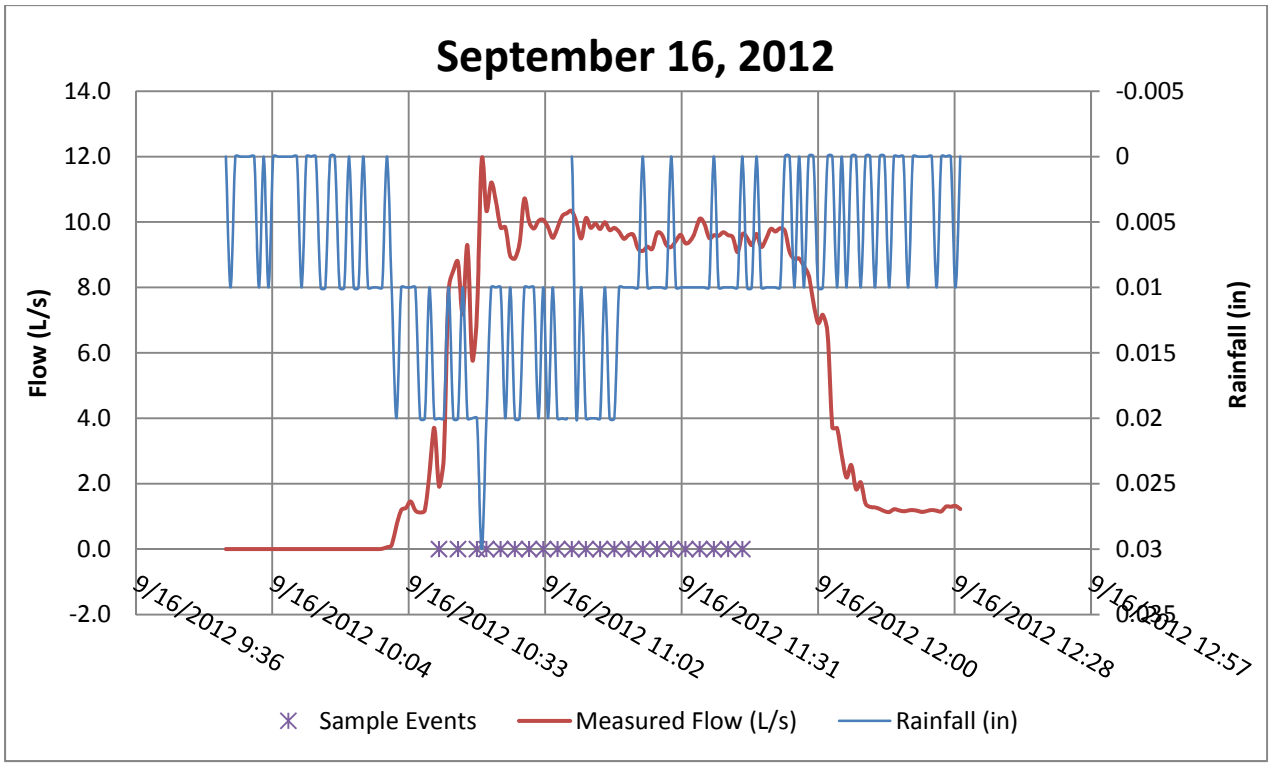
September 16, 2012
Flow (L/s)
Rainfall (in)
14.0
12.0
10.0
8.0
6.0
4.0
2.0
0.0
-2.0
-0.005
0
0.005
0.01
0.015
0.02
0.025
0.03
0.035
9/16/2012 9:36
9/16/2012 10:04
9/16/2012 10:33
9/16/2012 11:02
9/16/2012 11:31
9/16/2012 12:00
9/16/2012 12:28
9/16/2012 12:57
Sample Events
Measured Flow (L/s)
Rainfall (in)

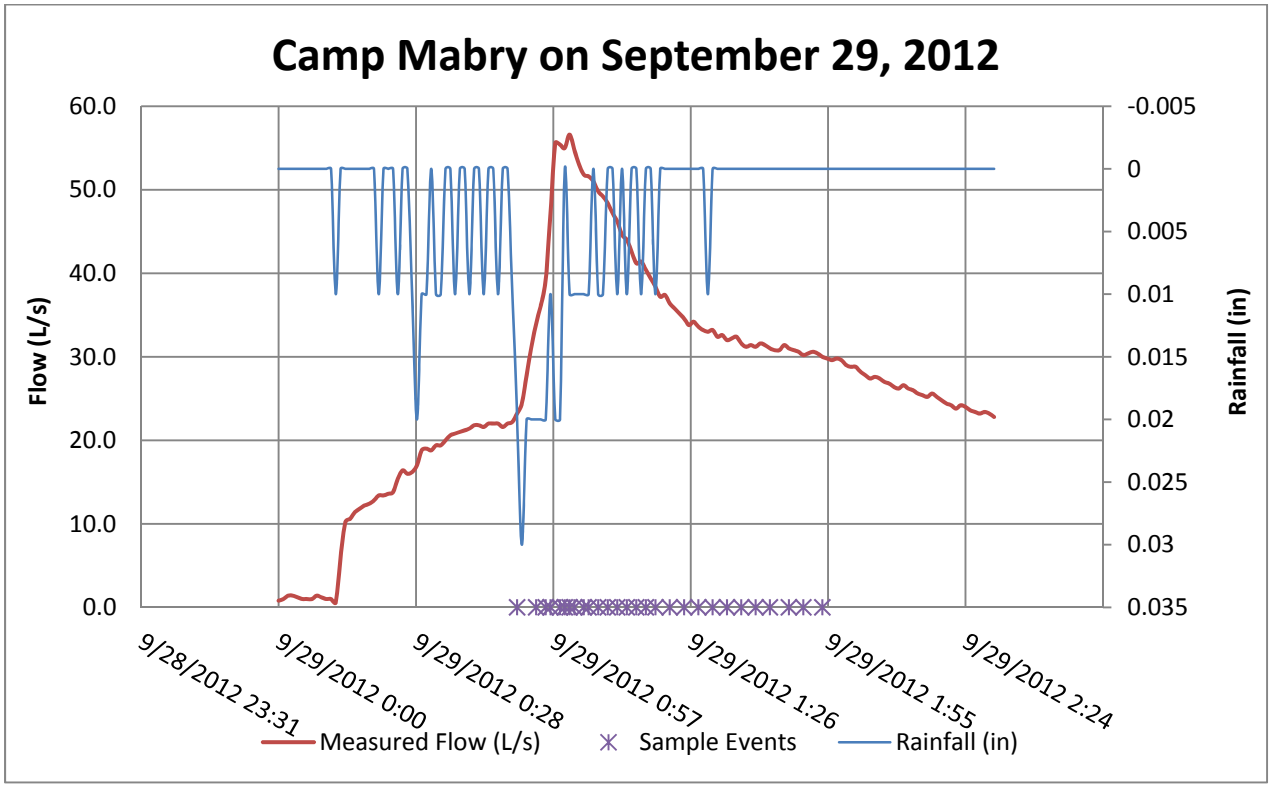
Camp Mabry on September 29, 2012
Flow (L/s)
Rainfall (in)
60.0
50.0
40.0
30.0
20.0
10.0
0.0
-0.005
0
0.005
0.01
0.015
0.02
0.025
0.03
0.035
9/28/2012 23:31
9/29/2012 0:00
9/29/2012 0:28
9/29/2012 0:57
9/29/2012 1:26
9/29/2012 1:55
9/29/2012 2:24
Measured Flow (L/s)
Sample Events
Rainfall (in)

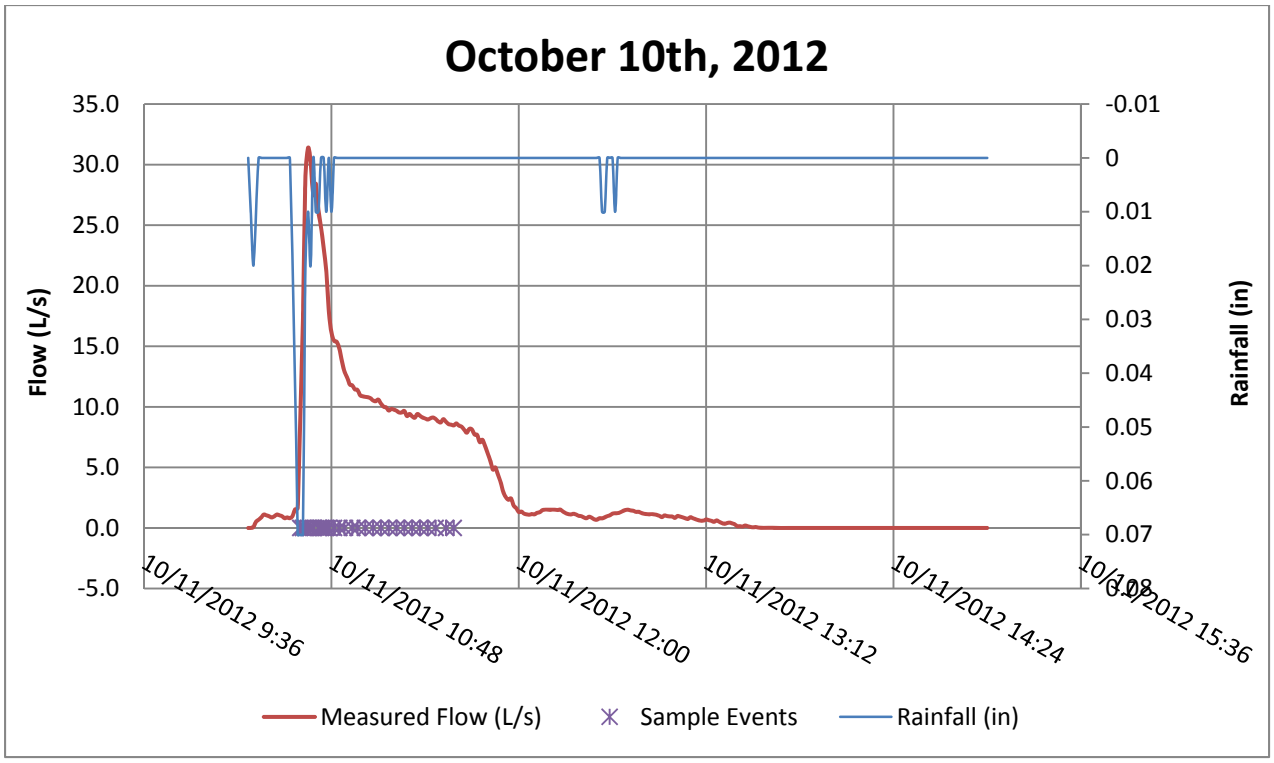
October 10th, 2012
Flow (L/s)
35.0
30.0
25.0
20.0
15.0
10.0
5.0
0.0
-5.0
-0.01
0
0.01
0.02
0.03
0.04
0.05
0.06
0.07
0.08
Rainfall (in)
10/11/2012 9:36
10/11/2012 10:48
10/11/2012 12:00
10/11/2012 13:12
10/11/2012 14:24
10/11/2012 15:36
Measured Flow (L/s)
Sample Events
Rainfall (in)

Camp Hubbard Hydrographs

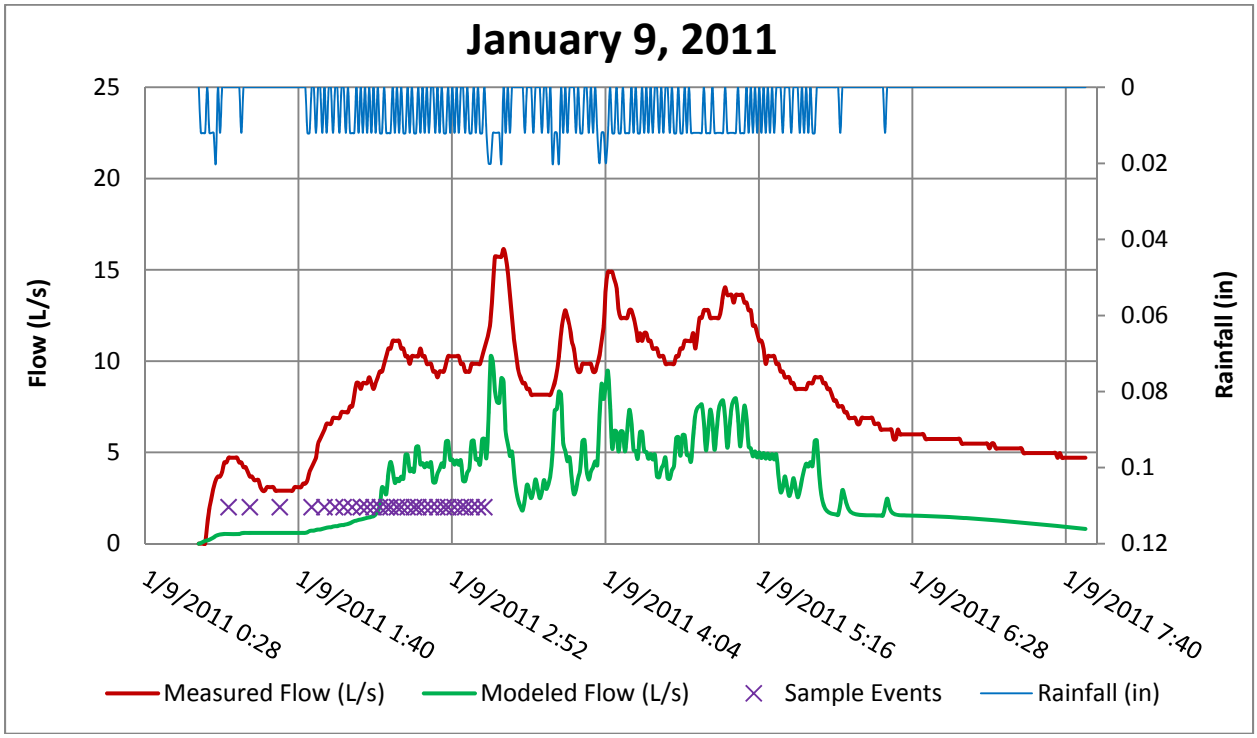

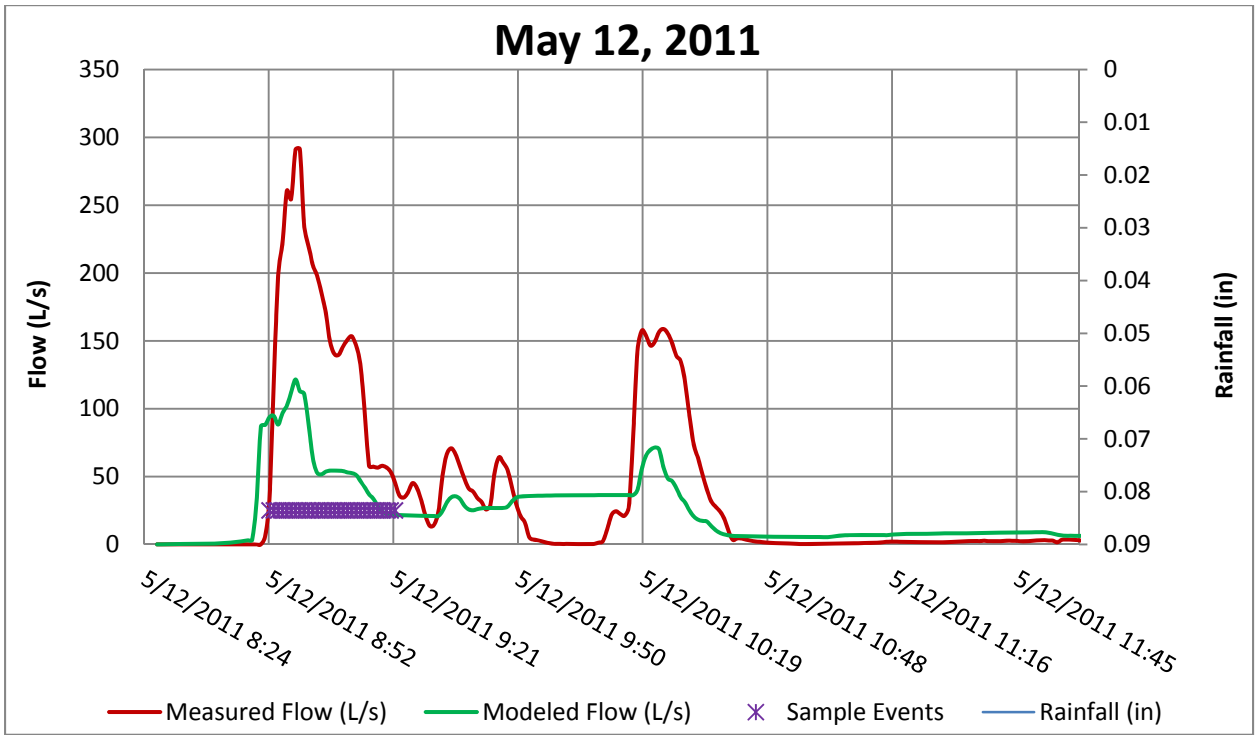

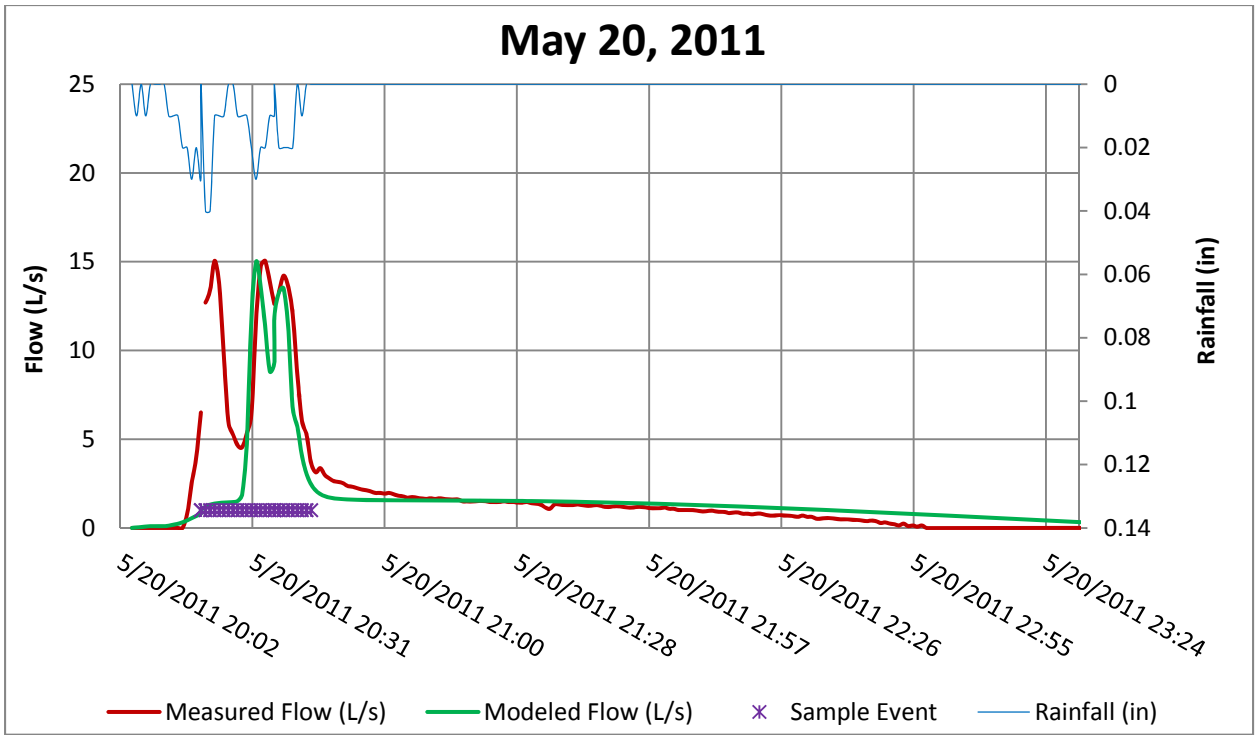
May 20, 2011
Flow (L/s)
Rainfall (in)
25
20
15
10
5
0
0
0.02
0.04
0.06
0.08
0.1
0.12
0.14
5/20/2011 20:02
5/20/2011 20:31
5/20/2011 21:00
5/20/2011 21:28
5/20/2011 21:57
5/20/2011 22:26
5/20/2011 22:55
5/20/2011 23:24
Measured Flow (L/s)
Modeled Flow (L/s)
Sample Event
Rainfall (in)

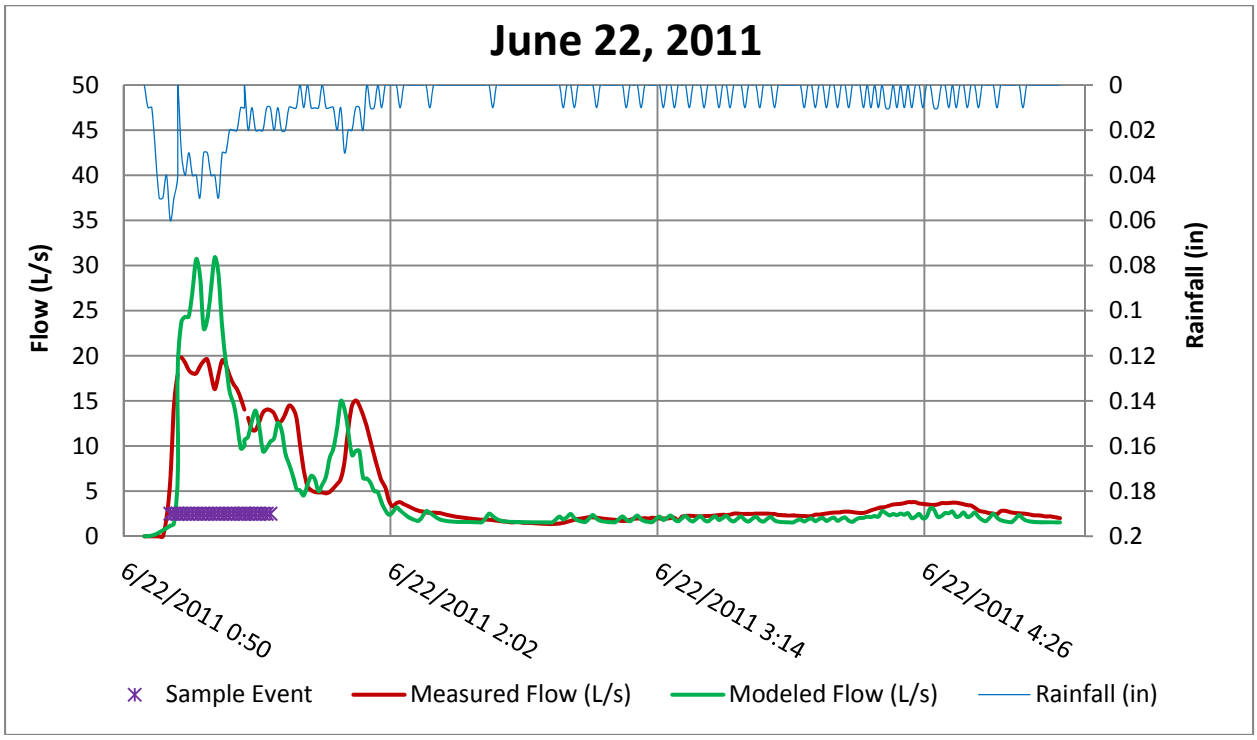
June 22, 2011
Flow (L/s)
Rainfall (in)
50
45
40
35
30
25
20
15
10
5
0
0
0.02
0.04
0.06
0.08
0.1
0.12
0.14
0.16
0.18
0.2
6/22/2011 0:50
6/22/2011 2:02
6/22/2011 3:14
6/22/2011 4:26
Sample Event
Measured Flow (L/s)
Modeled Flow (L/s)
Rainfall (in)

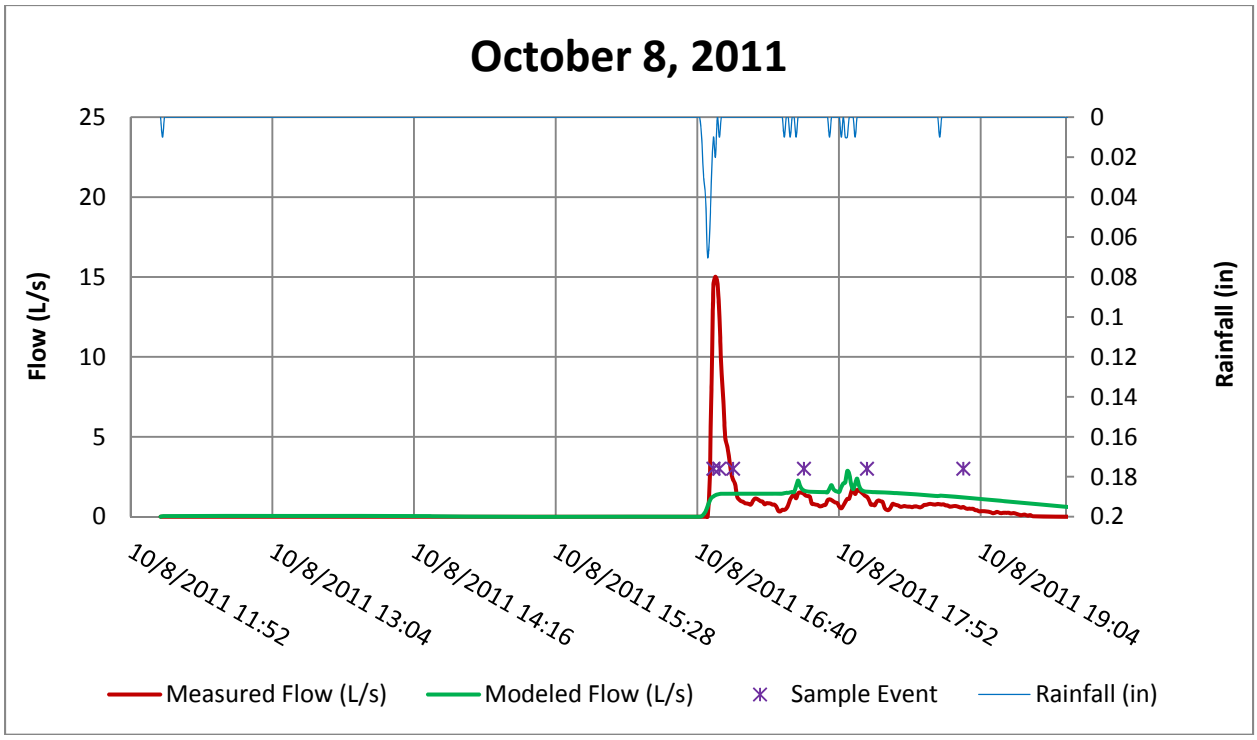
October 8, 2011
Flow (L/s)
Rainfall (in)
25
20
15
10
5
0
0
0.02
0.04
0.06
0.08
0.1
0.12
0.14
0.16
0.18
0.2
10/8/2011 11:52
10/8/2011 13:04
10/8/2011 14:16
10/8/2011 15:28
10/8/2011 16:40
10/8/2011 17:52
10/8/2011 19:04
Measured Flow (L/s)
Modeled Flow (L/s)
Sample Event
Rainfall (in)

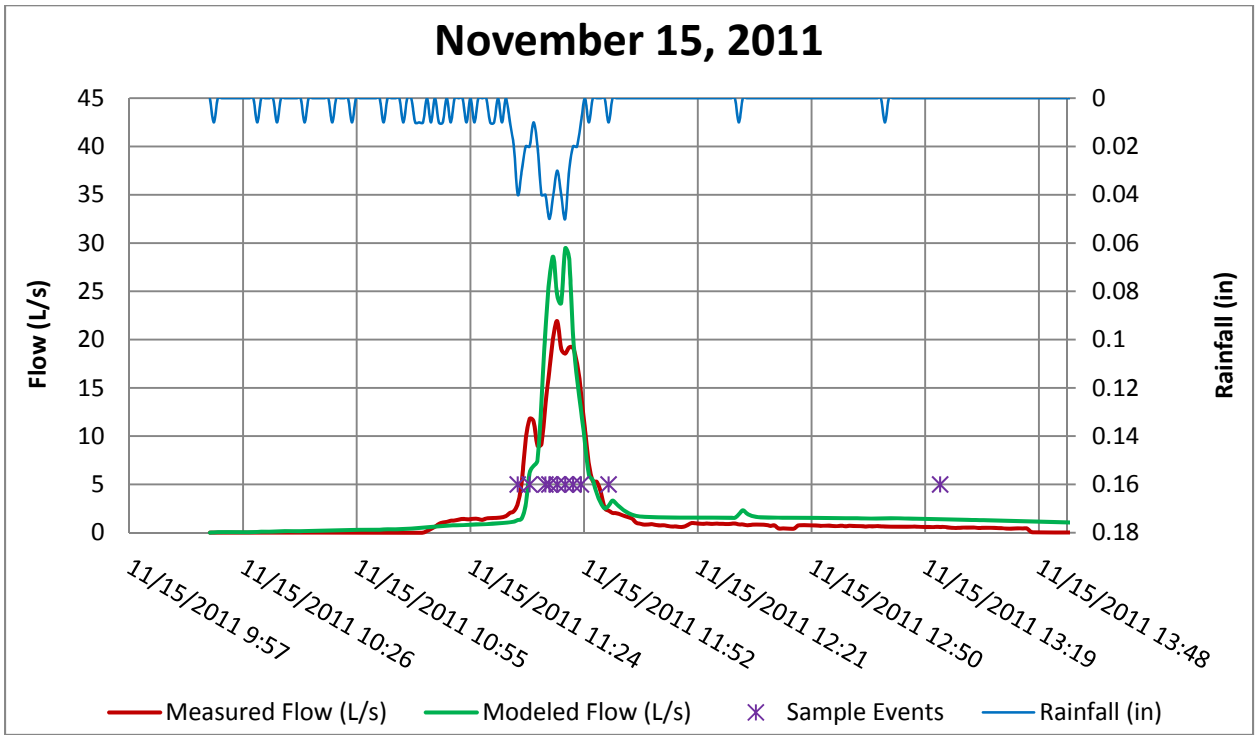
November 15, 2011
Flow (L/s)
Rainfall (in)
45
40
35
30
25
20
15
10
5
0
0
0.02
0.04
0.06
0.08
0.1
0.12
0.14
0.16
0.18
11/15/2011 9:57
11/15/2011 10:26
11/15/2011 10:55
11/15/2011 11:24
11/15/2011 11:52
11/15/2011 12:21
11/15/2011 12:50
11/15/2011 13:19
11/15/2011 13:48
Measured Flow (L/s)
Modeled Flow (L/s)
Sample Events
Rainfall (in)

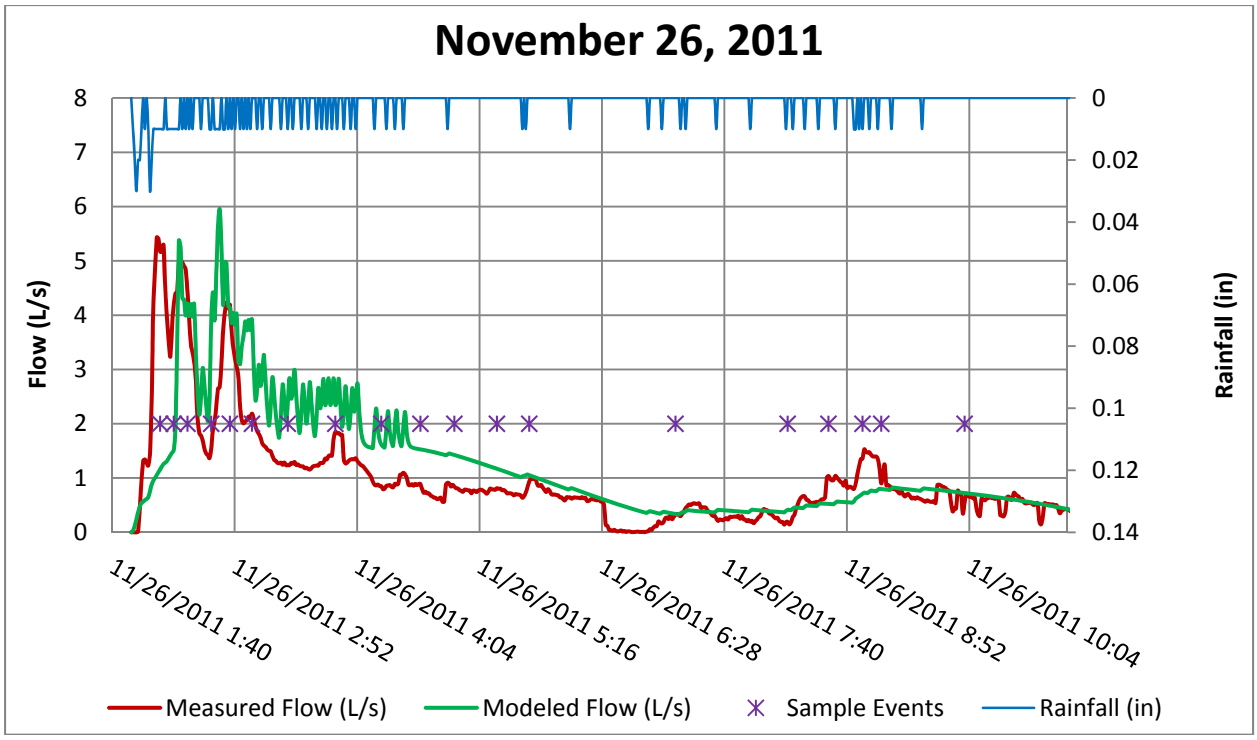
November 26, 2011
Flow (L/s)
Rainfall (in)
0
1
2
3
4
5
6
7
8
0
0.02
0.04
0.06
0.08
0.1
0.12
0.14
11/26/2011 1:40
11/26/2011 2:52
11/26/2011 4:04
11/26/2011 5:16
11/26/2011 6:28
11/26/2011 7:40
11/26/2011 8:52
11/26/2011 10:04
Measured Flow (L/s)
Modeled Flow (L/s)
Sample Events
Rainfall (in)

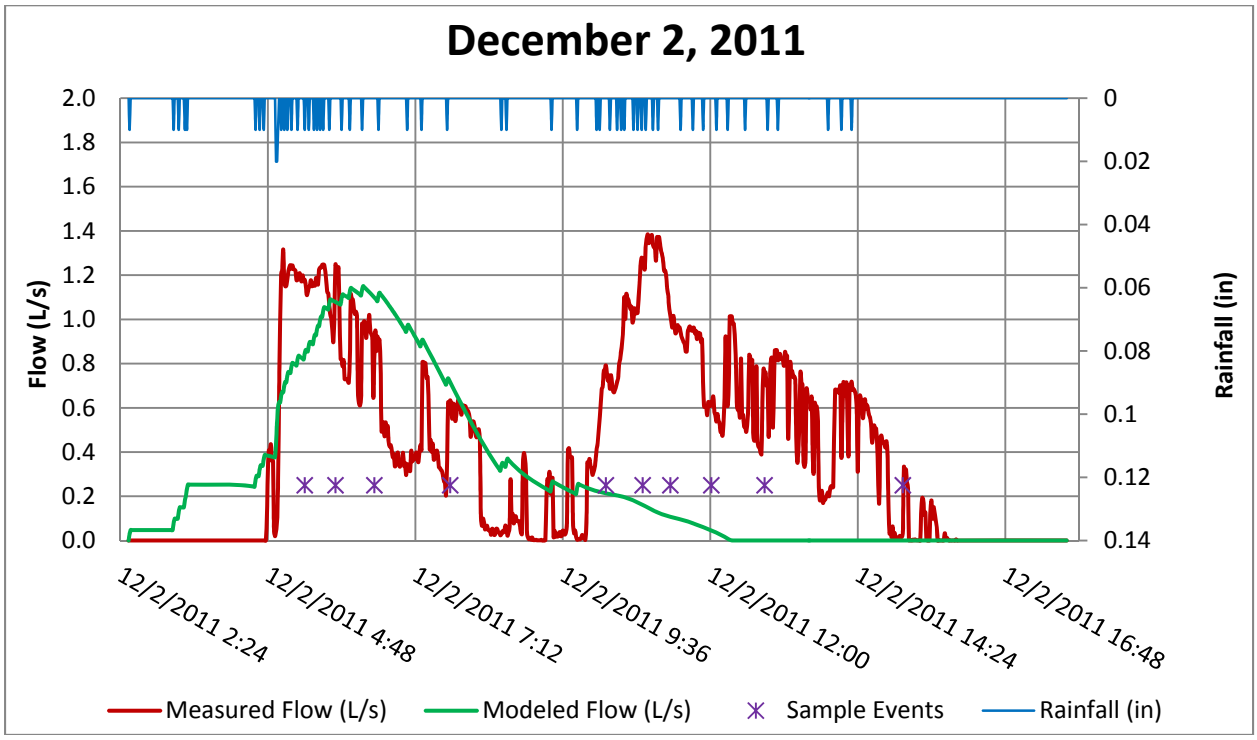
December 2, 2011
Flow (L/s)
Rainfall (in)
0.0
0.2
0.4
0.6
0.8
1.0
1.2
1.4
1.6
1.8
2.0
0
0.02
0.04
0.06
0.08
0.1
0.12
0.14
12/2/2011 2:24
12/2/2011 4:48
12/2/2011 7:12
12/2/2011 9:36
12/2/2011 12:00
12/2/2011 14:24
12/2/2011 16:48
Measured Flow (L/s)
Modeled Flow (L/s)
Sample Events
Rainfall (in)

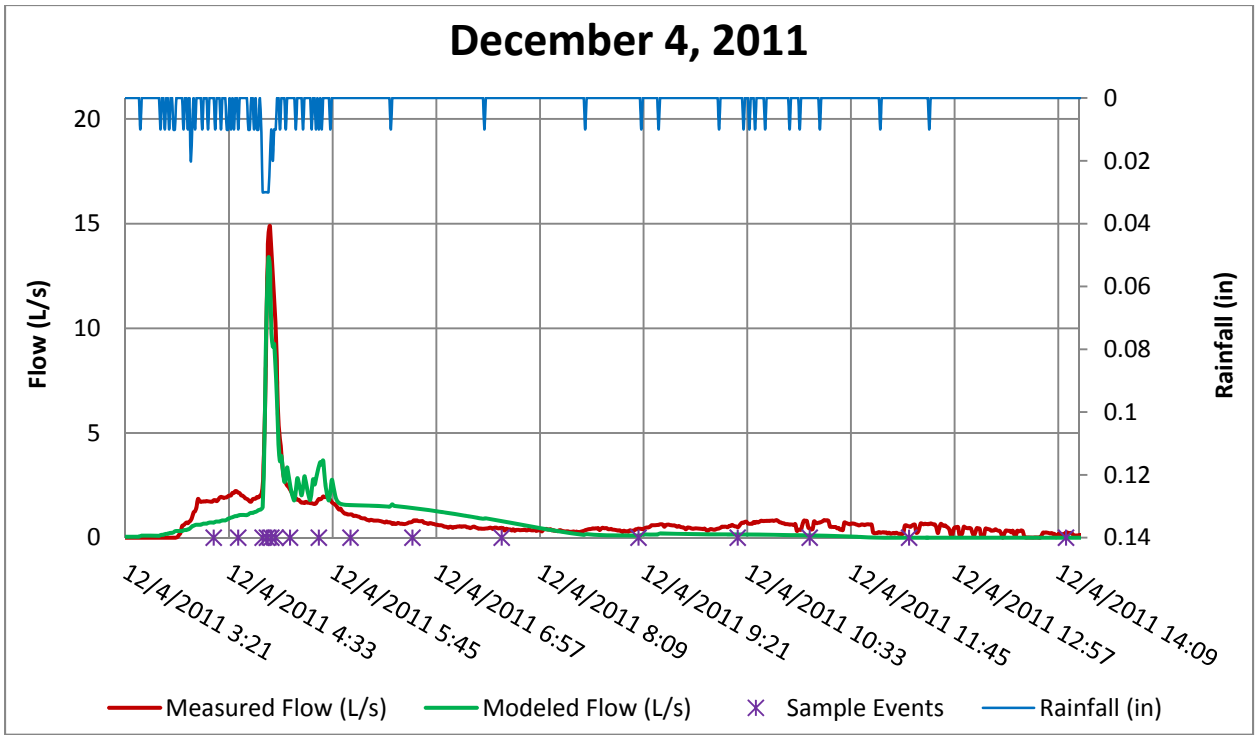
December 4, 2011
Flow (L/s)
Rainfall (in)
20
15
10
5
0
0
0.02
0.04
0.06
0.08
0.1
0.12
0.14
12/4/2011 3:21
12/4/2011 4:33
12/4/2011 5:45
12/4/2011 6:57
12/4/2011 8:09
12/4/2011 9:21
12/4/2011 10:33
12/4/2011 11:45
12/4/2011 12:57
12/4/2011 14:09
Measured Flow (L/s)
Modeled Flow (L/s)
Sample Events
Rainfall (in)

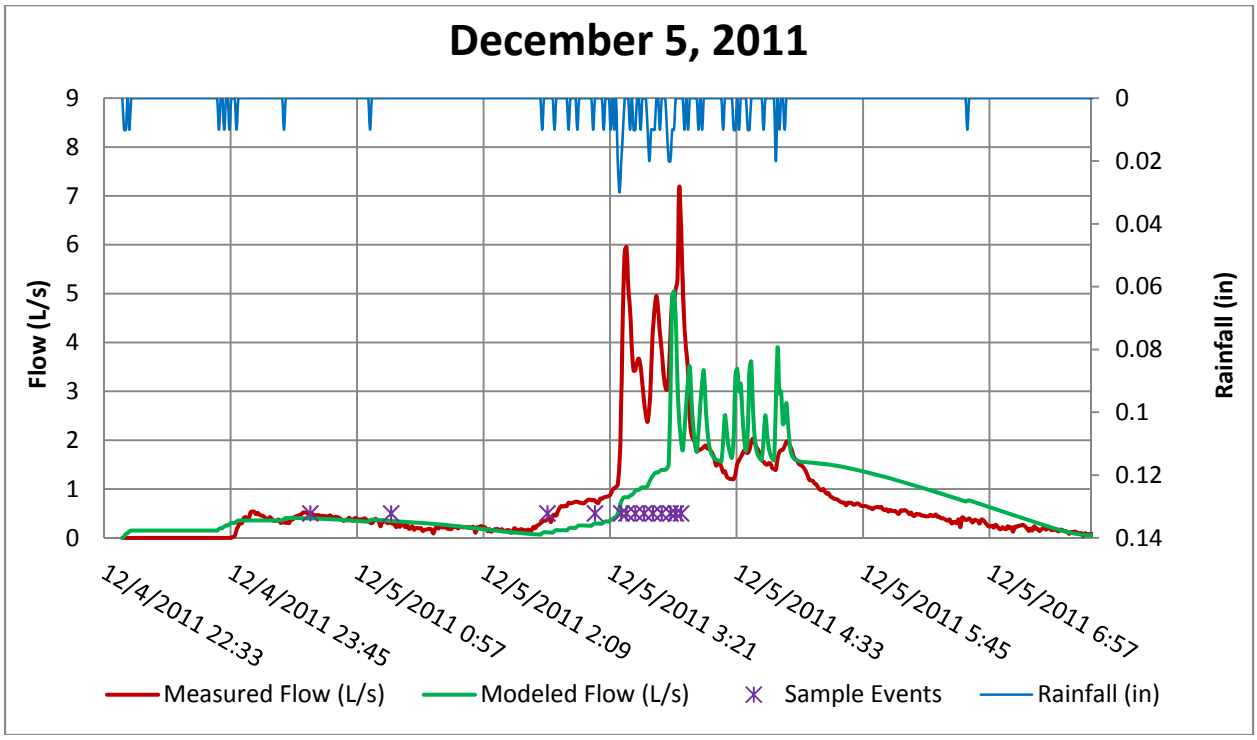
December 5, 2011
Flow (L/s)
Rainfall (in)
9
8
7
6
5
4
3
2
1
0
0
0.02
0.04
0.06
0.08
0.1
0.12
0.14
12/4/2011 22:33
12/4/2011 23:45
12/5/2011 0:57
12/5/2011 2:09
12/5/2011 3:21
12/5/2011 4:33
12/5/2011 5:45
12/5/2011 6:57
Measured Flow (L/s)
Modeled Flow (L/s)
Sample Events
Rainfall (in)

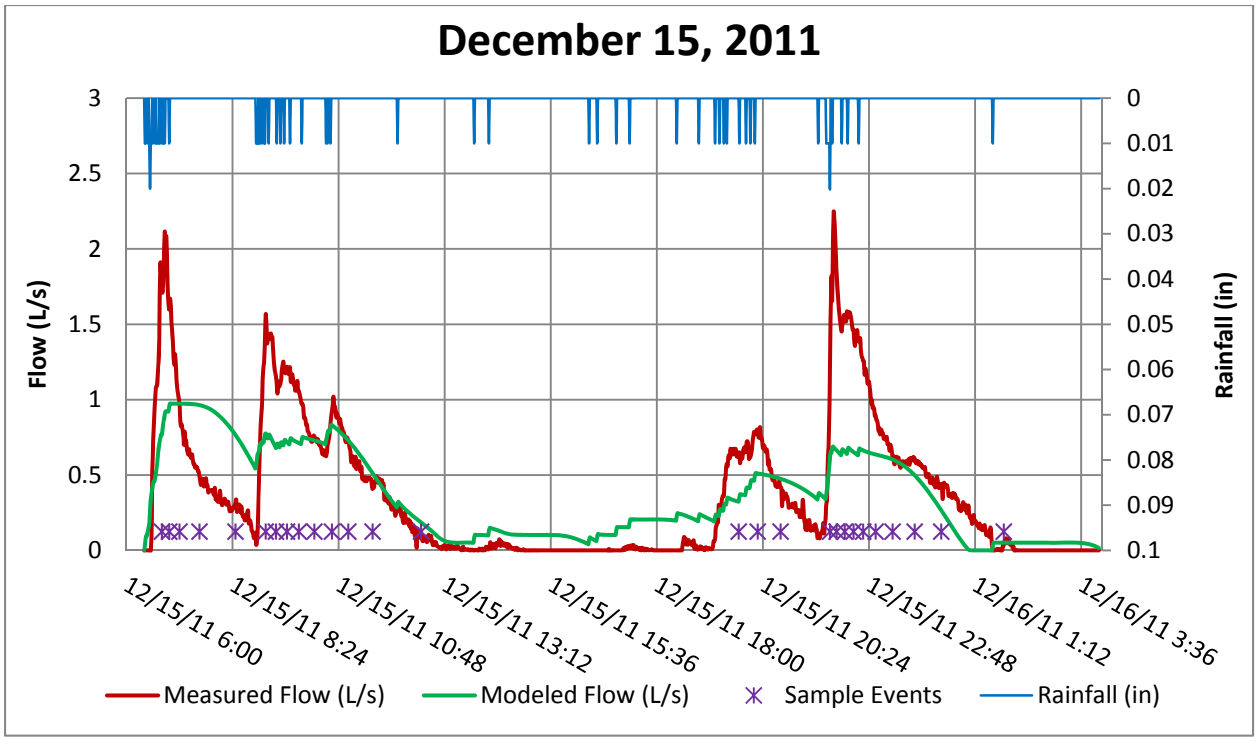
December 15, 2011
Flow (L/s)
Rainfall (in)
3
2.5
2
1.5
1
0.5
0
0
0.01
0.02
0.03
0.04
0.05
0.06
0.07
0.08
0.09
0.1
12/15/11 6:00
12/15/11 8:24
12/15/11 10:48
12/15/11 13:12
12/15/11 15:36
12/15/11 18:00
12/15/11 20:24
12/15/11 22:48
12/16/11 1:12
12/16/11 3:36
Measured Flow (L/s)
Modeled Flow (L/s)
Sample Events
Rainfall (in)

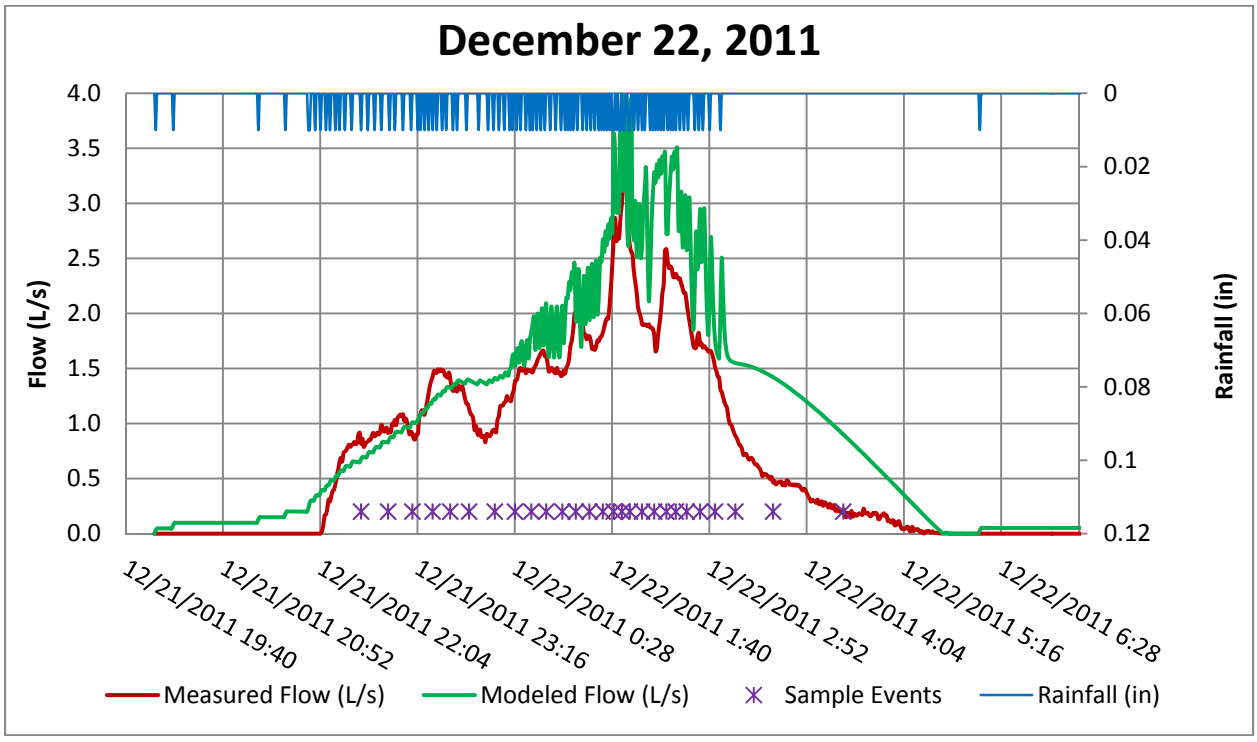
December 22, 2011
Flow (L/s)
Rainfall (in)
4.0
3.5
3.0
2.5
2.0
1.5
1.0
0.5
0.0
0
0.02
0.04
0.06
0.08
0.1
0.12
12/21/2011 19:40
12/21/2011 20:52
12/21/2011 22:04
12/21/2011 23:16
12/22/2011 0:28
12/22/2011 1:40
12/22/2011 2:52
12/22/2011 4:04
12/22/2011 5:16
12/22/2011 6:28
Measured Flow (L/s)
Modeled Flow (L/s)
Sample Events
Rainfall (in)

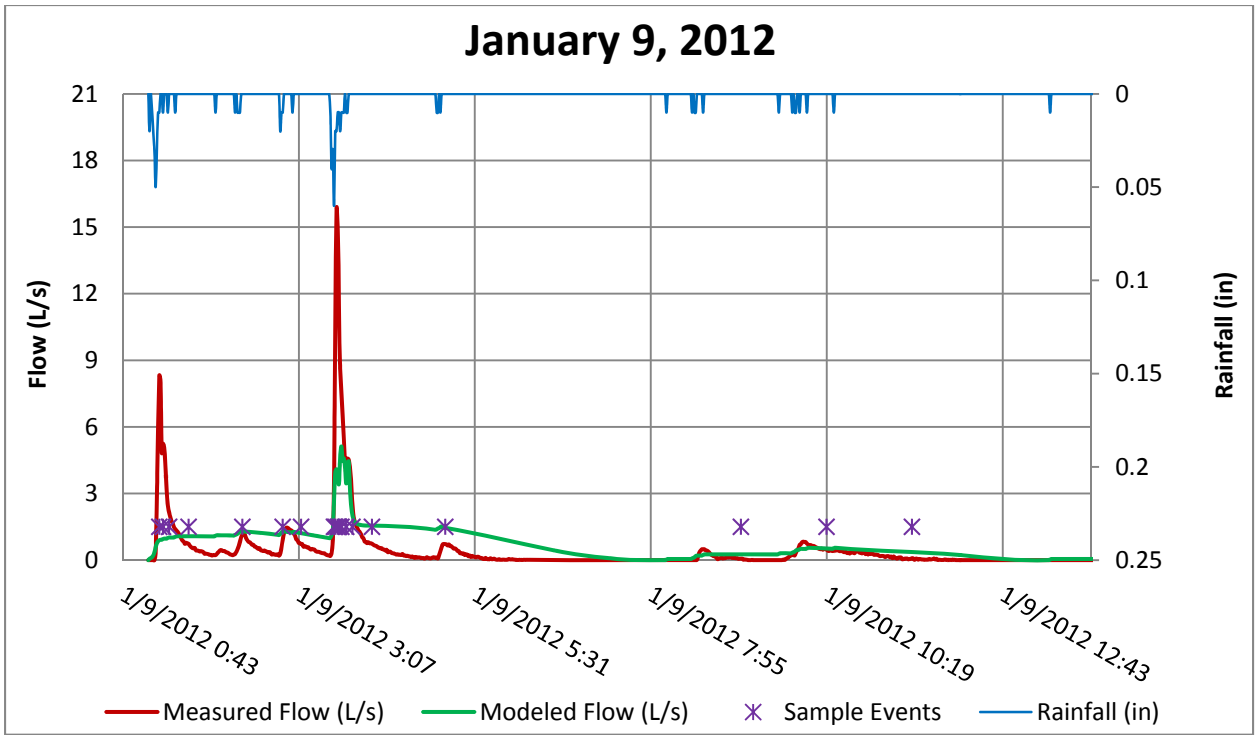
January 9, 2012
Flow (L/s)
Rainfall (in)
21
18
15
12
9
6
3
0
0
0.05
0.1
0.15
0.2
0.25
1/9/2012 0:43
1/9/2012 3:07
1/9/2012 5:31
1/9/2012 7:55
1/9/2012 10:19
1/9/2012 12:43
Measured Flow (L/s)
Modeled Flow (L/s)
Sample Events
Rainfall (in)

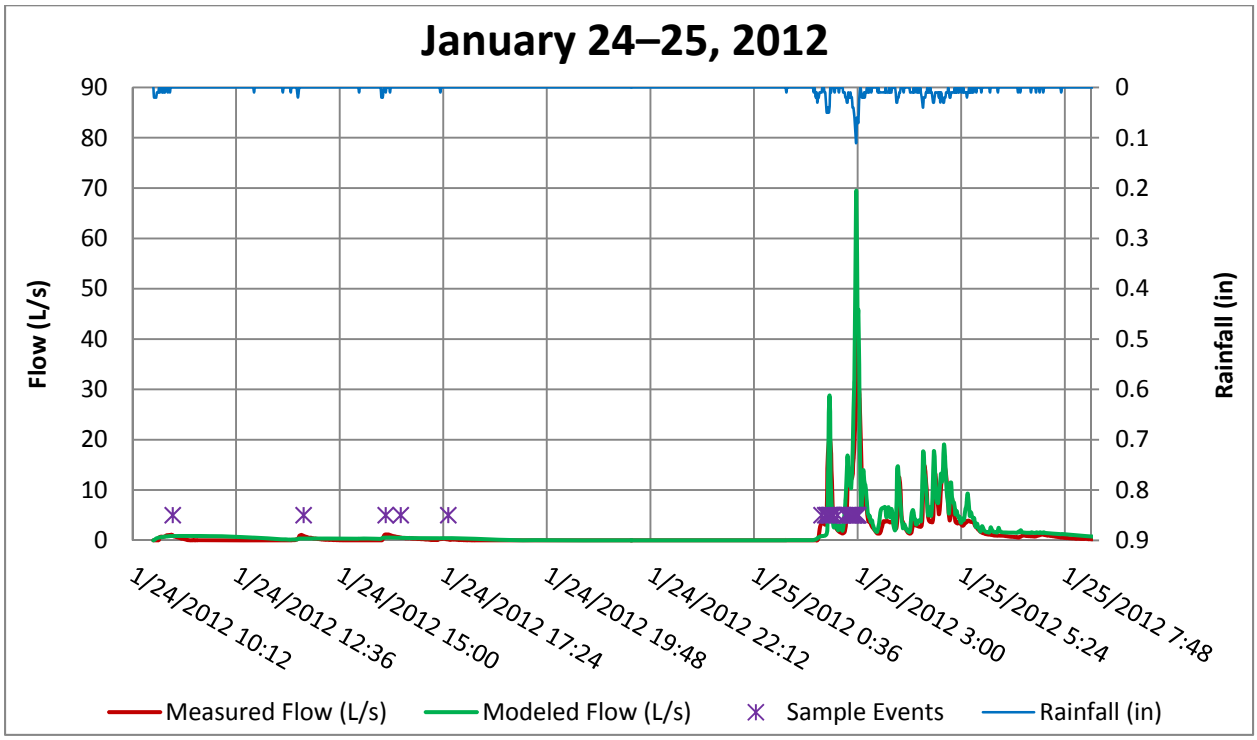
January 24–25, 2012
Flow (L/s)
Rainfall (in)
90
80
70
60
50
40
30
20
10
0
0
0.1
0.2
0.3
0.4
0.5
0.6
0.7
0.8
0.9
1/24/2012 10:12
1/24/2012 12:36
1/24/2012 15:00
1/24/2012 17:24
1/24/2012 19:48
1/24/2012 22:12
1/25/2012 0:36
1/25/2012 3:00
1/25/2012 5:24
1/25/2012 7:48
Measured Flow (L/s)
Modeled Flow (L/s)
Sample Events
Rainfall (in)

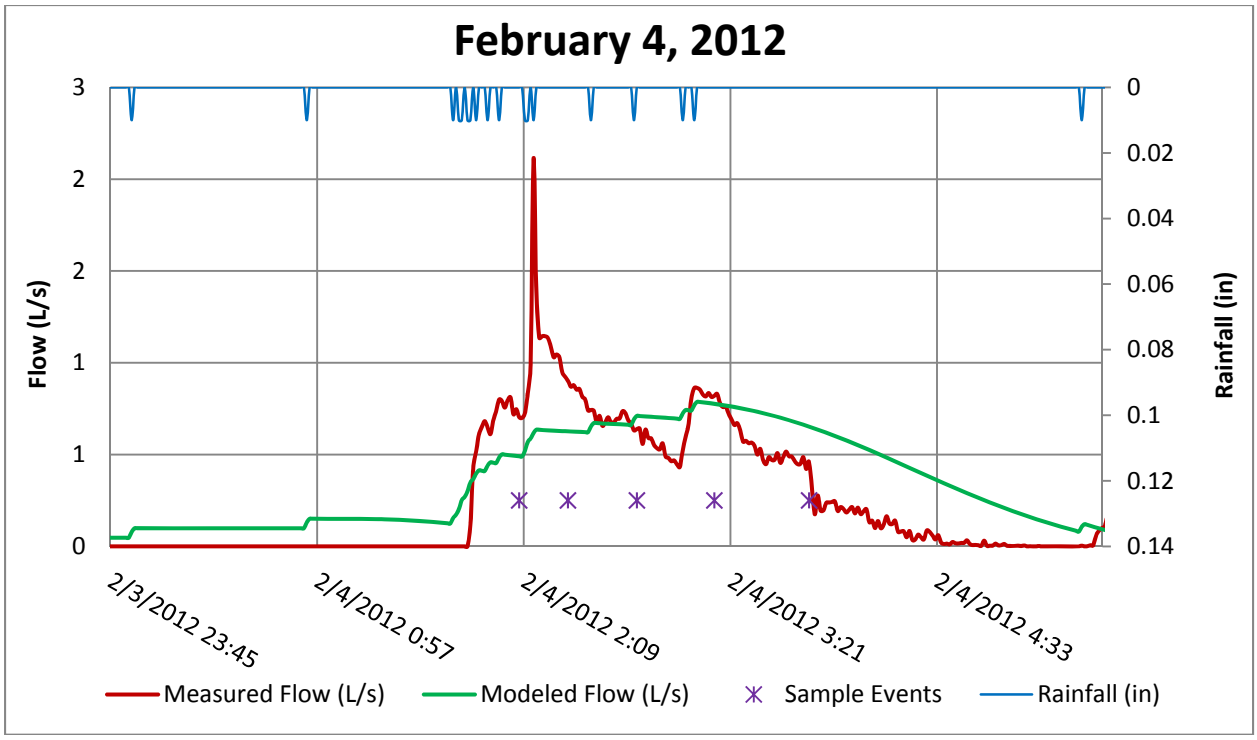
February 4, 2012
Flow (L/s)
Rainfall (in)
3
2
2
1
1
0
0
0.02
0.04
0.06
0.08
0.1
0.12
0.14
2/3/2012 23:45
2/4/2012 0:57
2/4/2012 2:09
2/4/2012 3:21
2/4/2012 4:33
Measured Flow (L/s)
Modeled Flow (L/s)
Sample Events
Rainfall (in)

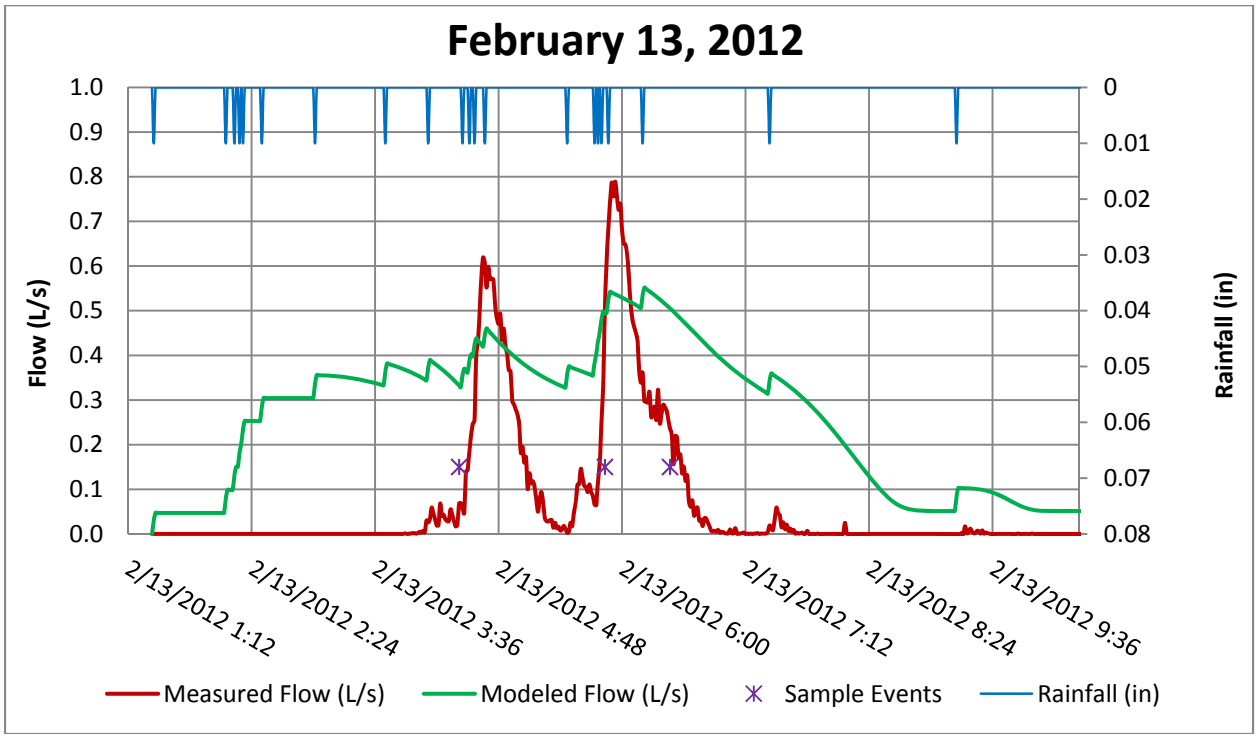
February 13, 2012
Flow (L/s)
Rainfall (in)
1.0
0.9
0.8
0.7
0.6
0.5
0.4
0.3
0.2
0.1
0.0
0
0.01
0.02
0.03
0.04
0.05
0.06
0.07
0.08
2/13/2012 1:12
2/13/2012 2:24
2/13/2012 3:36
2/13/2012 4:48
2/13/2012 6:00
2/13/2012 7:12
2/13/2012 8:24
2/13/2012 9:36
Measured Flow (L/s)
Modeled Flow (L/s)
Sample Events
Rainfall (in)

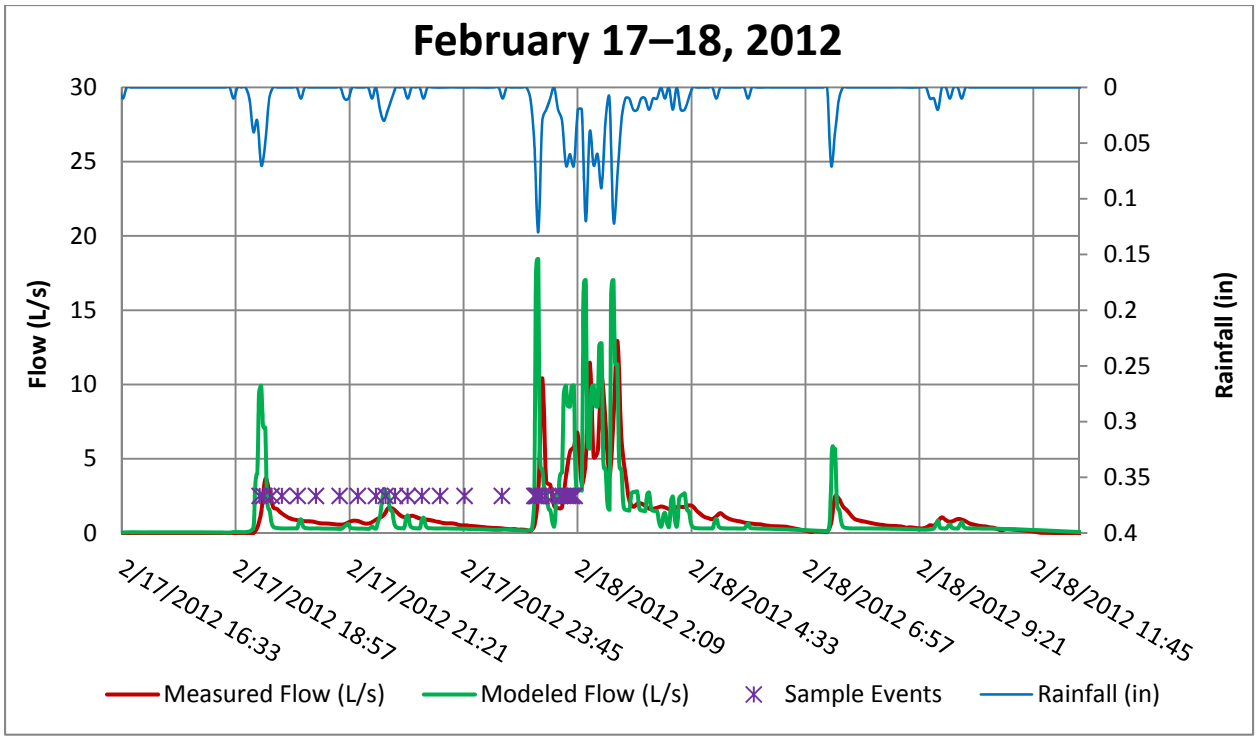
February 17–18, 2012
Flow (L/s)
Rainfall (in)
30
25
20
15
10
5
0
0
0.05
0.1
0.15
0.2
0.25
0.3
0.35
0.4
2/17/2012 16:33
2/17/2012 18:57
2/17/2012 21:21
2/17/2012 23:45
2/18/2012 2:09
2/18/2012 4:33
2/18/2012 6:57
2/18/2012 9:21
2/18/2012 11:45
Measured Flow (L/s)
Modeled Flow (L/s)
Sample Events
Rainfall (in)

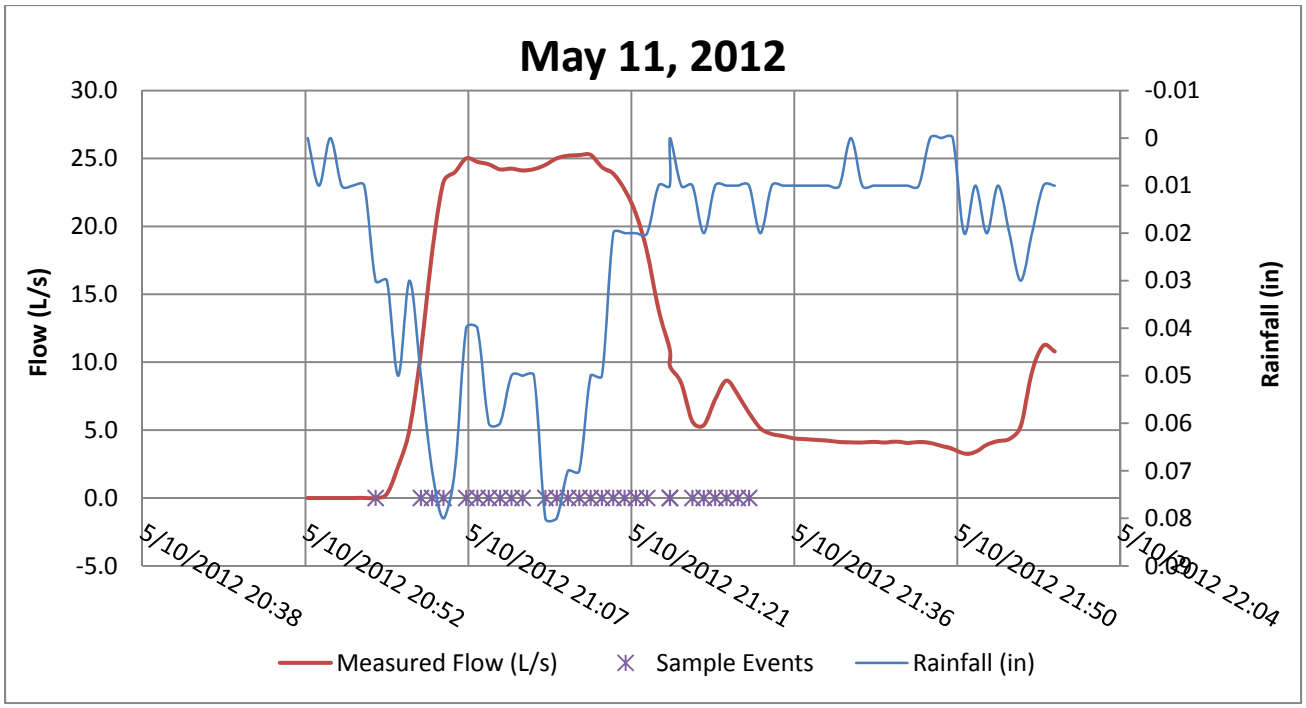
May 11, 2012
Flow (L/s)
Rainfall (in)
30.0
25.0
20.0
15.0
10.0
5.0
0.0
-5.0
-0.01
0
0.01
0.02
0.03
0.04
0.05
0.06
0.07
0.08
5/10/2012 20:38
5/10/2012 20:52
5/10/2012 21:07
5/10/2012 21:21
5/10/2012 21:36
5/10/2012 21:50
5/10/2012 22:04
Measured Flow (L/s)
Sample Events
Rainfall (in)

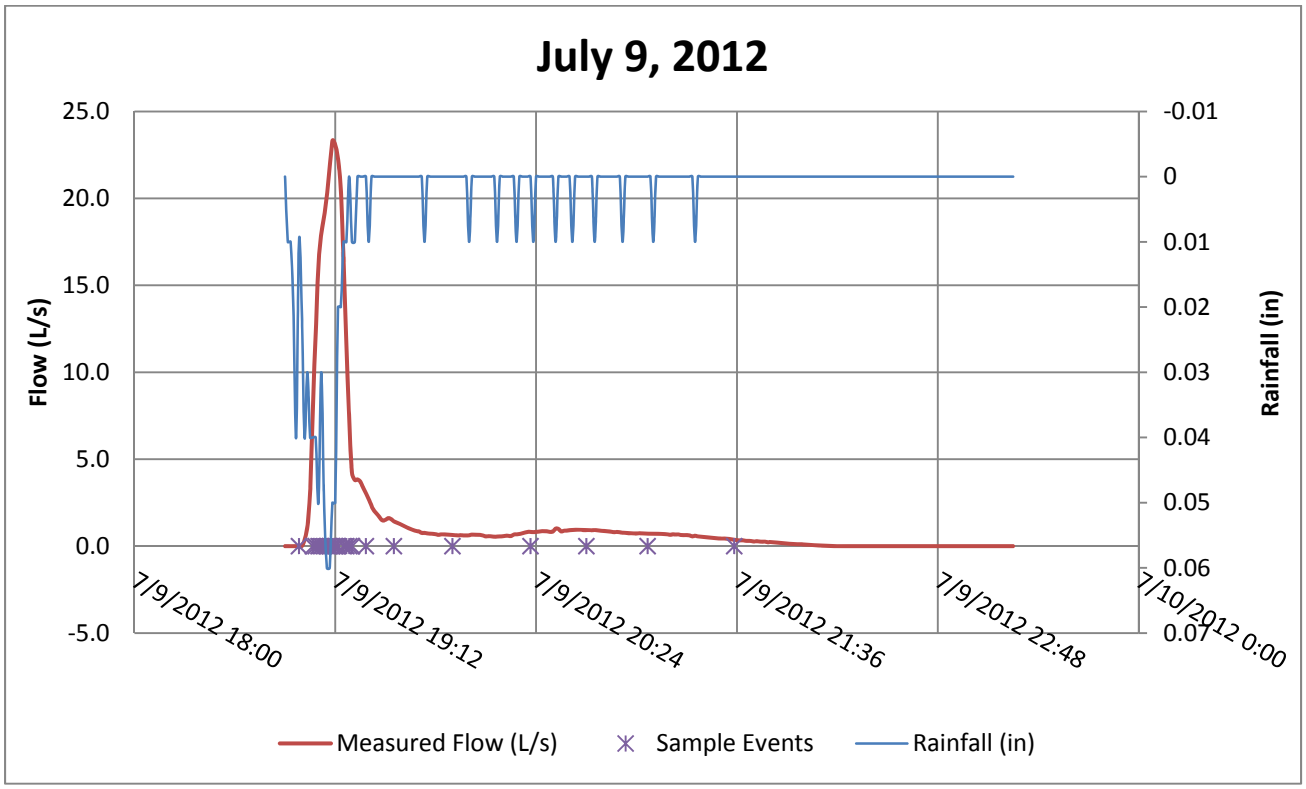
July 9, 2012
Flow (L/s)
Rainfall (in)
25.0
20.0
15.0
10.0
5.0
0.0
-5.0
-0.01
0
0.01
0.02
0.03
0.04
0.05
0.06
0.07
7/9/2012 18:00
7/9/2012 19:12
7/9/2012 20:24
7/9/2012 21:36
7/9/2012 22:48
7/10/2012 0:00
Measured Flow (L/s)
Sample Events
Rainfall (in)

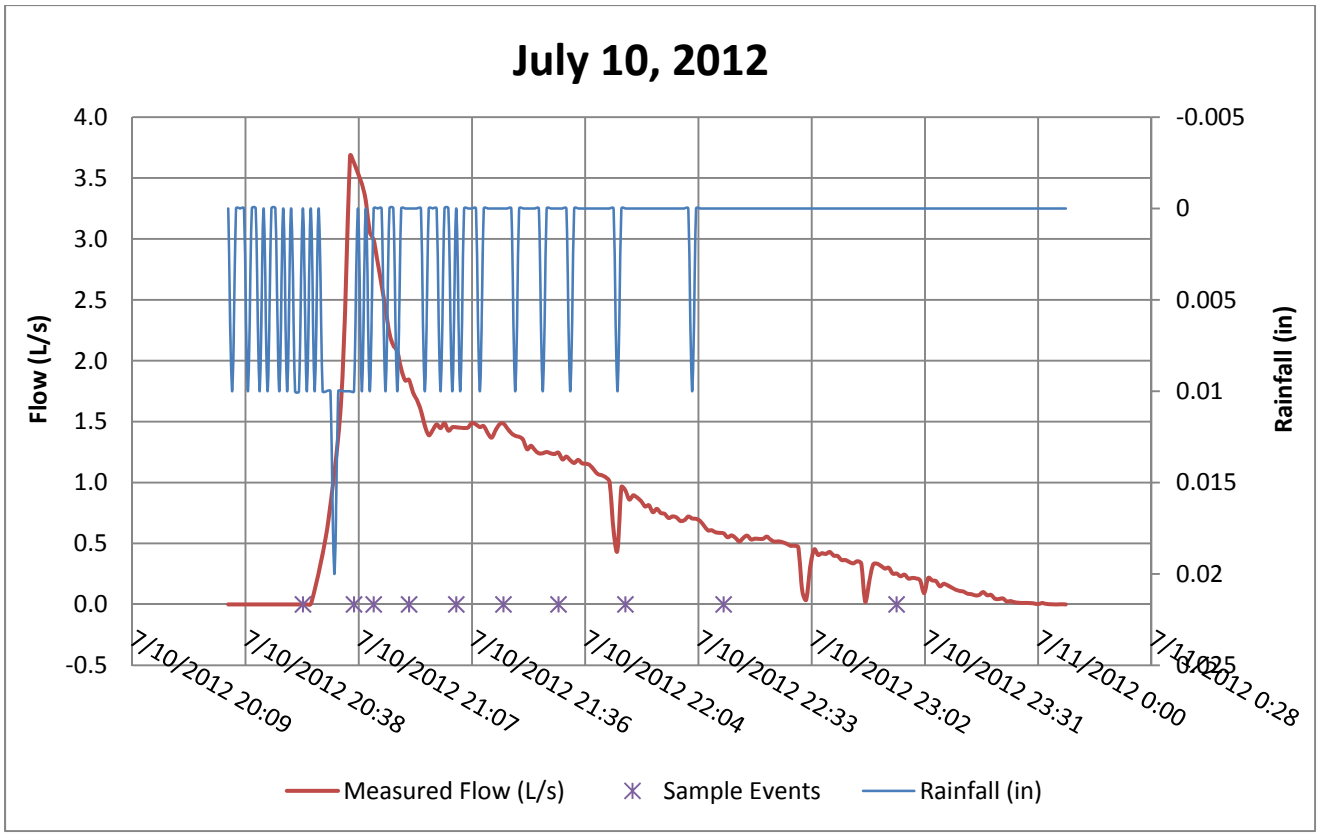
July 10, 2012
Flow (L/s)
Rainfall (in)
4.0
3.5
3.0
2.5
2.0
1.5
1.0
0.5
0.0
-0.5
-0.005
0
0.005
0.01
0.015
0.02
0.025
7/10/2012 20:09
7/10/2012 20:38
7/10/2012 21:07
7/10/2012 21:36
7/10/2012 22:04
7/10/2012 22:33
7/10/2012 23:02
7/10/2012 23:31
7/11/2012 0:00
7/11/2012 0:28
Measured Flow (L/s)
Sample Events
Rainfall (in)

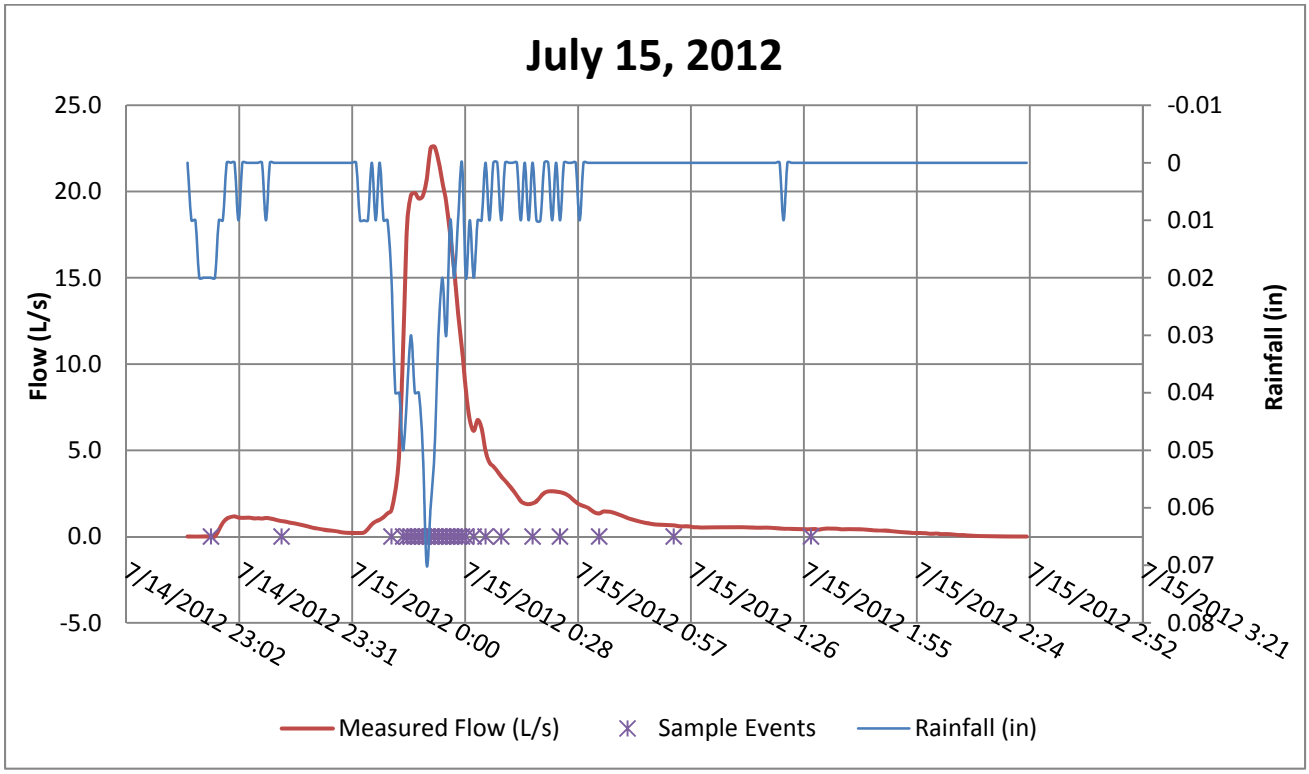
July 15, 2012
Flow (L/s)
Rainfall (in)
25.0
20.0
15.0
10.0
5.0
0.0
-5.0
-0.01
0
0.01
0.02
0.03
0.04
0.05
0.06
0.07
0.08
7/14/2012 23:02
7/14/2012 23:31
7/15/2012 0:00
7/15/2012 0:28
7/15/2012 0:57
7/15/2012 1:26
7/15/2012 1:55
7/15/2012 2:24
7/15/2012 2:52
7/15/2012 3:21
Measured Flow (L/s)
Sample Events
Rainfall (in)

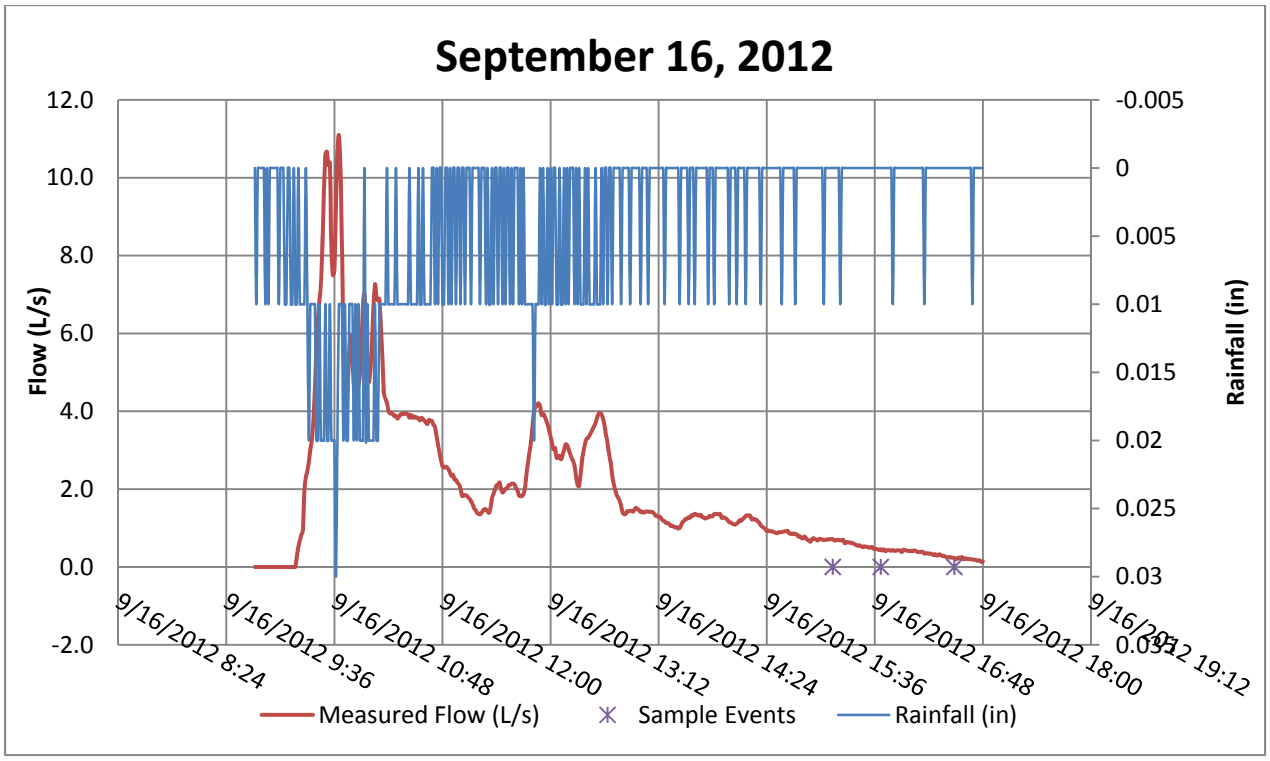
September 16, 2012
Flow (L/s)
Rainfall (in)
12.0
10.0
8.0
6.0
4.0
2.0
0.0
-2.0
-0.005
0
0.005
0.01
0.015
0.02
0.025
0.03
0.035
9/16/2012 8:24
9/16/2012 9:36
9/16/2012 10:48
9/16/2012 12:00
9/16/2012 13:12
9/16/2012 14:24
9/16/2012 15:36
9/16/2012 16:48
9/16/2012 18:00
9/16/2012 19:12
Measured Flow (L/s)
Sample Events
Rainfall (in)

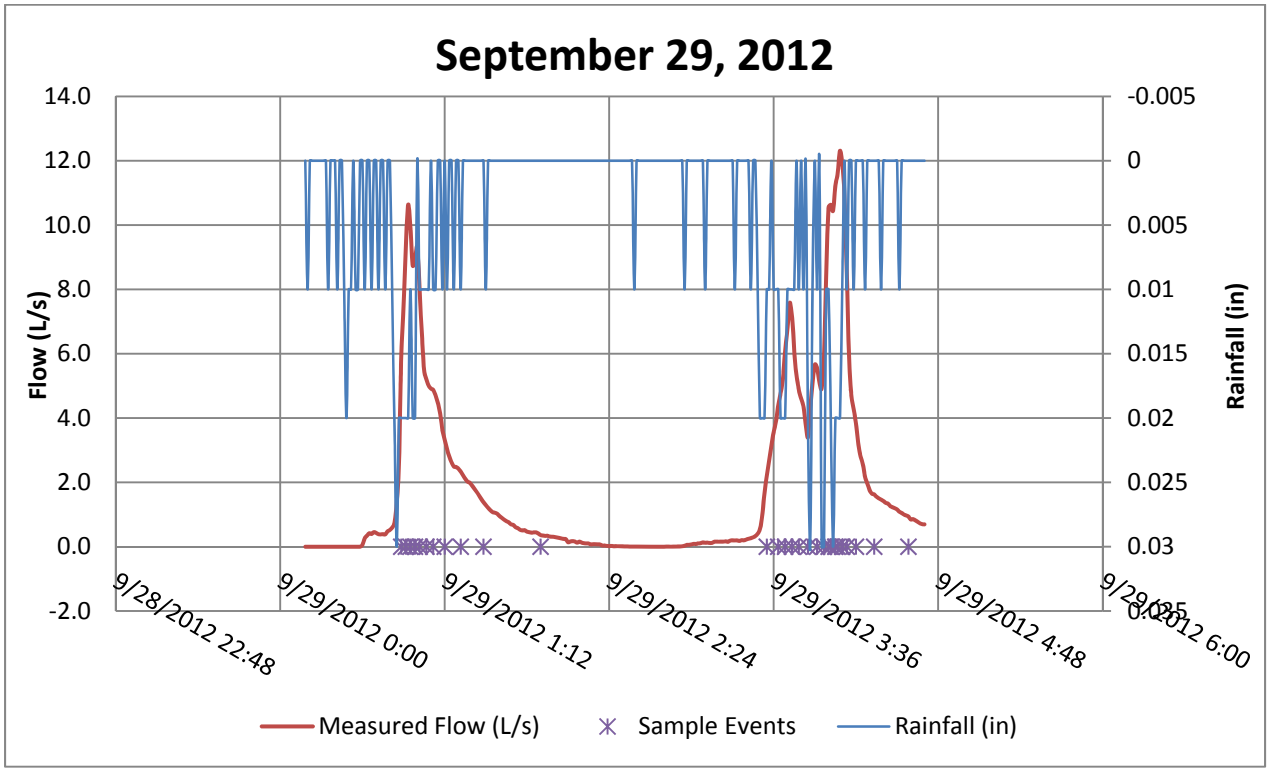
September 29, 2012
Flow (L/s)
Rainfall (in)
14.0
12.0
10.0
8.0
6.0
4.0
2.0
0.0
-2.0
-0.005
0
0.005
0.01
0.015
0.02
0.025
0.03
9/28/2012 22:48
9/29/2012 0:00
9/29/2012 1:12
9/29/2012 2:24
9/29/2012 3:36
9/29/2012 4:48
9/29/2012 6:00
Measured Flow (L/s)
Sample Events
Rainfall (in)

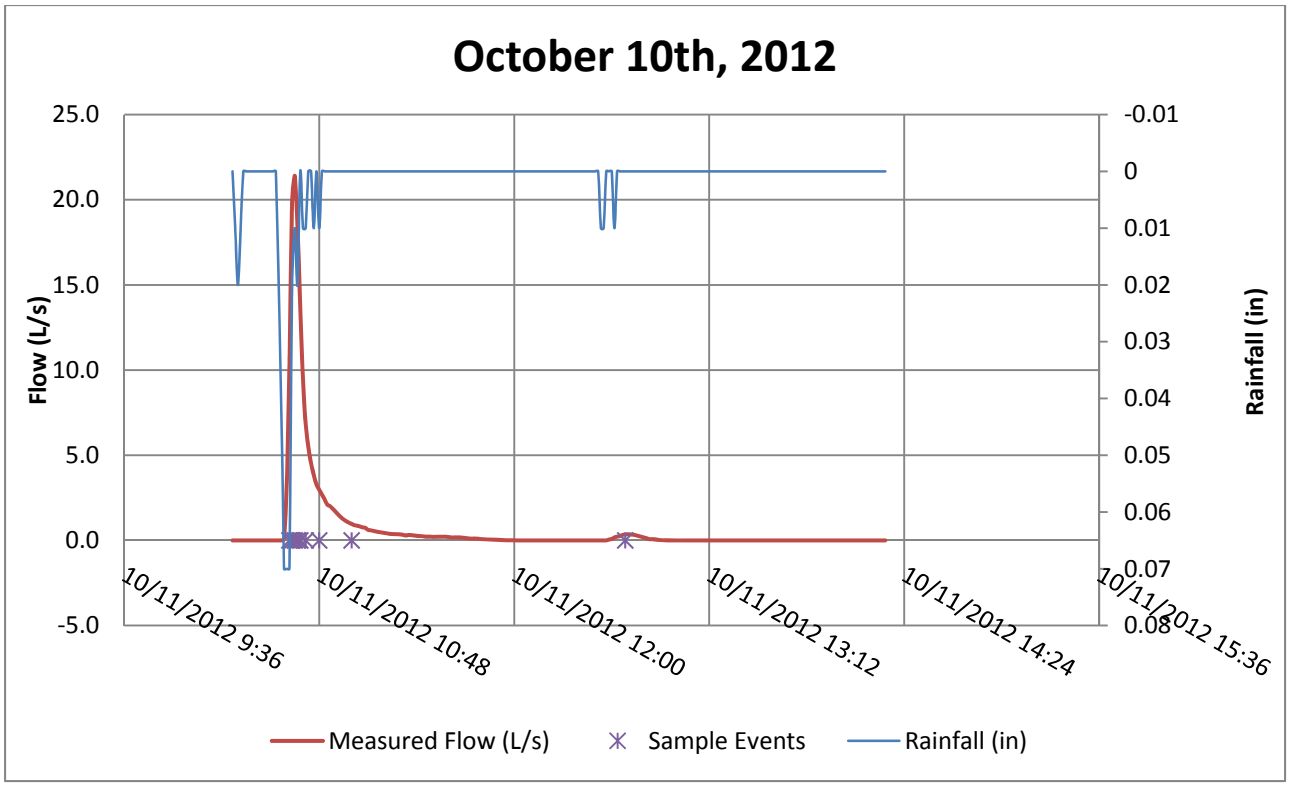
October 10th, 2012
Flow (L/s)
Rainfall (in)
25.0
20.0
15.0
10.0
5.0
0.0
-5.0
-0.01
0
0.01
0.02
0.03
0.04
0.05
0.06
0.07
0.08
10/11/2012 9:36
10/11/2012 10:48
10/11/2012 12:00
10/11/2012 13:12
10/11/2012 14:24
10/11/2012 15:36
Measured Flow (L/s)
Sample Events
Rainfall (in)

Appendix F: Water Depth Calculations

Water Depth Calculations (0%) Slope

Slope	0%	$Water\ Depth = (steady\ state - Baseline) * \sin\left(angle * \frac{\pi}{180}\right)$			
Angle	24.8 degrees				
Flow Rates	0.33-1.1 L/s/m				
Manometer	**Distance from beginning of reservoir (mm)**	**Baseline Monometer Readings**			
		no flow	no flow	no flow	no flow
Ruler	0				
7	548	128	128	128	128
2	966	130	130	130	130
8	1178	121	121	121	121
3	1295	126	126	126	126
4	1352	122	122	122	122
5	1373	120	120	120	120
6	1405	123	123	123	123
1(downstream)	1575	113	113	113	113
Manometer	**Distance from beginning of reservoir (mm)**	**Steady State Manometer Readings**			
		0.33L/s/m	0.55L/s/m	1.1L/s/m	1.2L/s/m
Ruler	0				
7	548	295	292	310	312
2	966	288	289	300	301
8	1178	266	274	289	292
3	1295	242	258	286	291
4	1352	218	232	275	266
5	1373	196	211	245	241
6	1405	195	203	232	228
1(downstream)	1575	113	113	113	142
Manometer	**Distance from beginning of reservoir (mm)**	**Calculated Water Depth (mm)**			
		0.1 L/s	0.55L/s/m	1.1L/s/m	1.2L/s/m
Ruler	0	69	70	75	76
7	548	70.0	68.8	76.3	77.2
2	966	66.3	66.7	71.3	71.7
8	1178	60.8	64.2	70.5	71.7
3	1295	48.7	55.4	67.1	69.2
4	1352	40.3	46.1	64.2	60.4
5	1373	31.9	38.2	52.4	50.8
6	1405	30.2	33.6	45.7	44.0
1(downstream)	1575				12.2

Water Depth Calculations (1.5%) Slope

Slope	1.5%	$Water\ Depth = (steady\ state - Baseline) * \sin\left(angle * \frac{\pi}{180}\right)$					
Angle	24.8 degrees						
Flow Rates	0.33-1.1 L/s/m						
Manometer	**Distance from beginning of reservoir (mm)**	**Baseline Monometer Readings**					
		no flow	no flow	no flow	no flow	no flow	no flow
Ruler	0						
7	548	203	203	203	203	203	203
2	966	188	188	188	188	188	188
8	1178	167	167	167	167	167	167
3	1295	165	165	165	165	165	165
4	1352	160	160	160	160	160	160
5	1373	157	157	157	157	157	157
6	1405	160	160	160	160	160	160
1(downstream)	1575	158	158	158	158	158	158
Manometer	**Distance from beginning of reservoir (mm)**	**Steady State Manometer Readings**					
		0.33L/s/m	0.55L/s/m	1.1L/s/m	0.66L/s/m	0.87L/s/m	0.99L/s/m
Ruler	0						
7	548	355	365	370	365	366	369
2	966	338	346	348	346	347	348
8	1178	301	317	330	324	327	330
3	1295	276	301	322	313	318	322
4	1352	247	268	303	287	301	298
5	1373	230	245	276	257	273	271
6	1405	225	237	264	252	262	254
1(downstream)	1575	158	158	165	158	158	158
Manometer	**Distance from beginning of reservoir (mm)**	**Calculated Water Depth (mm)**					
		0.33L/s/m	0.55L/s/m	1.1L/s/m	0.66L/s/m	0.87L/s/m	0.99L/s/m
Ruler	0	65	67	70	68	69	70
7	548	63.8	68.0	70.0	68.0	68.4	69.6
2	966	62.9	66.3	67.1	66.3	66.7	67.1
8	1178	56.2	62.9	68.4	65.9	67.1	68.4
3	1295	46.6	57.0	65.9	62.1	64.2	65.9
4	1352	36.5	45.3	60.0	53.3	59.1	57.9
5	1373	30.6	36.9	49.9	41.9	48.7	47.8
6	1405	27.3	32.3	43.6	38.6	42.8	39.4
1(downstream)	1575			2.9			

Water Depth Calculations (2.5%) Slope

Slope	2.5%	$Water\ Depth = (steady\ state - Baseline) * \sin\left(angle * \frac{\pi}{180}\right)$					
Angle	24.8 degrees						
Flow Rates	0.33-1.1 L/s/m						
Manometer	**Distance from beginning of reservoir (mm)**	**Baseline Monometer Readings**					
		no flow	no flow	no flow	no flow	no flow	no flow
Ruler	0						
7	548	245	245	245	245	245	245
2	966	212	212	212	212	212	212
8	1178	189	189	189	189	189	189
3	1295	182	182	182	182	182	182
4	1352	178	178	178	178	178	178
5	1373	175	175	175	175	175	175
6	1405	179	179	179	179	179	179
1(downstream)	1575	160	160	160	160	160	160
Manometer	**Distance from beginning of reservoir (mm)**	**Steady State Manometer Readings**					
		0.38L/s/m	0.55L/s/m	0.66L/s/m	0.87L/s/m	0.99L/s/m	1.1 L/s/m
Ruler	0						
7	548	398	400	407	407	408	409
2	966	367	373	376	378	379	380
8	1178	321	343	353	354	356	357
3	1295	294	318	332	342	343	345
4	1352	264	285	306	322	324	320
5	1373	248	262	273	295	297	295
6	1405	240	253	262	288	288	282
1(downstream)	1575	160	160	160	160	167	179
Manometer	**Distance from beginning of reservoir (mm)**	**Calculated Water Depth (mm)**					
		0.38L/s/m	0.55L/s/m	0.66L/s/m	0.87L/s/m	0.99L/s/m	1.1 L/s/m
Ruler	0	56	61	62	68	69	70
7	548	64.2	65.0	68.0	68.0	68.4	68.8
2	966	65.0	67.5	68.8	69.6	70.0	70.5
8	1178	55.4	64.6	68.8	69.2	70.0	70.5
3	1295	47.0	57.0	62.9	67.1	67.5	68.4
4	1352	36.1	44.9	53.7	60.4	61.2	59.6
5	1373	30.6	36.5	41.1	50.3	51.2	50.3
6	1405	25.6	31.0	34.8	45.7	45.7	43.2
1(downstream)	1575					2.9	7.9